Cytoplasmic location of translation controls protein output

by

Ellen Louise Horste

A Dissertation

Presented to the faculty of the Louis V. Gerstner, Jr.

Graduate School of Biomedical Sciences,

Memorial Sloan Kettering Cancer Center

in Partial Fulfillment of the Requirements for the Degree of

Doctor of Philosophy

New York, NY

June 2023

Christine Mayr, MD, PhD	Date
Dissertation Mentor	

DEDICATION

To my grandpa, Dr. Theodore Kenneth Sandberg. I hope you enjoy your new coffee table book.

ABSTRACT

The cytoplasm is highly compartmentalized, but the extent of subcytoplasmic mRNA localization in non-polarized cells is largely unknown. We used fluorescent particle sorting to determine mRNA enrichment in three unenclosed cytoplasmic compartments: the canonical rough endoplasmic reticulum (CRER), the TIS granule-associated rough endoplasmic reticulum (TGER), and the cytosol. Focusing our analysis on non-membrane protein-encoding mRNAs, we observed that 52% have a biased subcytoplasmic localization pattern which is determined by a combinatorial code of 3′UTR-bound RNA-binding proteins. Compartment-biased mRNAs differed in the functional classes of their encoded proteins. TGER-enriched mRNAs encode low-abundance proteins such as transcription factors, whereas CRER-enriched mRNAs encode highly expressed proteins. TGER/CRER-enriched mRNAs are more stable than cytosolic mRNAs, thus influencing protein output in a compartment-dependent manner. We observed that redirecting cytosolic mRNAs to the ER increases their protein expression by two-fold, independently of the bound RNA-binding proteins. In summary, the cytoplasm is functionally compartmentalized by local translation environments.

ACKNOWLEDGEMENTS

I would first like to acknowledge Christine Mayr for supporting me, challenging me, and trusting me to do great science over the past five years. You gave me every opportunity to succeed in science and beyond, I'm very grateful you took a chance on me. The Mayr Lab has always been a fantastic environment for science and I want to thank all past and present members, but especially: Sibylle Mitschka, Merv Fansler, Xiuzhen Chen, Vicky Luo, Ting Cai, Weirui Ma, Federica Lari, Neil Robertson, and Gang Zhen. I would also add Gaspare La Rocca to this list, who was not in the Mayr Lab but was a very supportive neighbor.

I would like to thank Andrea Schietinger who encouraged me to make meaningful, scientific contributions to her lab as a technician. Andrea, together with Mary Philip, were my first true scientific mentors, and they inspired me to pursue my PhD. Additionally- thanks both for convincing me not to go to medical school!

Thank you to the members of my thesis committee, Stewart Shuman and Philipp Niethammer, for all of your insightful criticisms and words of encouragement over the years. Thank you to Michael Kharas and Ben Kleaveland for thoughtfully reviewing this thesis.

I'm thankful for my wonderful GSK classmates- Corina Amor Vegas, Mariano Aufiero, Mollie Chipman, Florisela Herrejon Chavez, Buren Li, Adina Schonbrun,

Joe Shen, and Adele Whaley. Sadly, we are one fewer than we should be. To Jordan Aronowitz- I think of you often and wish you were here. Rest easy friend.

Thank you, GSK! Particularly Michael Overholtzer, Linda Burnley, David McDonagh, and Ken Marians.

Thank you to my family- Will, Barb, Tim, Caroline, Billy, Rose, and Pickle. You never asked too many questions about when I would be graduating, that was very much appreciated! And you all traveled to see me defend- even better! Love you all.

Finally, I would like to thank my husband, Charlie. Thank you for always taking an interest and singing my praises, even in my toughest times. I couldn't have done it without you!

TABLE OF CONTENTS

LIST OF TABLES

LIST OF FIGURES

LIST OF ABBREVIATIONS

AU-RBP: AU-rich element binding RNA-binding protein

CRER: Canonical rough endoplasmic reticulum

CY: Cytosol

ER: Endoplasmic reticulum

FACS: Fluorescence-activated cell sorting

iCLIP: Individual nucleotide resolution cross linking and immunoprecipitation

MCP: MS2 coat protein

RBP: RNA-binding protein

smRNA-FISH: Single molecule RNA fluorescent *in situ* hybridization

TGER: TIS granule and rough endoplasmic reticulum

TMT: Tandem mass tag

UTR: Untranslated Region

CHAPTER 1: INTRODUCTION

Our cells are immensely crowded and highly compartmentalized by both membrane-bound organelles and by higher order protein-nucleic acid complexes that partition bulk cytosol and nucleoplasm. Cellular organization is critical to ensuring that the billions of biomolecular interactions required to sustain life happen at the right place, at the right time, and for the appropriate duration. This is no trivial feat if you put yourself in the shoes of a single protein. From this vantage, the cell is about the size of four football fields and you are packed shoulder to shoulder with other proteins and nucleic acids. How will you ever find the specific proteins you are meant to interact with in this enormous, crowded milieu? Scientists have been fascinated by this question of protein complex assembly for decades. Early investigations often sought to reduce the complexity of the system by studying purified proteins, building multi-subunit protein complex machines in test tubes. Countless biochemistry experiments conducted over the years laid the foundation of our collective understanding of protein-protein interactions in principle. Today, we must embrace the complexity if we want to make meaningful contributions. On this note, I am proud to present my thesis work, which outlines a systems-level map of mRNA localization within the cytoplasm and demonstrates how cytoplasmic organization of mRNA contributes to protein output and thus, cellular activity.

Discovery of TIS Granules

Proteins are responsible for effectuating most cellular processes, but they do not work alone. Most proteins carry out their work in complex with other proteins and in some cases nucleic acids. The assembly of such protein complexes is a function of local protein concentration and the change in free energy associated with complex formation (Nooren and Thornton, 2003). As alluded to in the previous section, substantial coordination is required to optimize one or both parameters in order to form productive complexes efficiently and precisely in the vast and crowded cellular milieu. Cells employ several strategies to dynamically regulate the free energy landscape of protein-protein interactions including provision of metal ion or nucleoside-triphosphate cofactors, covalent modification of proteins such as phosphorylation or acetylation, and DNA/RNA allosteric substrates (Kuriyan and Eisenberg, 2007; Luo et al., 2023). In addition to promoting conformations which are energetically favorable to binding, cells can optimize effective protein concentration. Effective protein concentration can be increased by local translation of protein subunits, such as multi-subunit membrane channel proteins that are translated and assembled at the endoplasmic reticulum (ER) (Bonifacino et al., 1990; Zerangue et al., 1999) or synaptic proteins that are translated and assembled in neuronal synapses (Biederer et al., 2002; Hafner et al., 2019). Furthermore, the effect of local translation is potentiated by co-translational complex assembly, which has recently been shown to be a prevalent mechanism for assembly in eukaryotic cells (Badonyi and Marsh, 2022; Shiber et al., 2018).

By definition, co-translational protein complex assembly involves the protein-encoding mRNA, and our lab has a particular interest in the role mRNA plays in protein complex assembly. In 2015, Berkovits and Mayr demonstrated that the 3′untranslated region (3′UTR) of mRNA can mediate protein-protein interactions. In this study, it was shown that the long 3′UTR isoform of *CD47* is a scaffold for the assembly of the protein complex between CD47 and the adaptor protein SET (Berkovits and Mayr, 2015). Mechanistically, the RNA-binding protein HuR binds to AU-rich elements in the long 3′UTR isoform of *CD47* mRNA and recruits SET to the 3′UTR. As SET is tethered to the co-translational complex through the 3′UTR, its effective concentration is increased and its binding to the nascent polypeptide chain of CD47 is favored. The protein-protein interaction with SET results in efficient translocation of CD47 protein to the plasma membrane. Indeed, when CD47 is translated from the mRNA with the short 3′UTR, the HuR-SET-CD47 protein complex is not assembled, and CD47 protein is primarily localized to the ER. This finding represented a novel, 3′UTR -dependent mechanism for protein complex assembly.

As the binding of CD47 to SET has important downstream biological consequences, including protection from phagocytosis, the lab was motivated to identify additional RNA-binding proteins involved in the transfer of SET protein from the *CD47* 3′UTR to CD47 protein. My mentor Weirui Ma, who was a postdoc in the lab, addressed this question by performing an RNA-pulldown using the

minimal 3′UTR element required for CD47 surface localization followed by mass spectrometry analysis. This revealed the RNA-binding protein TIS11B (encoded by *ZFP36L1*), as the top hit. He reasoned that this factor is likely to be localized to the ER surface, the dominant site of *CD47* translation, and used immunofluorescence to confirm this. In this process he made another fascinating discovery which is that TIS11B forms a reticulated, mesh-like structure that is highly intertwined with the rough ER. Indeed, he showed that assembled TIS11B protein was necessary for SET transfer from the *CD47* 3′UTR to CD47 protein, and the reticulated structure is now known as the TIS granule network (Fig. 1.1A) (Ma and Mayr, 2018).

Prior to Weirui's discovery, TIS11B was characterized as a cytosolic RNA-binding protein, best known for its role in AU-rich element-mediated decay of cytokine and cell cycle factors (Stoecklin et al., 2002). TIS11B in its assembled state, TIS granules, was observed to take on additional functionality. It was shown that the long 3′UTR isoform of *CD47* is highly enriched in TIS granules and translated in the TIS granule-ER domain, however the short 3′UTR isoform of *CD47* is not enriched in TIS granules and is primarily translated on the ER membrane outside of TIS granules. Surprisingly, localization to TIS granules was found to be necessary and sufficient for SET binding: in the absence of TIS granules, SET does not bind CD47 even when translated from the long 3′UTR isoform. Conversely, when the short 3′UTR isoform of *CD47* was artificially expressed and translated in TIS granules, SET does bind the nascent protein. Thus rather than repressing AU-rich mRNAs, TIS granules appear to stabilize

localized transcripts and provide a favorable environment for co-translational protein complex assembly (Ma and Mayr, 2018).

TIS granules are present under steady-state cultivation conditions and have been observed across diverse human and mouse cell types, including human induced pluripotent stem cells (Ma and Mayr, 2018). Due to their ubiquitous nature and large size, we hypothesized that TIS granules facilitate many additional biomolecular interactions. To discover more functions of the TIS granule network, I set out to characterize the mRNA landscape of TIS granules and the functional consequences of mRNA localization to TIS granules. The following sections provide a conceptual overview of how this work integrates with and builds upon what is currently known about mRNA localization and sub-cellular organization.

mRNA localization

Spatial organization of mRNAs has been observed across species and cell types but is particularly well-studied in the context of polarized or asymmetric cell types (Martin and Ephrussi, 2009). Specific localization of mRNAs within the cytoplasm confers both spatial and temporal control of protein output and has been shown to be critically important in embryonic development, maintenance of synaptic plasticity in neurons, nutrient absorption in the gut, and cell migration. Recent studies demonstrated that a majority of mRNAs have a distinct spatial localization in polarized cell types such as neurons, intestinal epithelial cells, or cells of the early fly embryo (Glock et al., 2021; Hüttelmaier et al., 2005; Lécuyer et al., 2007; Moor et al., 2017; Tushev et al., 2018), which enables the local

control of protein production and activity (Biever et al., 2019; Buxbaum et al., 2015; Moretti et al., 2015). An outstanding question in the field is the extent to which the transcriptome adopts distinct spatial localization patterns in non-polarized cells, as it stands to reason that the energetic and regulatory benefits of mRNA compartmentalization are, to varying extents, universal across cell types.

For mRNAs encoding membrane and secretory proteins, mRNA localization to the ER membrane has been observed across many cell types and is a well characterized mechanism to support co- and post-translational membrane insertion of membrane and secretory proteins (Rapoport, 2007; Ast et al, 2013; Chartron et al 2016). Additionally, a growing body of evidence suggests that a substantial fraction of non-membrane protein encoding mRNAs are translated on the ER surface (Fazal et al., 2019; Jan et al., 2014; Reid and Nicchitta, 2012), despite lacking a signal peptide sequence. The functional implications are less obvious in this scenario, but one hypothesis is that the ER surface is a more efficient platform for protein synthesis than the cytosol and non-membrane protein encoding mRNAs may localize there as a means of increasing their translation rates. Two observations of distinct experimental methods support this hypothesis: 1) a greater fraction of mRNAs translated at the ER surface are found in polysomes than mRNAs translated in the cytosol, and 2) translation rates measured by single molecule imaging of reporter mRNAs are higher at the ER than in the cytosol (Reid and Nicchitta, 2012; Voigt et al., 2017). Thus, the

ER membrane may play an underappreciated role in translational regulation of non-membrane, non-secreted proteins.

Still, the vast majority of mRNAs do not encode membrane proteins, and little is known about how this subset localizes at steady state. One study began to address this with a dual mRNA localization-local translation screen on 500 mRNAs in HeLa cells. The investigation revealed distinct spatial patterning of 32/500 mRNAs. For 11/32 mRNAs, localization was translation dependent (Chouaib, et al 2020). However, contrary to the stark spatial enrichments observed for synaptic mRNAs in synapses or membrane-encoding mRNAs on the ER, the localization enrichments in this study were highly variable. For example, on average 11% of mRNA molecules localize to protrusions with cell-to-cell variability of 0-60%. This suggests that localization can be dynamic and tuned to the needs of the particular cell. In support of this, a separate study recently demonstrated that the dual targeting of the guanine nucleotide exchange factor NET1 to the nucleus and the cytoplasm is dependent on *NET1* mRNA location and translation rate. *NET1* transcripts in the perinuclear region have slow rates of translation, allowing the nascent polypeptide to bind importins and be transported to the nucleus. *NET1* transcripts in the periphery have a high rate of translation, which allows for competitive binding of CASK protein and RhoA association, trapping NET1 in the cytosol to promote cell adhesion and migration (Gasparski, et al 2023).

A comprehensive assessment of the field reveals an interesting theme: to date, mRNA localization has almost exclusively been investigated as a binary mechanism for local protein synthesis, meaning an mRNA is either “properly localized” to support a specific cellular process, or the mRNA is “mis-localized” and the cellular process is disrupted. For example, the “proper” functional location for *oskar* mRNA in *Drosophila* oocytes is the posterior pole. If *oskar* mRNA is mis-localized to elsewhere in the oocyte, anterior-posterior axis segmentation of the developing embryo is abolished (Kim-Ha et al., 1991). However, a new research area is emerging that focuses on multi-functional outcomes of heterogenous mRNA localization patterns. In this context, an mRNA does not have a singular “proper” translational environment, and the local translational environment itself can regulate the function or activity of the encoded protein. This type of localization-dependent regulation is exemplified by the difference in activity of protein encoded by *CD47* translated in TIS granules versus the ER, or *NET1* and *RAB13* translated in the periphery versus the perinuclear region (Ma and Mayr 2018; Muissoglu et al 2020; Gasparski et al 2022; Gasparski et al 2023). The work described in this thesis comprises a transcriptome-wide analysis of the mechanisms and functional outcomes of this type of mRNA localization in non-polarized cells at steady state. It is among the first of its kind in this nascent field and provides a foundation for others to build upon.

Experimental Introduction

At the outset of my thesis work the objective was to determine the broader biological significance of TIS granules. To begin, we set out to identify the mRNAs that are enriched in TIS granules since we knew 1) TIS granules promote 3′UTR-dependent protein-protein interactions, and 2) mRNA scaffolds the reticulated, mesh-like morphology in TIS granules (Ma and Mayr, 2018; Ma et al 2021). The first major challenge in this endeavor was the purification of TIS granules, and this challenge was two-fold. First, TIS granules are not enclosed by a membrane and therefore we had to develop an appropriate lysis method to maintain their structural integrity. Second, TIS granules are highly intertwined with the membrane-bound ER, which is contiguous with the nuclear membrane, thus the isolation method had to be optimized to separate TIS granules from the ER and the nucleus. At this time, several methods had been developed by other groups to investigate subcellular transcriptomics including RNA sequencing (RNA-seq) after biochemical fractionation, APEX-seq, MERFISH, and fluorescent particle sorting (Fazal *et al.*, 2019; Hubstenberger et al., 2017; Khong et al., 2017; Mili et al., 2008; Moor *et al.*, 2017; Xia et al., 2019). Application of these methods identified mRNAs that localize to cellular protrusions of migrating fibroblasts and distinguished between mRNAs that localize to the apical or basal sides of gut epithelial cells (Mili *et al.*, 2008; Moor *et al.*, 2017). These methods also determined the transcriptomes of cytoplasmic condensates such as P bodies or stress granules (Hubstenberger *et al.*, 2017; Khong *et al.*, 2017) and

identified mRNAs associated with membrane-bound organelles such as the ER or mitochondria (Fazal *et al.*, 2019; Qin et al., 2021).

I first tested biochemical fractionation, but the unique morphology and extensive intercalation with membrane bound organelles precluded the use of this technique. Proximity labeling was also ruled out based on the observation that TIS11B protein is present in cells in two assembly states: soluble TIS11B and TIS granules. Ultimately, I found success combining a mechanical lysis method with the elegant method used to purify P-bodies, so called fluorescence activated particle sorting (Hubstenberger *et al.*, 2017). Despite substantial effort, I was unable to completely separate TIS granules from the ER membrane and therefore we refer to sorted TIS granules as TIS granules-ER (TGER) particles.

After performing initial RNA-seq experiments on TGER particles we realized that we needed additional subcellular reference points in order to identity mRNAs that are overrepresented in TIS granules. The ER was an obvious choice due to its physical association with TIS granules *in vivo* and in sorted particles. Therefore, we used the same fluorescent particle sorting method to sort ER particles that we not associated with TIS11B, herein referred to as canonical rough ER (CRER) particles, and sequenced the ER-bound mRNAs. In addition, we sequenced digitonin-extracted cytosolic mRNAs, as the cytosol has thus far been considered the primary site of translation for non-membrane protein encoding mRNAs. We could then make comparisons across the transcriptomes of the three

subcytoplasmic compartments and identify mRNAs that were overrepresented in one compartment relative to the others. This is how the project evolved from an investigation of TIS granules to a broader study of sub-cytoplasmic mRNA localization.

Our systems-level analysis resulted in several unexpected observations. In addition to ~1,700 mRNAs that encode membrane proteins, we detected more than 2,100 mRNAs that encode non-membrane proteins with a biased localization to TGER or CRER, indicating that the ER membrane is a general translation compartment and is not restricted to membrane and secretory proteins. As the association of membrane-protein encoding mRNAs with the ER is well-characterized, we focused our analysis on mRNAs that encode non-membrane proteins. For more than half of them, we observed a biased localization to one of the three subcytoplasmic compartments. The localization pattern was largely controlled by a combinatorial code of the 3′UTR-bound RBPs TIS11B, TIA1/L1, and LARP4B. Compartment-enriched mRNAs differed substantially in their production and degradation rates as well as in the functional classes and expression levels of their encoded proteins. In addition to RBPs, we found that the location of translation has an independent effect on protein expression. We observed that redirecting cytosolic mRNAs to the rough ER membrane increased their steady-state protein expression levels by two-fold, indicating that the ER environment promotes protein expression. These results are detailed in the next section.

Figure 1.1 TIS granules intertwined with the rough ER.

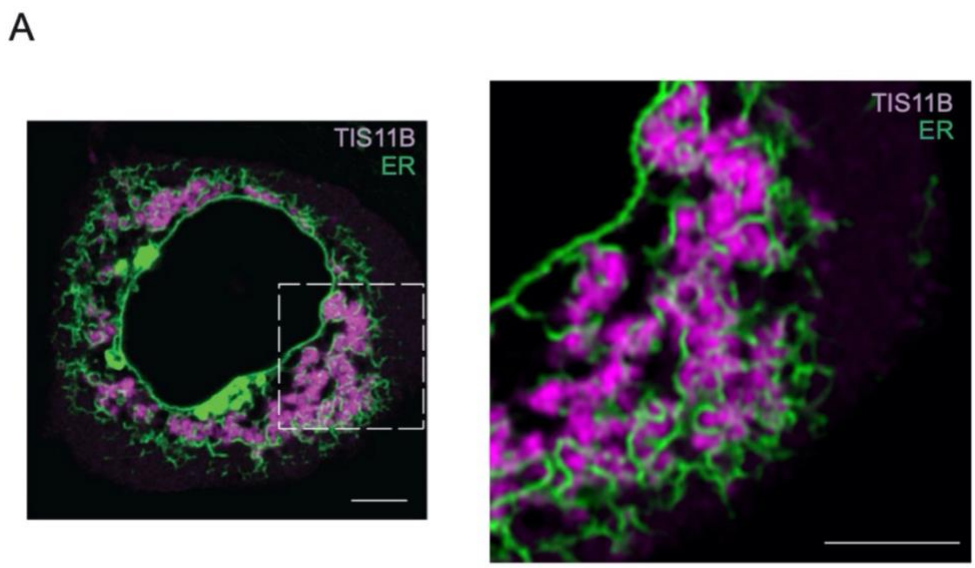

(A) Confocal live cell imaging of HeLa cells after transcfection with mCherry-TIS11B and GFP-SEC61B to visualize the ER. Right: higher magnification of the demarcated region (Ma and Mayr, 2018). Scale bar, 5 μm.

CHAPTER 2: RESULTS

Approach to determine subcytoplasmic mRNA localization

We set out to study differential mRNA localization across three major unenclosed cytoplasmic compartments in non-polarized human HEK293T cells under steady-state cultivation conditions. We determined the mRNAs enriched at the cytosolic surface of the ER – the largest cytoplasmic organelle, and TIS granules, an ER-associated condensate network, as well as the cytosol (Fig. 2.1A, B). For simplicity, we consider here the sum of the three compartments as the universe of cytoplasmic mRNAs.

To identify TIS granule-localized mRNAs, we used fluorescent particle sorting followed by RNA-seq. After transfecting cells with fluorescently tagged TIS11B to label TIS granules, we used mechanical lysis and differential centrifugation to isolate the cytoplasmic membrane fraction which was followed by flow cytometry-based sorting of TIS11B-positive particles (Fig. 2.2A, 2.2B). DAPI staining allowed us to identify and discard nuclei that were still associated with the ER and TIS granules and to isolate TIS11B-positive particles free of nuclei. To investigate if the obtained particles were pure TIS granules or if they contained ER membrane, we double-labeled TIS granules and the rough ER membrane, followed by particle sorting and confocal microscopy. This revealed that the TIS11B-positive particles cannot be separated from the rough ER membrane and therefore, we call them TIS granule ER (TGER) particles (Fig. 2.1C).

To isolate the canonical rough ER (CRER), we labeled the rough ER membrane with fluorescently tagged SEC61B and isolated CRER particles with the same

strategy. We obtained particles similar in size to TGER particles (Fig. 2.1C, Fig. 2.2C). To isolate cytosolic mRNAs, we used digitonin extraction (Liu and Fagotto, 2011). The extracted cytosol was not contaminated by nuclei or the ER, but it contained cytosolic proteins, including unassembled TIS11B protein and GAPDH which was used as positive control (Fig. 2.2D).

We performed RNA-seq to determine the mRNA composition in the three fractions. The biological replicates of the compartment samples were highly reproducible (Fig. 2.2E). We focused our analysis on protein-coding mRNAs. Previous analyses showed that most mRNAs that encode membrane or secretory proteins are translated on the ER, whereas mRNAs that encode non-membrane proteins are translated in the cytosol (Fazal *et al.*, 2019; Jan *et al.*, 2014). Consistent with this, we observed distinct partitioning patterns between the two groups across the three compartments (Fig. 2.2F).

mRNAs that encode membrane and secretory proteins are strongly enriched on the CRER membrane

Based on the different partitioning patterns, we analyzed the mRNAs that encode membrane or secretory proteins separately from the mRNAs that encode non-membrane proteins. Proteins that contain either a signal sequence or transmembrane domain are defined as secretory or membrane proteins and are encoded by 23% of mRNAs expressed in HEK293T cells, whereas the remaining 77% encode non-membrane proteins. We determined the compartment-specific partition coefficients in each group: For each gene, we calculated the fraction of

mRNA transcripts that localize to TGER, the CRER, or the cytosol and observed the expected baseline distributions across the three compartments (Fig. 2.2F). For mRNAs that encode membrane/secretory proteins, we observed 69% (*N* = 1,476) to be enriched at the CRER (Fig. 2.2G). When comparing the CRER membrane-enriched mRNAs with analyses from alternative isolation methods, we detected approximately 80% overlap among the ER membrane-enriched mRNAs, supporting the validity of our purification strategy (Fig. 2.2H) (Fazal *et al.*, 2019; Reid and Nicchitta, 2012).

A third of mRNAs that encode non-membrane proteins have an ER-biased localization

For mRNAs that encode non-membrane proteins, the baseline partitioning across the three compartments was more even. For a typical mRNA, we observed that roughly a third of transcripts localizes to TGER, CRER or to the cytosol (Fig. 2.2F). Next, we identified mRNAs whose transcript localization was biased towards a single compartment. We considered an mRNA to be compartment-enriched if the fraction of transcripts that localize to one compartment is 1.25-fold higher than the median fraction observed in the compartment. With this strategy, we identified 1246 mRNAs enriched in TGER, 919 non-overlapping mRNAs enriched on the CRER, and 1481 mRNAs enriched in the cytosol (Fig. 2.1D, 2.2I). The remaining 3369 mRNAs were not enriched in a single compartment and are considered to have an unbiased localization pattern (Fig. 2.1D, Table 1). To illustrate the compartment-biased localization, for individual mRNAs, we depicted the fraction of transcripts observed in the three compartments (Fig.

2.1E). Presented are examples obtained from the top 10%, bottom 10% and the median fraction of compartment-enriched transcripts, showing that the transcript enrichment is relative (Fig. 2.1E). Overall, we found that 52% of mRNAs that encode non-membrane proteins have a biased localization pattern to a single subcytoplasmic compartment in steady-state conditions of non-polarized cells. Taken together, for the two ER-associated compartments (TGER and CRER), we found enrichment of mRNAs that encode membrane or secretory proteins, but we detected even more mRNAs that encode non-membrane proteins enriched (Fig. 2.1F). Dozens of these mRNAs have been found previously by several other groups (Chen et al., 2011; Cui et al., 2012; Diehn et al., 2006; Lerner et al., 2003; Reid and Nicchitta, 2012; Voigt *et al.*, 2017) but the extent of localization of mRNAs that encode non-membrane proteins to TGER or CRER was previously unknown. This suggests that the rough ER membrane is a general translation compartment not restricted to membrane or secretory proteins. All remaining analyses were performed on mRNAs that encode non-membrane proteins.

Validation of subcytoplasmic mRNA localization patterns by single-molecule RNA-FISH

To validate mRNA localization across the three compartments, we performed single-molecule (sm) RNA-FISH on endogenous mRNAs predicted to localize to TGER or to the cytosol (Boraas et al., 2021). The TGER domain was visualized using fluorescently tagged TIS11B. To quantify compartment localization for individual mRNAs, we determined the area occupied by TGER or the cytosol in

each cell and calculated the expected distribution of mRNA foci across the two compartments. We determined the fold-change between the foci observed in each compartment and the foci expected to be in each compartment. Our smRNA-FISH experiment confirmed enrichment of all candidates predicted to be overrepresented in the TGER domain. mRNAs predicted to be biased to the cytosol were not enriched in the TGER domain and were even excluded from the TGER domain in some samples (Fig. 2.1G, 2.1H, 2.2J, 2.2K, Table 2.1).

The fine reticulated structure of the ER membrane makes it challenging to perform a similar colocalization analysis for the CRER. ER-localized mRNAs are tethered to the ER and are relatively resistant to digitonin extraction compared to cytosolic mRNAs (Cui *et al.*, 2012; Lerner *et al.*, 2003). To validate the enrichment of mRNAs on the CRER, we performed smRNA-FISH before and after digitonin extraction and calculated the fraction of retained mRNAs. We observed significantly higher retention rates for mRNAs predicted to be CRER-localized compared to mRNAs predicted to be cytosolic (Fig. 2.1I, 2.1J, 2.2L, 2.2M, Table 2.1). Based on our high validation rates for mRNAs that localize to the three investigated cytoplasmic compartments, we conclude that about half (52%) of mRNAs that encode non-membrane proteins have a biased subcytoplasmic localization pattern.

mRNA and protein levels strongly correlate with the location of translation

Next, we characterized the features of compartment-enriched mRNAs and found substantial differences in their steady-state mRNA and protein levels (Fig. 2.3A,

2.3B). We observed that TGER-enriched mRNAs have the lowest steady-state expression levels and encode proteins with the lowest expression levels (Fig. 2.3A, 2.3B). To examine if the low mRNA levels are caused by mRNA degradation, we estimated mRNA half-lives by analyzing Precision Run-On sequencing (Pro-seq) and RNA-seq data (Fig. 2.3C, 2.3D, Fig. 2.4A) (Blumberg et al., 2021; Patel et al., 2020). Pro-seq values can be treated as transcription rates and RNA-seq data can be viewed as a measure of RNA concentration to estimate RNA decay rates required for a steady-state equilibrium (Blumberg *et al.*, 2021). For TGER-enriched mRNAs, we observed that the low steady-state mRNA levels were not primarily caused by a low mRNA stability. Instead, these mRNAs had the lowest transcription rates which suggests that these mRNAs are either produced at a low rate or have high cotranscriptional degradation rates (Fig. 2.3C, 2.3D) (Smalec et al., 2022).

Cytosol-enriched mRNAs showed the highest degree of mRNA regulation with high production and high degradation rates (Fig. 2.3C, 2.3D). CRER-enriched mRNAs encode proteins with the highest expression levels, particularly when considering their intermediate steady-state mRNA levels (Fig. 2.3A, 2.3B). The compartment-enriched mRNAs also showed differences in their gene architectures. Cytosolic mRNAs have shorter 3′UTRs that are GC-rich and contain fewer AU-rich elements (Fig. 2.4B-D). Furthermore, CRER-enriched mRNAs encode the largest proteins which are more than twice as large as proteins encoded by cytosol-enriched mRNAs (Fig. 2.4E).

Consistent with the observed differences in steady-state protein expression levels, compartment-enriched mRNAs encode substantially different functional gene classes (Huang da et al., 2009). TGER-biased mRNAs are strongly enriched in zinc fingers and transcription factors (Fig. 2.3E). CRER-biased mRNAs are enriched in helicases, cytoskeleton-binding proteins and chromatin regulators which represent large proteins that are highly expressed in cells (Fig. 2.3F). Cytosol-enriched mRNAs often encode smaller proteins involved in the regulation of translation or splicing (Fig. 2.3G).

The TGER region supports active translation

Transcription factors are known to be expressed at lower abundance levels than non-transcription factors (Vaquerizas et al., 2009). Our analysis suggests that proteins that need to be expressed at low levels, such as transcription factors, are translated in the TGER domain (Fig. 2.3A, 2.3B, 2.3E). To obtain direct evidence for translation in the TGER domain, we applied the SunTag system to simultaneously visualize mRNAs and their nascent proteins in TGER and in the cytosol (Fig. 2.4F, 2.4G) (Yan et al., 2016). We confirmed that the TGER domain represents a translation environment for mRNAs (Ma and Mayr, 2018). We observed that the number of mRNA foci in TGER was five-fold lower compared to the cytosol. However, the proportion of mRNA translated was similar in TGER and the cytosol (Fig. 2.4H, 2.4I). Taken together, our data show that the TGER translation environment is not repressive and that the low expression level of

TGER-translated proteins is predominantly a result of their low nuclear gene expression (Fig. 2.3A, 2.3C).

Lack of 3'UTRs in expression constructs causes default mRNA localization to the cytosol

Our next goal was to identify the RBPs responsible for mRNA enrichment in the three compartments (Fig. 2.1D, 2.1E). As TIS11B is the scaffold protein of TIS granules, we performed iCLIP of TIS11B in HEK293T cells (Fig. 2.6A, 2.6B). We confirmed that the top binding motif of TIS11B in 3′UTRs of mRNAs is the canonical AU-rich element (UAUUUA) (Fig. 2.6C). To perform a comprehensive analysis on localization regulators, we analyzed additional CLIP datasets (Küspert et al., 2015; Zhao et al., 2021). Altogether, we correlated the 3′UTR binding pattern of 170 RBPs with mRNA enrichment in the three subcytoplasmic compartments. Among them, we found that the 3′UTR CLIP peak distributions of 25 RBPs were biased towards one of the three compartments. We applied logistic regression and identified seven RBPs whose binding contributed significantly to mRNA localization to the three compartments. They include TIS11B, HuR, PUM2, HNRNPC, TIA1/L1, LARP4B and METAP2 (Fig. 2.5A). As a previous CLIP analysis showed that peaks for TIA1 and TIAL1 cannot be distinguished (Wang et al., 2010), we used the sum of peaks from TIA1 and TIAL1 to obtain the values for TIA1/L1.

Among all mRNAs that encode non-membrane proteins, we observed 2154 without binding sites for any of the seven RBPs. Comparing mRNAs with CLIP

peaks for the seven RBPs with mRNAs lacking the RBPs, we observed increased cytosolic localization for the latter group (Fig. 2.6D, 2.6E). This suggests that they either contain binding sites for RBPs that were not studied by us or that these mRNAs localize to the cytosol by default. Two candidates (*LHPP, PTP4A3*) whose subcytoplasmic mRNA localization was experimentally verified by us did not contain binding sites for any of the seven RBPs. As these mRNAs localized to the cytosol in the presence or absence of their 3′UTRs, our data support a model of default cytosolic localization (Fig. 2.5B-D, 2.8A).

AU-RBPs promote mRNA localization to TGER or CRER, whereas LARP4B promotes cytosolic localization

Next, we focused on RBPs that differentially localize mRNAs to the ER-associated TGER or CRER regions versus the cytosol. Our CLIP analysis suggested that presence of LARP4B or METAP2 enhanced cytosolic mRNA localization. In contrast, the presence of all other RBPs, including TIS11B, HuR, PUM2, HNRNPC, and TIA1/L1, which bind to U-rich or AU-rich sequences (called here AU-RBPs) enhanced localization to either TGER or CRER (Fig. 2.5A, 2.5E-H) (Hafner et al., 2010; Lebedeva et al., 2011; Meyer et al., 2018; Mukherjee et al., 2011; Wang *et al.*, 2010; Yugami et al., 2020). Although both LARP4B and METAP2 binding were correlated with cytosolic mRNA localization, few mRNAs (N = 90) were exclusively bound by METAP2, whereas 740 were exclusively bound by LARP4B (Fig. 2.6F, 2.6G). We experimentally validated the localization pattern of three mRNAs (*SF3A2, MAP2K2, MLST8*) that were only

bound by LARP4B or METAP2 and confirmed their cytosolic localization (Fig. 2.5B, Fig. 2.1H).

In contrast, all validated candidates with predominant binding of AU-RBPs (*DNAJB1, BAG3, DUSP1, ALDH18A1, TES, IQGAP1, FOS, THAP1, FBXL3,* and *HSPA1B*) localized to TGER or CRER (Fig. 2.5B, Fig. 2.1H, 2.1J, Fig. 2.5I-K, 2.8B). For a selection of candidates, those expressed with and without their 3′UTRs, we observed that TGER enrichment was dependent on presence of their 3′UTRs, suggesting AU-RBP binding is required for mRNA localization to these compartments (Fig. 2.5I-K, 2.8A-B). In total, we experimentally confirmed differential mRNA localization to TGER/CRER versus the cytosol for all 15 tested candidates.

These experiments demonstrate that the presence of AU-RBPs strongly determines mRNA localization to TGER/CRER, whereas their absence promotes localization to the cytosol. Taken together with the observations that TGER/CRER mRNAs have very high AU content and are strongly enriched in AU-rich elements in their 3′UTRs (Fig. 2.5L, 2.5M), this region can be considered an AU compartment. mRNAs with a high AU content have a higher mRNA stability than the non-enriched (Fig. 2.5N), as was reported previously (Courel et al., 2019; Litterman et al., 2019). They also have longer 3′UTRs and lower pre-mRNA production rates (Fig. 2.6H, 2.6I).

The ratio of 3'UTR-bound TIS11B versus TIA1/L1 differentiates between TGER and CRER

Next, we set out to identify the RBP drivers that distinguish between different regions of the AU compartment. 3′UTRs bound by either TIS11B, HuR or PUM2 significantly promoted mRNA localization to TGER (Fig. 2.10A). However, few mRNAs were exclusively bound by HuR (*N* = 124), PUM2 (*N* = 38) or HNRNPC (*N* = 2) (Fig. 2.10B). While 441 mRNAs were exclusively bound by TIS11B, 230 mRNAs were only bound by TIA1/L1 and most mRNAs were cobound by TIS11B and TIA1/L1 (Fig. 2.7A, *N* = 862). Whereas presence of TIS11B positively correlated with TGER localization, presence of TIA1/L1 negatively correlated with it (Fig. 2.7B, 2.7C). For the cobound mRNAs, the ratio of 3′UTR-bound TIS11B over TIA1/L1 was strongly associated with TGER localization (Fig. 2.7B). In contrast, mRNAs predominantly bound by TIA1/L1 correlated best with localization to CRER (Fig. 2.7C).

mRNAs with 3′UTR-bound TIS11B had the highest number of AU-rich elements and the lowest pre-mRNA production rates (Fig. 2.7D, 2.7E). As all mRNAs in the AU compartment had generally high mRNA stability rates, the low production rates of TIS11B-bound mRNAs were associated with low steady-state mRNA and protein levels (Fig. 2.7F-H). In contrast, mRNAs predominantly bound by TIA1/L1 had significantly higher pre-mRNA production rates, and higher steady-state mRNA and protein levels (Fig. 2.7E-H). TIS11B or TIA1/L1-bound mRNAs also differed in the length and AU content of their 3′UTRs (Fig. 2.10C, 2.10D). Our analysis showed that although the presence of AU-RBPs is associated with high mRNA stability, different AU-RBPs, such as TIS11B or TIA1/L1 have a

differential influence on subcytoplasmic mRNA localization and are associated with vastly different abundance levels.

3′UTR-bound TIAL1 localizes non-membrane protein-encoding mRNAs to the ER

Our CLIP data analysis suggested that TIA1/L1-bound mRNAs are enriched on the CRER, which has never been reported (Fig. 2.7A, 2.7C). To validate TIA1/L1-dependent mRNA localization to the ER, we used the MS2 tethering system to mimic 3′UTR-binding of TIA1/L1 (Fig. 2.9A). We generated a GFP-tagged reporter mRNA that contains MS2-binding sites as 3′UTR (Berkovits and Mayr, 2015; Bertrand et al., 1998; Lee and Mayr, 2019). Coexpression of mCherry-tagged MS2 coat protein (MCP) fused to TIAL1 tethers TIAL1 to the 3′UTR of the reporter mRNA (Fig. 2.9A). As control, mCherry-tagged MCP was tethered to the GFP reporter mRNA.

Coexpression of the reporter mRNA and MCP resulted in evenly distributed cytosolic expression of both MCP protein and reporter mRNA, due to the absence of a specific RBPs (Fig. 2.9C-E). In contrast, coexpression of the reporter mRNA and MCP-TIAL1 resulted in perinuclear, reticulated expression of MCP-TIAL1 with the mRNA reporter predominantly localized to the rough ER (Fig. 2.9B-E). Colocalization was assessed by RNA-FISH of the GFP-tagged reporter mRNA and simultaneous visualization of the rough ER through fluorescently tagged SEC61B. Using line diagrams of the fluorescence intensities, we quantified the overlap between the reporter mRNAs and the ER

(Fig. 2.9C-E). In the presence of MCP-TIAL1, we observed higher correlation coefficients between the reporter mRNA and the ER (Fig. 2.9E). This result indicates that 3′UTR-bound TIAL1 causes localization of non-membrane protein encoding mRNAs to the rough ER surface.

3'UTR-bound TIAL1 increases protein expression

For endogenous mRNAs, our analysis suggested that TIA1/L1-bound mRNAs are highly abundant at steady-state and encode highly expressed proteins (Fig. 2.7G, 2.7H). Using the mRNA reporter, we investigated the contribution of TIAL1 to steady-state protein expression. We used FACS to measure GFP protein expression of the mRNA reporter with and without tethering of TIAL1 to the 3′UTR (Fig. 2.9A, Fig. 2.12A-C). We observed a 3.5-fold increase in protein expression upon 3′UTR-tethering of TIAL1 compared to tethering of MCP alone (Fig. 2.9F, 2.9G). We confirmed the TIA1/L1-dependent increase in protein expression using a second GFP reporter (Fig. 2.12D-F). To determine if the increase in protein expression was a consequence of increased mRNA stability, we measured *GFP* reporter mRNA abundance in cells expressing the TIAL1 tether and cells expressing the MCP tether (Fig 2.9H). We observed no change in reporter mRNA abundance and determined that the increased protein expression was independent of mRNA stability. As TIAL1 promotes translation of mRNAs on the ER membrane, it was unclear if increased protein expression was caused by TIAL1 or by a potentially unique translation environment provided by the rough ER membrane. For example, it was reported that mRNAs that encode

non-membrane proteins contain 1.4-fold more ribosomes when translated on the ER membrane than when translated in the cytosol (Voigt *et al.*, 2017).

TIAL1 cooperates with the rough ER environment to promote protein expression

To disentangle the effects of TIAL1 and the ER membrane on protein expression, we tethered the reporter mRNA directly to the ER surface by fusing MCP to SEC61B, a subunit of the translocon complex in the rough ER (Fig. 2.11A). MCP-SEC61B perfectly colocalized with the ER and recruited reporter mRNAs to the ER (Fig. 2.11B, 2.12G-I). However, reporter protein expression only increased by 1.25-fold compared to the tethering of MCP alone, accompanied by no change in reporter mRNA abundance (Fig. 2.11B-E). We used a second ER localization reporter by fusing MCP to TRAPα, which represents a different subunit of the translocon complex and obtained a similar result. We observed an increase in protein expression by 1.5-fold when the reporter mRNA was tethered to TRAPα (Fig. 2.12J-M). These results suggested that the ER membrane environment has a significant but small stimulatory effect on protein expression.

Next, we investigated if the TIAL1-dependent increase in protein expression is intrinsic to TIAL1 or if it depends on its localization to the ER membrane. We added a CAAX motif to TIAL1 to localize the TIAL1-bound mRNA reporter to the plasma membrane instead of the ER membrane (Fig. 2.11F). The CAAX signal is a prenylation motif that efficiently localized MCP and MCP-TIAL1 to the plasma membrane (Fig. 2.11G) (Yan *et al.*, 2016). Translation of the TIAL1-bound mRNA reporter at the plasma membrane increased protein expression by 1.8-fold (Fig.

2.11H, 2.11I). As translation of the TIAL1-bound reporter at the ER membrane resulted in two-fold higher protein expression than its translation at the plasma membrane (Fig. 2.11I), our result suggested that TIAL1 cooperates with the environment on the rough ER membrane to promote protein expression. As the RBPs bound to the reporter mRNA were identical in these experiments, our results demonstrate that the subcytoplasmic location of translation controls steady-state protein expression levels by two-fold when comparing plasma and ER membranes.

The repressive effect of unassembled TIS11B on protein expression is overcome by its localization to rough ER membrane

Next, we examined if the environment on the rough ER membrane also promotes protein expression of mRNAs bound by other RBPs, including TIS11B (Fig. 2.13A, 2.13B). In cells expressing GFP- or mCherry-TIS11B fusion constructs, about 30% form TIS granules at steady state (Fig. 2.14A, 2.14B) (Ma and Mayr, 2018). However, we noticed that addition of MCP to TIS11B fusion constructs resulted in limited TIS granule formation and predominant expression of unassembled TIS11B in the cytosol (Fig. 2.14A, 2.14B). In the unassembled state, binding of MCP-TIS11B to reporter mRNA repressed reporter protein expression by two-fold and decreased reporter mRNA abundance by 1.4-fold, compared to tethering of MCP alone (Fig. 2.13C-E). This result is consistent with previous reports that suggested that unassembled TIS11B represses the expression of certain cytokine mRNAs and cell cycle regulators (Galloway et al.,

2016; Lykke-Andersen and Wagner, 2005; Stoecklin *et al.*, 2002). In contrast, fusing TIS11B to MCP-SEC61B localizes TIS11B and the bound reporter mRNA to the rough ER, and this overcomes the repressive effect of unassembled TIS11B, increasing protein expression by two-fold and recovering reporter mRNA abundance (Fig. 2.13A-E). The two-fold increase in protein expression was recapitulated with a second reporter and indicates that the repressive effect on protein expression mediated by cytosolic, unassembled TIS11B, which is at least partially driven by destabilization of mRNA, is overcome by translation of the TIS11B-bound mRNA in the TGER region (Fig. 2.13D, Fig. 2.14C-E).

Taken together, we observed that 3′UTR-bound TIAL1 has a promoting effect on protein expression, whereas the binding of TIS11B is repressive. These results confirm the primary regulatory impact of RBPs on steady-state protein expression (Fig. 2.11H, 2.13D). Moreover, protein expression is additionally regulated by the subcytoplasmic location of translation in a manner that is independent of the bound RBP (Fig. 2.11H, 2.13D). Our findings show that relocalization of mRNAs that encode non-membrane proteins to the rough ER membrane stimulates their protein expression by two-fold, regardless of the bound RBPs (Fig. 2.13F).

Figure 2.1 Strategy to determine subcytoplasmic mRNA localization.

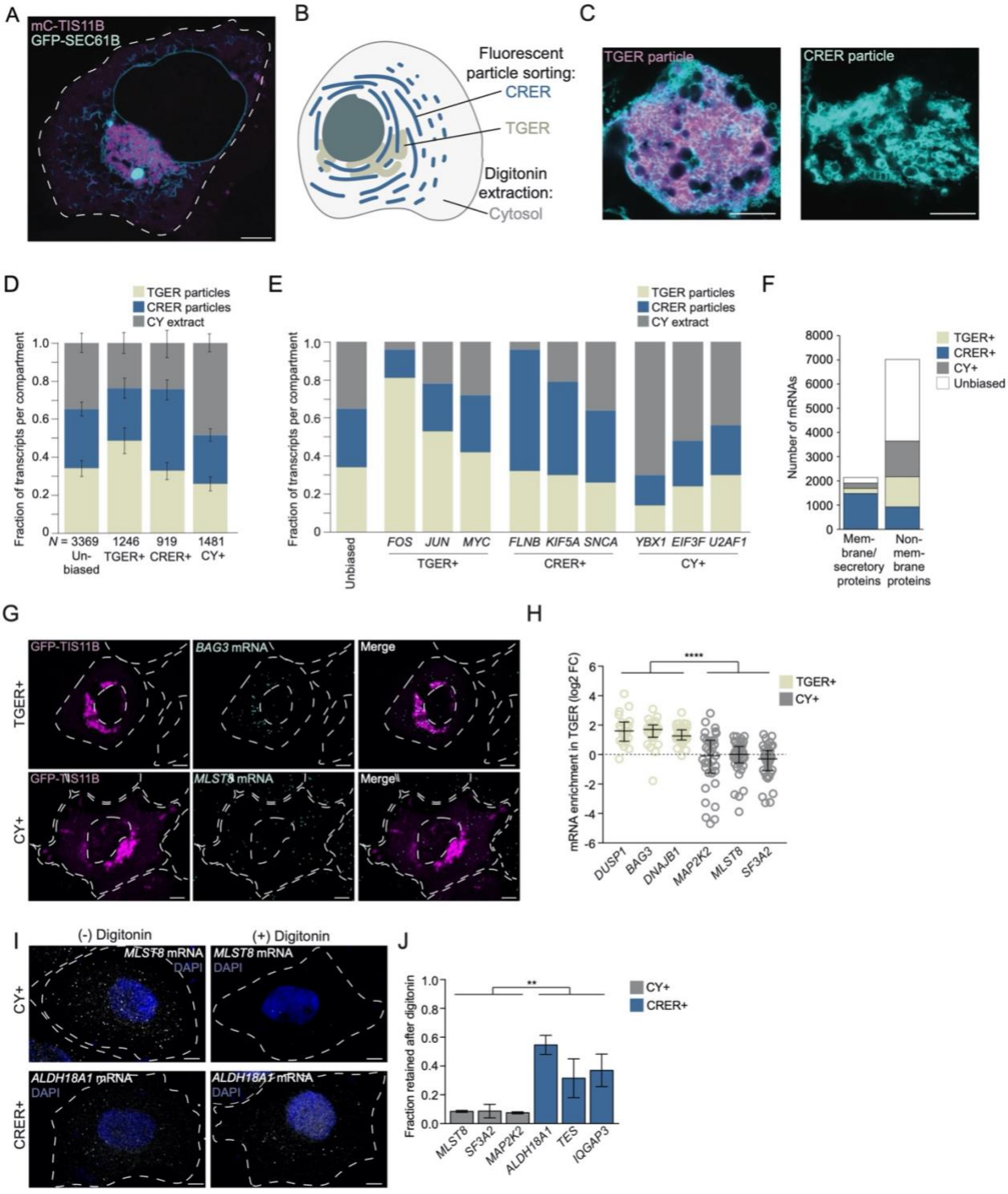

Figure 2.1 Strategy to determine subcytoplasmic mRNA localization.

(A) Confocal live cell imaging of HeLa cells after transfection of mCherry (mC)-TIS11B (magenta) to visualize TIS granules and of GFP-SEC61B to visualize the rough ER (teal). Scale bar, 5 µm.
(B) Schematic showing purification strategy to identify mRNAs within three cytoplasmic compartments, including TGER (beige), CRER (blue), and the cytosol (grey).
(C) As in (A), but after sorting of fluorescent particles. Shown is a TGER particle (left) and a CRER particle (right). Scale bar, 5 µm.
(D) Stacked bar plot showing fraction of transcripts that localize to each of the three cytoplasmic compartments for TGER-enriched (TGER+, *N* = 1246), CRER-enriched (CRER+, *N* = 919), cytosol-enriched (CY+, *N* = 1481) mRNAs or for mRNAs without enrichment in a single compartment (unbiased, *N* = 3369). Shown is the mean ± standard deviation for each compartment.
(E) As in (D), but shown is the fraction of transcripts that localize to each of the three subcytoplasmic compartments for representative examples (partition coefficient). Shown are examples from the top 10%, the bottom 10%, and the median of TGER-enriched, CRER-enriched, and cytosol-enriched mRNAs.
(F) The number of compartment-enriched mRNAs is shown separately for mRNAs that encode membrane or secretory proteins versus non-membrane proteins.
(G) Single-molecule (sm) RNA-FISH of the indicated endogenous mRNAs (teal) in HeLa cells. TIS granules were visualized by using GFP-TIS11B (magenta). Cell and nuclear boundaries are indicated by the dotted lines. Representative images are shown. Scale bar, 5 µm.
(H) Quantification of (G). Colocalization of smRNA-FISH foci and TIS granules was determined. Shown is the log2 fold-change (FC) of the observed over expected TGER localization based on the relative area of TIS granules and the cytosol in each cell. Each cell is represented by one dot and the summarized data from three independent experiments is shown. Number of cells analyzed, *DUSP1, N* = 21; *BAG3, N* = 25; *DNAJB1, N* = 32; *MAP2K2, N* = 45; *MLST8, N* = 38; *SF3A2, N* = 37. Representative images are shown in Fig. 2.2J and 2.2K. Differential localization between TGER+ and CY+ mRNAs: Mann-Whitney test, ****, *P* = 3 x 10-20. *SF3A2* mRNA is significantly depleted from TIS granules, Mann-Whitney test, *P* = 0.004.
(I) Shown are smRNA-FISH foci of endogenous mRNAs in HeLa cells before (-) and after (+) digitonin treatment. Cell and nuclear boundaries are indicated by the dotted lines. Representative images are shown. Scale bar, 5 µm.
(J) Quantification of (I). Shown is the fraction of digitonin-resistant smRNA-FISH foci of endogenous mRNAs as mean ± std of three independent experiments. Number of cells analyzed, *MLST8, N* = 70; *SF3A2, N* = 67; *MAP2K2, N* = 48; *ALDH18A1, N* = 63; *TES, N* = 81; *IQGAP3, N* = 50. Representative images are shown in Fig. 2.2L and 2.2M. T-test for independent samples, **, P = 0.008.

Figure 2.2 Strategy to determine subcytoplasmic mRNA localization continued.

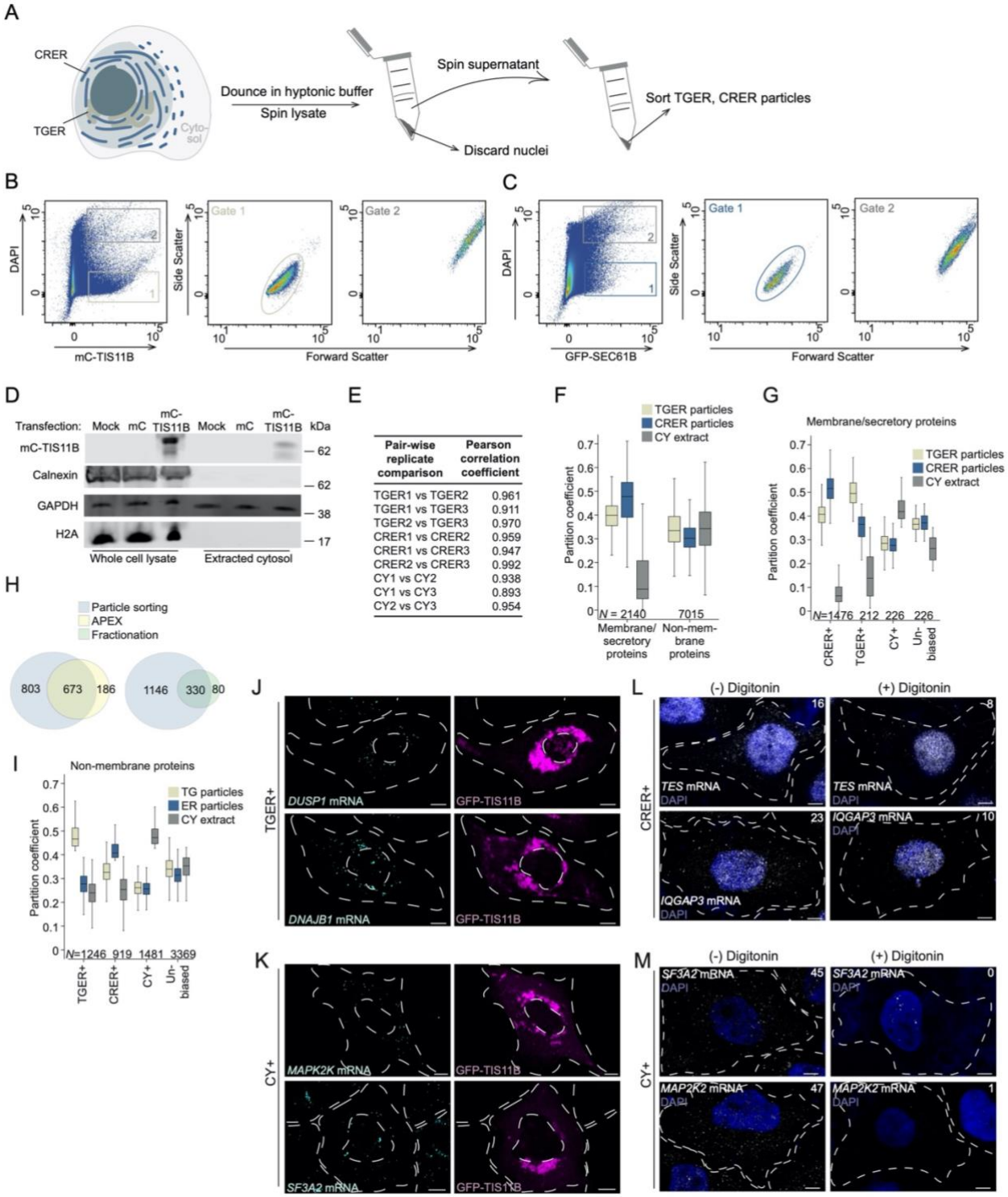

Figure 2.2 Strategy to determine subcytoplasmic mRNA localization continued.

(A) Cell fractionation strategy to obtain the cytoplasmic membrane fraction. Transfected HEK293T cells were lysed in hypotonic buffer, followed by douncing and differential centrifugation at 600 g to pellet nuclei and the supernatant was subsequently spun at 7000 g. The pellet contains the cytoplasmic membrane fraction that was used for subsequent fluorescent particle sorting.
(B) FACS plot showing mCherry-TIS11B-positive TGER particles costained with DAPI to segregate TGER particles from nuclear contamination. Gate (1) contains TGER particles, whereas gate (2) contains TGER particles bound to nuclei, indicated by DAPI stain and larger size.
(C) As in (B) but shown are GFP-SEC61B-positive CRER particles costained with DAPI. Gate (1) contains CRER particles, whereas gate (2) contains CRER particles bound to nuclei, indicated by DAPI stain and larger size.
(D) Immunoblot showing markers used to evaluate the quality of the digitonin-based cytosol extraction. H2A antibody was used as marker for nuclear components, Calnexin was used as ER marker and GAPDH was used as cytosolic protein. Unassembled TIS11B was observed in the cytosol after transfection with mCherry-tagged TIS11B. Marker expression in whole cell lysates serves as control. mC, mCherry.
(E) Pearson correlation coefficients for mRNA expression levels for biological replicates on subcytoplasmic compartments.
(F) Baseline distribution of partition coefficients across the three investigated cytoplasmic compartments is shown separately for mRNAs that encode membrane/secretory proteins and mRNAs that encode non-membrane proteins.
(G) Distribution of partition coefficients in each fractionation sample for compartment-enriched mRNAs that encode membrane/secretory proteins.
(H) Overlap of CRER-enriched mRNAs that encode membrane/secretory proteins (N = 1476) with previous datasets that used alternative isolation methods. APEX-seq, $X2$ =127, P < 0.0001 Fractionation dataset, $X2$ = 803, P < 0.0001.
(I) Distribution of partition coefficients in each fractionation sample for compartment-enriched mRNAs that encode non-membrane proteins.
(J) smRNA-FISH of endogenous mRNAs (teal), predicted to localize to the TGER in HeLa cells. The TGER domain is visualized by GFP-TIS11B (magenta). Cell and nuclear boundaries are indicated by the dotted lines. Representative images are shown. Scale bar, 5 µm. Shown are representative images for *DUSP1* and *DNAJB1.*
(K) As in (J), but for endogenous mRNAs predicted to localize to the cytosol in HeLa cells. Shown are representative images for *MAP2K2* and *SF3A2*.
(L) smRNA-FISH of endogenous mRNAs predicted to localize to the CRER. Shown are HeLa cells before (-) and after (+) digitonin treatment. Cell and nuclear boundaries are indicated by the dotted lines, number of foci counted in each image indicated in white. Representative images for *TES* and *IQGAP3* are shown. Scale bar, 5 µm.
(M) As in (L), but for endogenous mRNAs predicted to localize to the cytosol in HeLa cells. Shown are representative images for *SF3A2* and *MAP2K2.*

Figure 2.3 Characteristics of compartment enriched mRNAs.

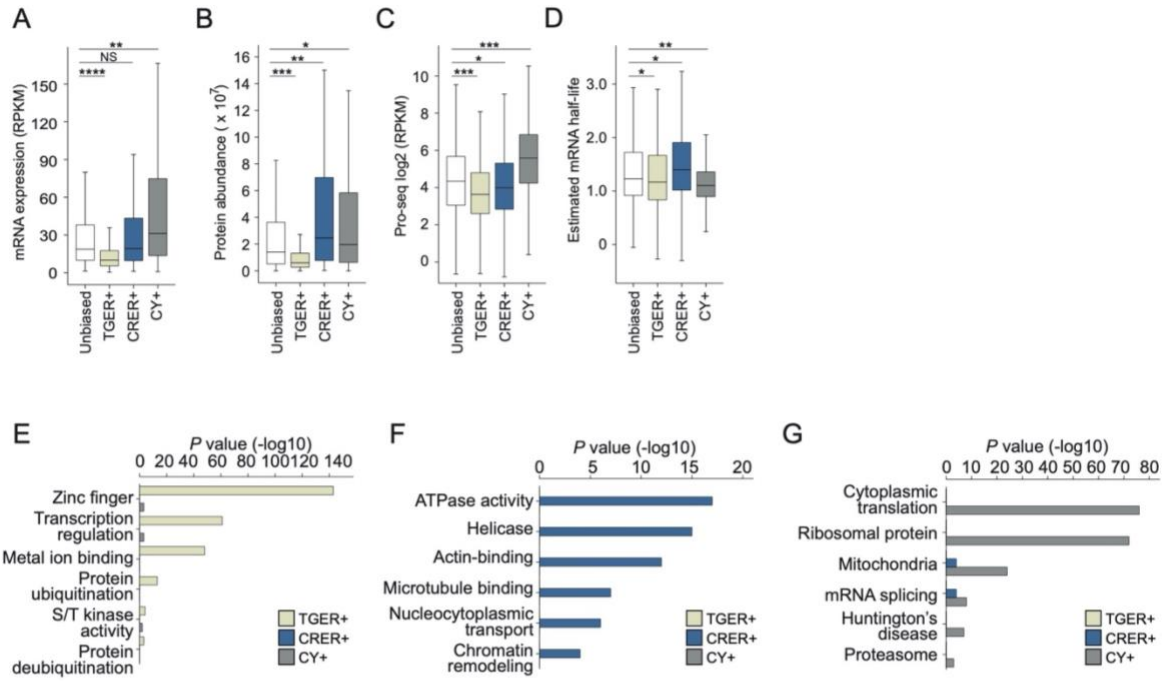

(A) Steady-state mRNA abundance levels obtained from whole cell lysates. TGER+, *N* = 1246; CRER+, *N* = 919, CY+, *N* = 1481; unbiased, *N* = 3369. Mann Whitney test: *, 1 x 10-3 >*P*> 1 x 10-9; **, 1 x 10-10 >*P*> 1 x 10-20; ***, 1 x 10-21 >*P*> 1 x 10-80; ****, 1 x 10-81 >*P*> 0. RPKM, reads per kilobase of transcript per million reads mapped.
(B) As in (A), but steady-state protein levels obtained from whole cell lysates. TGER+, *N* = 469; CRER+, *N* = 638; CY+, *N* = 833; unbiased, *N* = 2001. *P* value categories as in (A), exact *P* values are listed in Table 2.2.
(C) As in (A), but Pro-seq levels are shown, which indicate transcription rates. TGER+, *N* = 1222; CRER+, *N* = 896; CY+, *N* = 1425; unbiased, *N* = 3268. *P* value categories as in (A), exact *P* values are listed in Table 2.2.
(D) As in (C), but estimated mRNA half-lives are shown. *P* value categories as in (A), exact *P* values are listed in Table 2.2.
(E) Gene ontology analysis for TGER-enriched mRNAs. Shown are the top six functional gene classes and their Benjamini-Hochberg adjusted *P* values for categories that are significantly and uniquely enriched in TGER+ mRNAs. The Benjamini-Hochberg adjusted *P* values for the same categories for CRER+ and CY+ mRNAs are shown for comparison reasons.
(F) As in (E), but for CRER-enriched mRNAs.
(G) As in (E), but for mRNAs enriched in the cytosol.

Figure 2.4 The TGER domain is an active translation compartment.

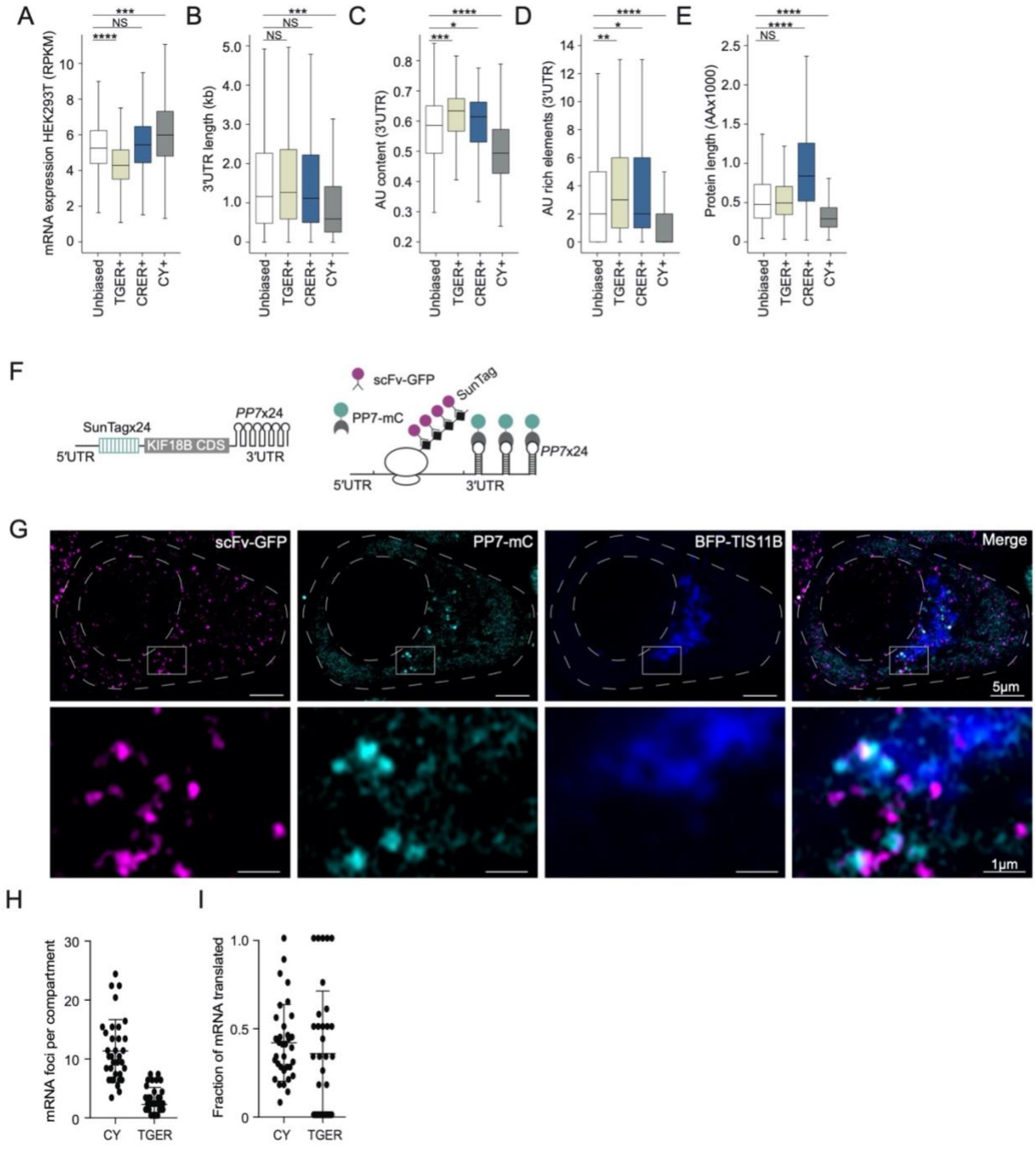

Figure 2.4 The TGER domain is an active translation compartment.

(A) As in Fig. 2.3C, but steady-state mRNA abundance levels of compartment-enriched mRNAs obtained by RNA-seq from whole cell lysates of HEK293 cells. This sample was used together with the Pro-seq sample to estimate mRNA half-lives. Mann Whitney test: *, 1 x 10-3 > *P*> 1 x 10-9; **, 1 x 10-10 > *P*> 1 x 10-20; ***, 1 x 10-21 > *P*> 1 x 10-80; ****, 1 x 10-81 > *P*> 0. RPKM, reads per kilobase of transcript per million reads mapped.
(B) As in Fig. 2.3A, but 3′UTR length of mRNAs enriched in the indicated compartments is shown. *P* value categories as in (A), exact *P* values are listed in Table 2.2.
(C) As in (B), but the fraction of adenosines or uridines in 3′UTRs of mRNAs enriched in the indicated compartments is shown. *P* value categories as in (A), exact *P* values are listed in Table 2.2.
(D) As in (B), but the number of AU-rich elements (AUUUA) in 3′UTRs of mRNAs enriched in the indicated compartments is shown. *P* value categories as in (A), exact *P* values are listed in Table 2.2.
(E) As in (B), but size of mRNA-encoded proteins enriched in the indicated compartments is shown. *P* value categories as in (A), exact *P* values are listed in Table 2.2.
(F) Schematic of the reporter mRNA used with the SunTag system to measure nascent protein synthesis. CDS, coding sequence. The KIF18B construct was used previously (Yan et al., 2016).
(G) Confocal imaging of HeLa cells stably expressing SunTag reporter proteins svFc-GFP and mCherry-tagged PP7 protein (mC-PP7) co-transfected with two constructs (i) BFP-TIS11B to visualize the TGER domain and (ii) SunTag-labeled mRNA encoding KIF18B and PP7-binding sites. The *KIF18B* mRNA is visualized by mC-PP7 binding (teal) whereas the KIF18B protein is visualized by svFc-GFP binding (magenta). Foci with co-localization of mRNA and protein represent nascent protein synthesis and are indicative of active translation. A representative example is shown. White box indicates area depicted at 6X magnification in the lower panel. Scale bar, 5 μm (top panel), 1 μm (bottom panel).
(H) Quantification of the experiment from (G). Shown are the number of mRNA foci in TGER or the cytosol (CY) using the Suntag reporter from (F). *N* = 24 cells were analyzed.
(I) As in (H), but shown are the mRNAs that are actively translated in each compartment, which were identified by counting the teal and magenta-double positive foci.

Figure 2.5 Presence of AU-RBPs promotes mRNA localization to TGER or

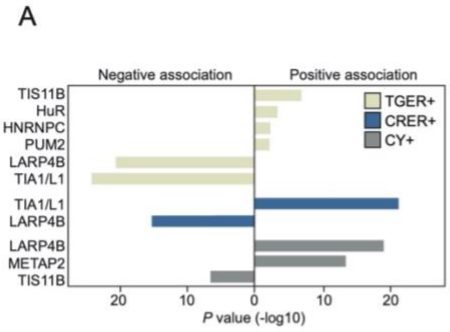

B

	Number of RBP peaks in 3'UTR							Predicted by CLIP	Observed experimentally
Gene name	TIS11B	HuR	PUM2	HNRNPC	TIA1/L1	LARP4B	METAP2		
LHPP	0	0	0	0	0	0	0	CY	CY
PTP4A3	0	0	0	0	0	0	0	CY	CY
MAP2K2	0	0	0	0	0	0	5	CY	CY
MLST8	0	0	0	0	0	6	4	CY	CY
SF3A2	0	0	0	0	0	5	0	CY	CY
FOS	3	0	0	0	0	0	0	TGER	TGER
THAP1	15	2	4	0	0	0	0	TGER	TGER
FBXL3	45	2	4	0	8	0	0	TGER	TGER
HSPA1B	10	0	0	0	49	0	0	CRER	TGER
DNAJB1	21	0	0	0	3	7	0	TGER	TGER
BAG3	11	0	4	0	0	0	0	TGER	TGER
DUSP1	7	0	2	4	32	8	0	CRER	TGER
ALDH18A1	10	0	0	0	16	5	0	CRER	CRER
TES	11	2	5	3	58	7	0	CRER	CRER
IQGAP3	0	0	0	0	4	0	0	CRER	CRER

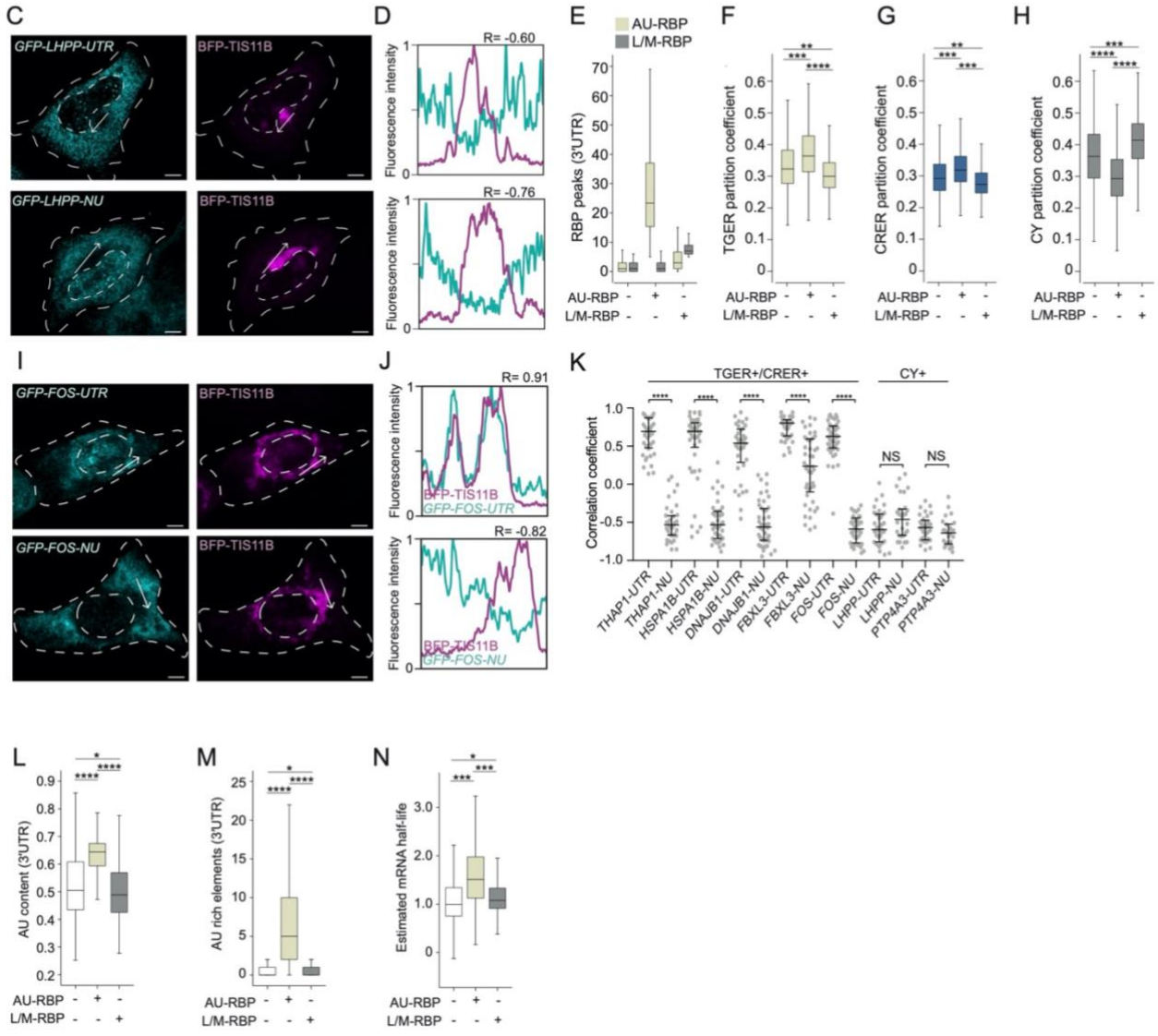

CRER.

Figure 2.5 Presence of AU-RBPs promotes mRNA localization to TGER or CRER.

(A) 3′UTR-bound RBPs that are positively or negatively associated with mRNAs enriched in the three subcytoplasmic compartments. Shown are the -log10 transformed *P* values obtained from logistic regression (see Table 2.2).
(B) Predicted and observed subcytoplasmic mRNA localization for experimentally validated candidates. Shown are the number of RBP CLIP peaks used for localization prediction for each candidate.
(C) RNA-FISH of GFP mRNA after transfection of a GFP-fused LHPP coding region together with the *LHPP 3′UTR* (*LHPP-UTR*) or without the *LHPP 3′UTR* (*LHPP-NU*, no UTR) in HeLa cells (teal). Cotransfection of GFP-TIS11B to visualize TIS granules (magenta). Scale bar, 5 μm.
(D) Line diagrams showing the fluorescence intensities obtained at the position of the arrows from (C). The Pearson's correlation coefficients of the fluorescence intensities are shown.
(E) The number of 3′UTR CLIP peaks is shown for the following mRNA groups: mRNAs not bound by any of the seven RBPs (*N* = 2154), bound by AU-RBPs (*N* = 1695), bound by L/M-RBP (sum of LARP4B and METAP2 CLIP peaks), *N* = 825.
(F) Shown is the fraction of mRNA transcripts that localize to TGER for the groups from (E). Mann Whitney tests were performed. *P* value categories as in Fig. 2.3A, exact *P* values are listed in Table 2.2.
(G) As in (F), but shown is the fraction of mRNA transcripts that localize to CRER for the groups from (E).
(H) As in (F), but shown is the fraction of mRNA transcripts that localize to the cytosol for the groups from (E).
(I) RNA-FISH of GFP mRNA after transfection of a GFP-fused *FOS* coding region together with the *FOS 3′UTR* (*FOS-UTR*) or without the *FOS 3′UTR* (*FOS-NU*, no UTR) in HeLa cells (teal). Cotransfection of GFP-TIS11B to visualize TIS granules (magenta). Scale bar, 5 μm.
(J) Line diagrams showing the fluorescence intensities obtained at the position of the arrows from (I). The Pearson's correlation coefficients of the fluorescence intensities are shown.
(K) As in (J) but shown are the Pearson's correlation coefficients of additional mRNAs expressed from cDNAs either containing or lacking their corresponding 3′UTRs. Corresponding RNA-FISH images are shown in (C) and Fig 2.8. Two line profiles were generated for each cell. Number of cells analyzed, *FOS-UTR N* = 14, *FOS-NU N* = 18, *THAP1-UTR N* = 15, *THAP1-NU N* = 18, *HSPA1B-UTR N* = 18, *HSPA1B-NU N* = 15, *DNAJB1-UTR*
N = 13, DNAJB1-NU *N* = 18, FBXL3-UTR *N* = 12, FBXL3-NU *N* = 16, LHPP-UTR *N* = 16, LHPP-NU *N* = 12, *PTP4A3-UTR N* = 14, *PTP4A3-NU N* = 11. Mann-Whitney test, ****, $P < 0.0001$, NS, not significant; *LHPP: UTR* vs *NU*; $P = 0.1447$; *PTP4A3 UTR* vs *NU*; $P = 0.1126$.
(L) As in (F), but shown is the AU content in 3′UTRs. Mann Whitney test, *P* value categories as in Fig. 2.3A, exact *P* values are listed in Table 2.2.
(M) As in (L), but the number of AU-rich elements in 3′UTRs is shown.
(N) As in (M), but estimated mRNA half-lives are shown.

Figure 2.6 CLIP analysis of RBPs.

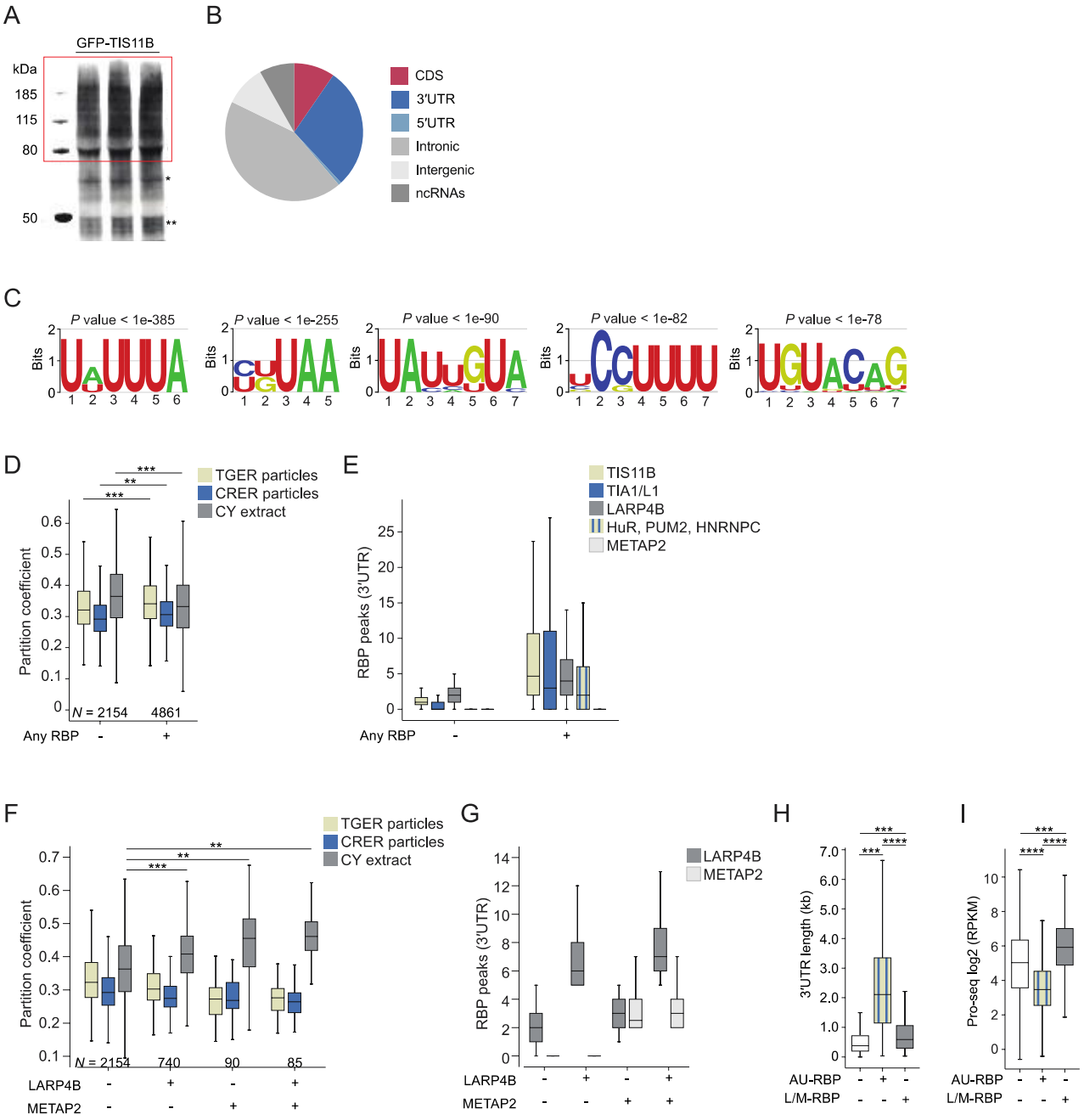

Figure 2.6 CLIP analysis of RBPs.

(A) Gel showing samples used for iCLIP of GFP-tagged TIS11B. The region outlined in red was used for iCLIP sample preparation.
(B) TIS11B iCLIP tag distribution obtained from HEK293T cells.
(C) The top five motifs that were enriched within TIS11B peaks in 3′UTRs compared to all nucleotides in 3′UTRs. Shown are *P* values obtained by HOMER.
(D) Fraction of mRNA transcripts that localize to TGER, CRER, or the cytosol for the indicated groups of mRNAs. mRNAs that are not bound by any of the seven RBPs (no RBP, *N* = 2154) are compared to mRNAs that are targets for at least one of the seven RBPs (RBP, *N* = 4861). Mann Whitney test was performed. *P* value categories as in (A), exact *P* values are listed in Table 2.2.
(E) The number of 3′UTR CLIP peaks is shown for the mRNA groups from (D).
(F) Fraction of mRNA transcripts that localize to TGER, CRER, or the cytosol for the indicated groups of mRNAs. mRNAs that are not bound by any of the seven RBPs (*N* = 2154) are compared to mRNAs that are only bound by LARP4B (*N* = 740), or METAP2 (*N* = 90), or both (*N* = 85). Mann Whitney test was performed. *P* value categories as in (A), exact *P* values are listed in Table 2.2.
(G) The number of CLIP peaks is shown for the mRNA groups from (F).
(H) As in Fig. 3L, but 3′UTR length is shown. Mann Whitney test, *P* value categories as in Fig. 2.3A, exact *P* values are listed in Table 2.2.
(I) As in (H), but Pro-seq values are shown.

Figure 2.7 The ratio of 3′UTR-bound TIS11B over TIA1/L1 differentiates between TGER and CRER.

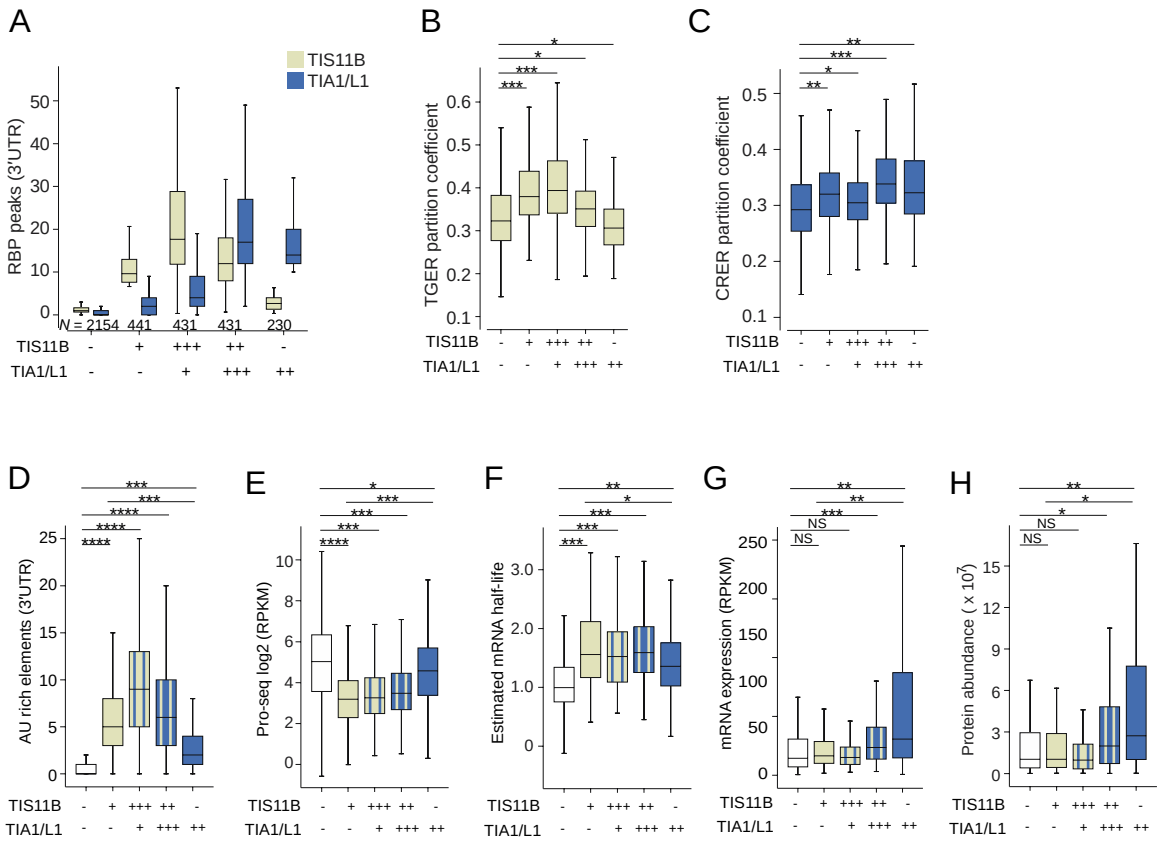

(A) The number of CLIP peaks for subgroups of AU-RBPs is shown. (-/-), no RBP, *N* = 2154; TIS11B only (+/-), N = 441; TIA1/L1 only (-/++), *N* = 230; TIS11B > TIA1/L1 (+++/+), *N* = 431; TIS11B < TIA1/L1 (++/+++), *N* = 431.
(B) Shown is the fraction of mRNA transcripts that localize to TGER for the groups from (A). *P* value categories as in Fig. 2.3A, exact *P* values are listed in Table 2.2.
(C) Shown is the fraction of mRNA transcripts that localize to CRER for the groups from (A). *P* value categories as in Fig. 2.3A, exact *P* values are listed in Table 2.2.
(D) Number of AU-rich elements in 3′UTRs is shown for the groups from (A). *P* value categories as in Fig. 2.5F, exact *P* values are listed in Table 2.2.
(E) As in (D), but shown are Pro-seq levels.
(F) As in (D), but shown are estimated mRNA half-lives.
(G) As in (D), but shown are steady-state mRNA abundance levels obtained from whole cell lysates.
(H) As in (D), but shown are steady-state protein levels obtained from whole cell lysates.

Figure 2.8 mRNA localization to TGER is controlled by 3′UTRs.

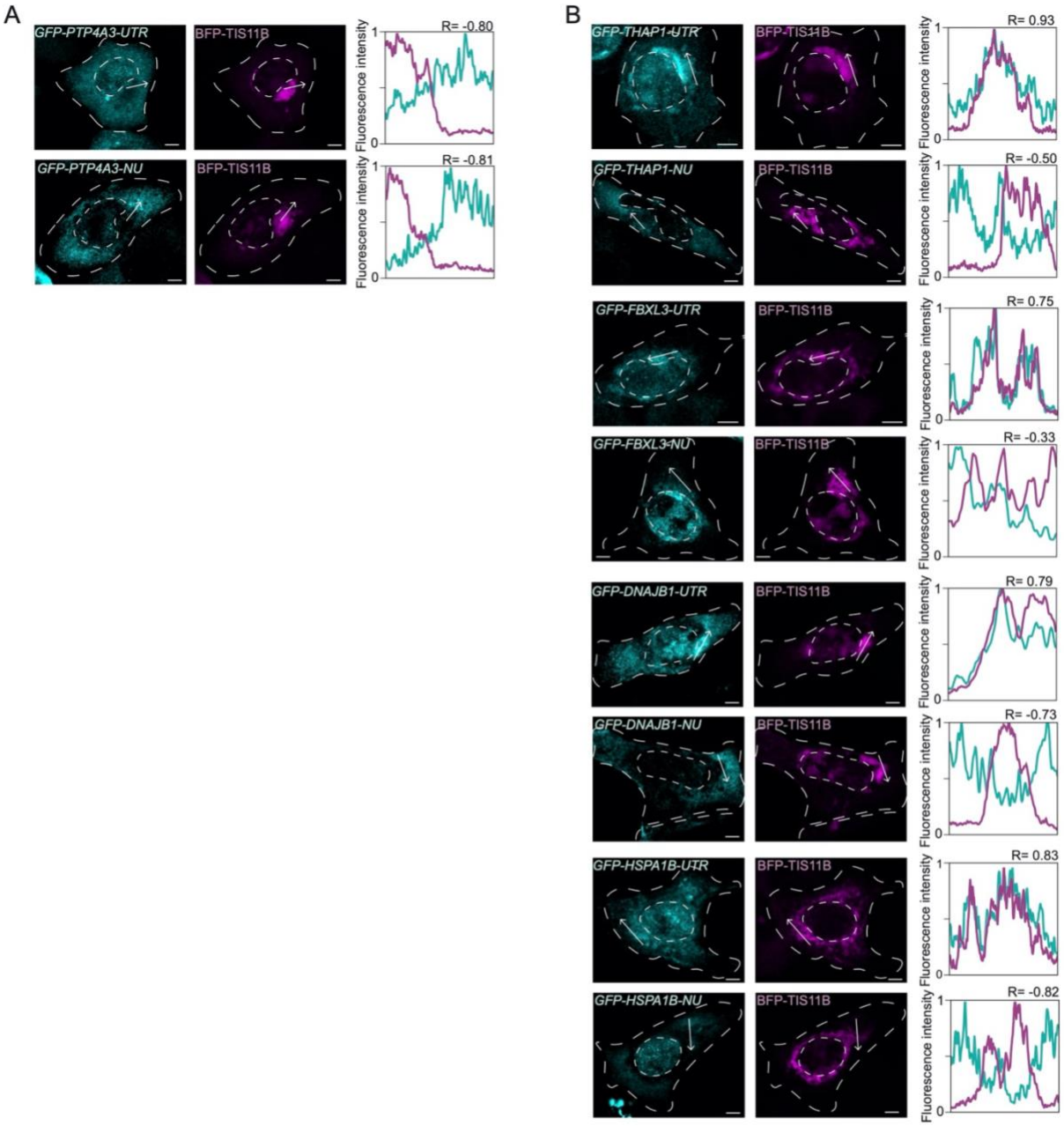

RNA-FISH of mRNAs after transfection of cDNA GFP-fusion constructs containing the indicated coding regions, either including (UTR) or excluding the respective 3'UTRs (NU, no UTR) in HeLa cells (teal). BFP-TIS11B was cotransfected to visualize the TGER domain (magenta). Scale bar, 5 µm. Line diagrams depicting the fluorescence intensities obtained at the position of the arrows are shown with the Pearson's correlation coefficients of the fluorescence intensities. Shown are representative images for cytosol- or TGER-enriched mRNAs.
(A) *PTP4A* does not contain 3'UTR peaks for any of the seven RBPs and is predicted to localize to the cytosol.
(B) *THAP1, FBXL3, DNAJB1,* and *HSPA1B* are predicted to localize to TGER in the presence of their 3'UTRs.

Figure 2.9 TIAL1 dependent mRNA localization to the rough ER increases protein expression.

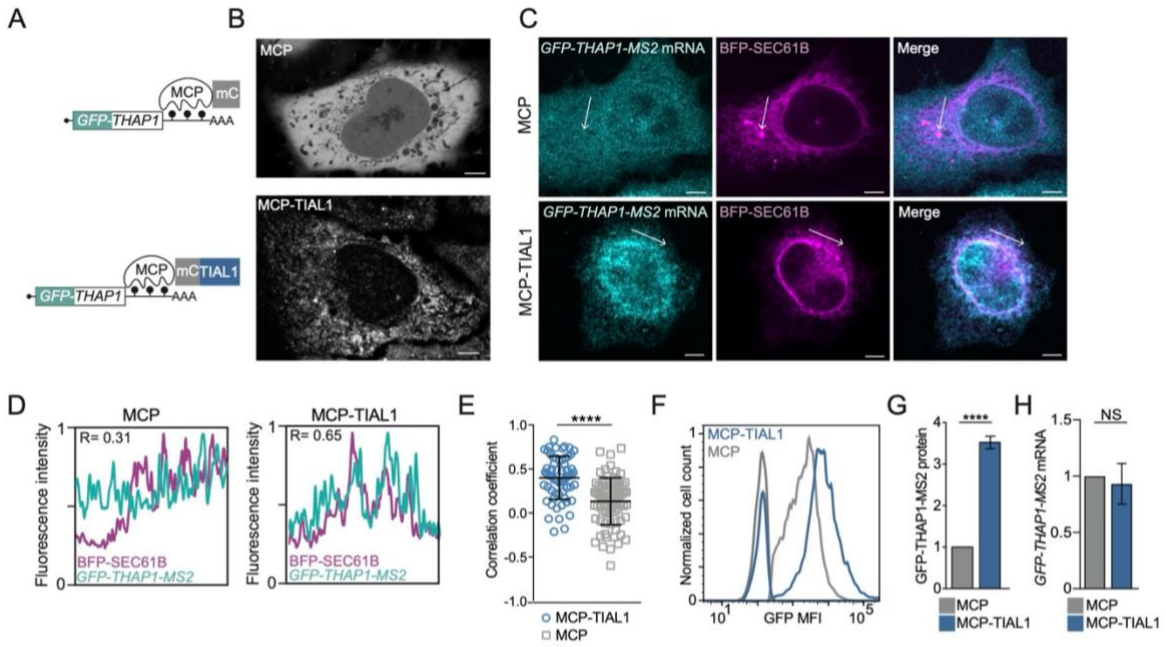

(A) Schematic of the mRNA reporter used to validate the effect of a single 3′UTR-bound RBP on mRNA localization and to investigate the resulting protein expression. The GFP-tagged reporter mRNA contains the THAP1 coding region and MS2 hairpins as a 3′UTR, which allow binding of the cotransfected MS2 coat protein (mCherry-tagged MCP). Fusion of TIAL1 to MCP tethers it to the 3′UTR of the reporter mRNA. mC, mCherry.
(B) Confocal live cell imaging of HeLa cells expressing mC-tagged MCP (top) or mC-tagged MCP-TIAL1 (bottom). Scale bar, 5 µm.
(C) RNA-FISH of the GFP reporter mRNA (teal) from (A) in HeLa cells coexpressing the indicated MCP-fusion construct together with BFP-SEC61B to visualize the rough ER (magenta). Representative confocal images are shown. Scale bar, 5 µm.
(D) Line profiles of the fluorescence intensities obtained from the arrows shown in (C) together with the obtained Pearson's correlation coefficients.
(E) Quantification of the Pearson's correlation coefficients between the GFP reporter mRNA and the rough ER in the experiment shown in (C). Two line profiles were generated for each cell. For MCP, $N = 26$ cells were analyzed and for MCP-TIAL1 $N = 21$ were analyzed. The horizontal line denotes the median and the error bars denote the 25th and 75th percentiles. Mann-Whitney test, ****, $P < 0.0001$.
(F) GFP protein expression of the reporter mRNA in HeLa cells measured by FACS for the samples from (A). Representative histograms are shown. The histograms on the left indicate GFP-negative cell populations.
(G) Quantification of the experiment shown in (F). Shown is the mean ± std of five independent experiments. T-test for independent samples, ****, $P = 0.0003$.
(H) *GFP* reporter mRNA abundance in HeLa cells measured by qRT-PCR for the samples from (A). Shown in the mean ± std of three independent experiments after normalization to *GAPDH*. NS, not significant.

Figure 2.10 CLIP peaks that different between TGER and CRER.

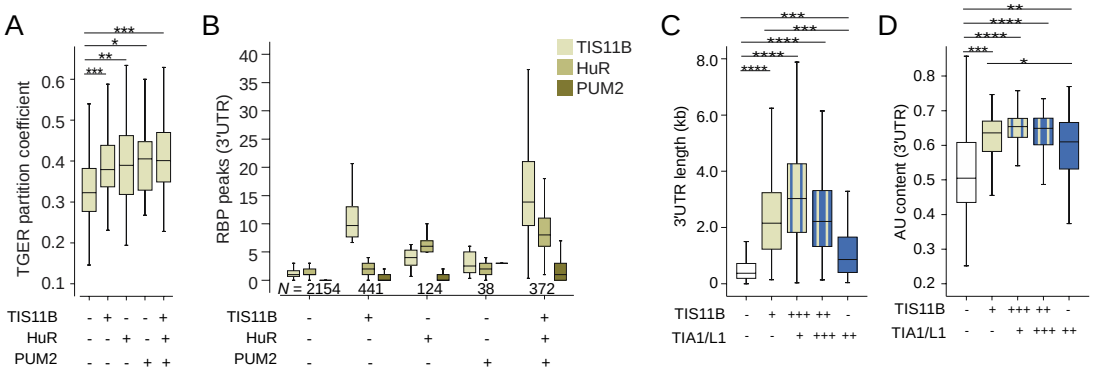

(A) Fraction of mRNA transcripts that localize to TGER for different groups of mRNAs: no RBP, *N* = 2154; TIS11B only, *N* = 441; HuR only, *N* = 124; PUM2 only, *N* = 38; HNRNPC only, *N* = 2 (not shown); any combination of the four RBPs, *N* = 372. Mann Whitney test, *P* value categories as in Fig. 2.3A, exact *P* values are listed in Table 2.2.
(B) The number of CLIP peaks for the groups from (A) are shown.
(C) As in Fig. 2.7D, but 3′UTR length is shown. Mann Whitney test, *P* value categories as in Fig. 2.3A, exact *P* values are listed in Table 2.2.
(D) As in (C), but AU content in the 3′UTR is shown.

Figure 2.11 3′UTR-bound TIAL1 cooperates with the rough ER membrane environment to increase protein expression.

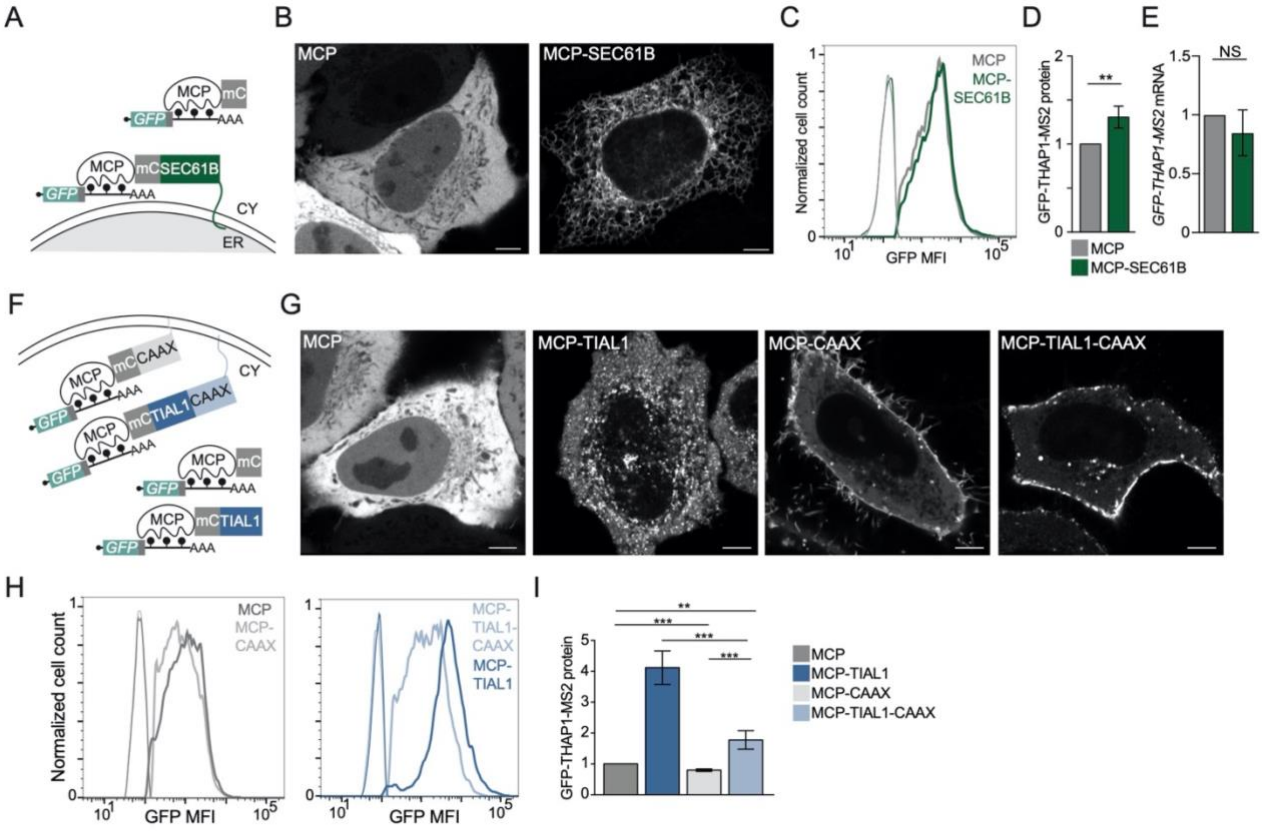

(A) Schematic of a GFP-tagged mRNA reporter that investigates the influence of subcellular mRNA localization on protein expression. Fusion of MCP to SEC61B localizes the GFP reporter mRNA (shown as in Fig. 2.9A) to the rough ER membrane, whereas MCP alone localizes it to the cytosol.
(B) Confocal live cell imaging of HeLa cells expressing mC-tagged MCP (left) or mC-tagged MCP-SEC61B (right). Scale bar, 5 µm.
(C) GFP protein expression of the mRNA reporter measured by FACS in HeLa cells coexpressing the mRNA reporter together with the indicated MCP-fusion constructs. Representative histograms are shown. GFP-negative populations are plotted on the left side.
(D) Quantification of the experiment from (C). Shown is the mean ± std of four independent experiments. T-test for independent samples, **, P =0.0026.
(E) *GFP* reporter mRNA abundance measured by qRT-PCR in HeLa cells co-expressing the mRNA reporter together with the indicated MCP-fusion constructs. Shown in the mean ± std of three independent experiments after normalization to *GAPDH*. NS, not significant
(F) As in Fig. 2.7D, but addition of a prenylation signal (CAAX) localizes the TIAL1-bound GFP reporter mRNA to the plasma membrane. In the absence of CAAX, the TIAL1-bound reporter mRNA localizes to the rough ER.
(G) Confocal live cell imaging of HeLa cells expressing the indicated constructs. Scale bar, 5 µm.
(H) GFP protein expression of the mRNA reporter measured by FACS in HeLa cells coexpressing the mRNA reporter together with the indicated MCP-fusion constructs. Representative histograms are shown. GFP-negative populations are plotted on the left side.
(I) Quantification of the experiment from (G). Shown is the mean ± std of four independent experiments. T-test for independent samples, ****, P < 0.0006, **, P = 0.002.

Figure 2.12 mRNA localization-dependent protein expression of GFP reporter.

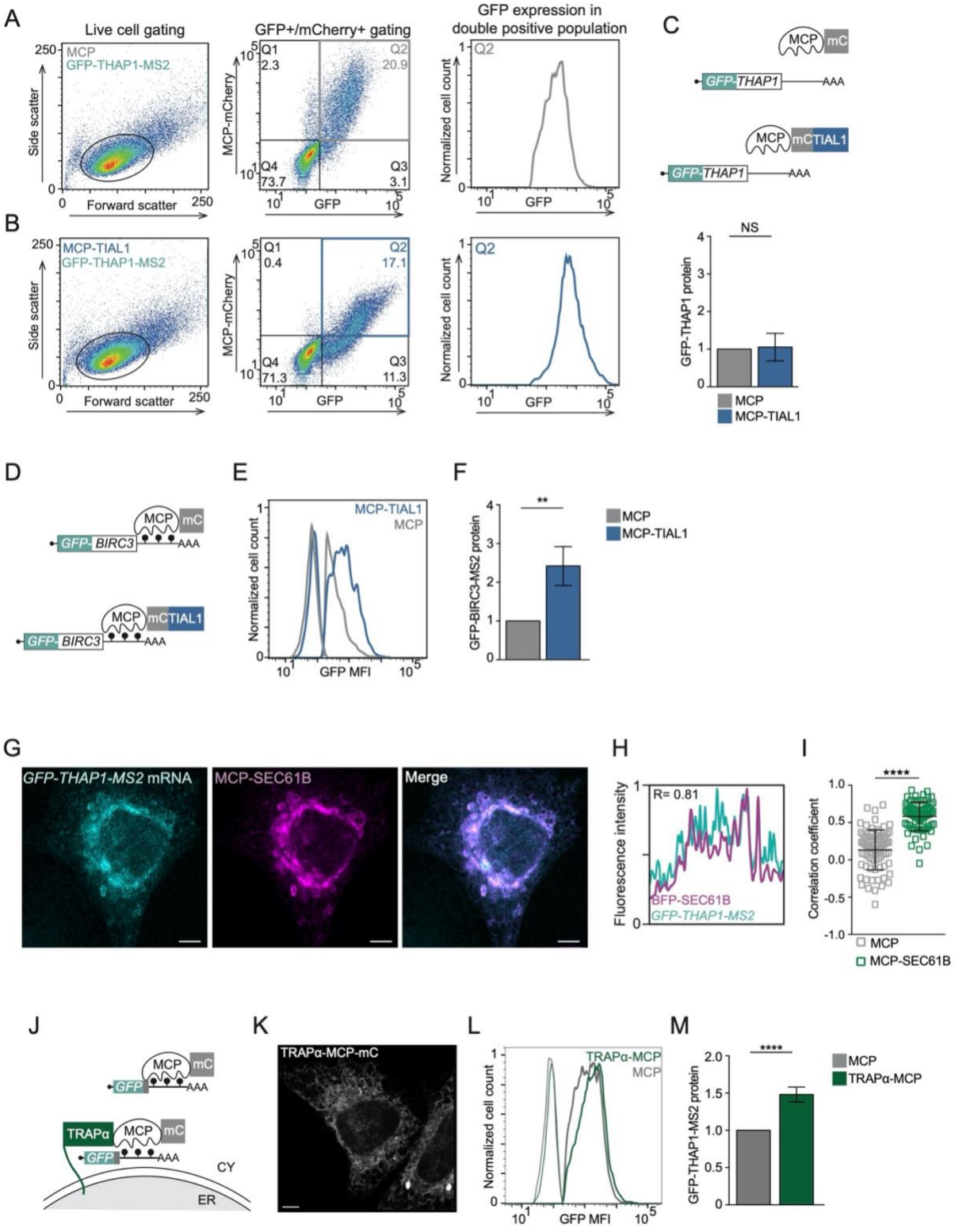

Figure 2.12 mRNA localization-dependent protein expression of GFP reporter.

(A) Gating strategy to assess GFP protein expression of the reporter mRNA by FACS. Left panel shows the ungated population of HeLa cells coexpressing MCP-mCherry and the *GFP-THAP1-MS2* reporter, separated by size (forward scatter) and granularity (side scatter). The black circle indicates the live cells that were used for subsequent analysis. Middle panel, the GFP- and mCherry-double positive population was gated to obtain the GFP mean fluorescence values (MFI, right panel) which corresponds to the reported GFP protein expression values.
(B) As in (A), but HeLa cells coexpressing MCP-mCherry-TIAL1 and the *GFP-THAP1-MS2* reporter.
(C) As in Fig. 2.10A and 2.10G, but the MS2 sites in the GFP reporter were omitted. Coexpression of MCP-mCherry-TIAL1 does not result in the binding of MCP to the reporter mRNA without MS2 sites. This experiment serves as control for the effect of TIA1L1 overexpression on reporter mRNA expression.
(D) Schematic of a second mRNA reporter used to validate the effect of a single 3′UTR-bound RBP on protein expression. The GFP-tagged reporter mRNA contains the BIRC3 coding region and MS2 hairpins as 3′UTR, which allow binding of the co-transfected MS2 coat protein (mCherry-tagged MCP). Fusion of TIAL1 to MCP tethers TIAL1 to the 3′UTR of the reporter mRNA. mC, mCherry.
(E) GFP protein expression of the reporter mRNA from (D) in HeLa cells, coexpressing the indicated MCP-fusion constructs, measured by FACS. Representative histograms are shown. The histograms on the left indicate GFP-negative cell populations.
(F) Quantification of the experiment shown in (E). Shown is the mean ± std of five independent experiments. T-test for independent samples, **, $P = 0.005$.
(G) RNA-FISH of the GFP reporter mRNA (teal) from Fig. 2.11A in HeLa cells coexpressing MCP-mCherry-SEC61B (magenta) to visualize colocalization between the mRNA and the rough ER membrane. Representative confocal images are shown. Scale bar, 5 µm.
(H) Line profiles of the fluorescence intensities of the arrows from (G).
(I) Quantification of the experiment from (G). Two line profiles were generated for each cell. The Pearson's correlation coefficients between the reporter mRNA and the ER were determined. For MCP, $N = 26$ cells were analyzed, for MCP-SEC61B, $N = 26$ cells were analyzed. The horizontal line denotes the median and the error bars denote the 25th and 75th percentiles. Mann-Whitney test, ****, $P < 0.0001$.
(J) Schematic of a second GFP-tagged mRNA reporter that investigates the influence of subcellular mRNA localization on protein expression. Fusion of MCP to TRAPα localizes the GFP reporter mRNA to the ER membrane, whereas MCP alone localizes it to the cytosol.
(K) Confocal live cell imaging of HeLa cells expressing mC-tagged TRAPα-MCP. Scale bar, 5 µm.
(L) GFP protein expression of the reporter mRNAs from (J) coexpressing the indicated MCP-fusion constructs in HeLa cells measured by FACS. Representative histograms are shown. The histograms on the left indicate GFP-negative cell populations.
(M) Quantification of the experiment from (L). Shown is the mean ± std of four independent experiments. T-test for independent samples, ****, $P < 0.0001$.

Figure 2.13 Relocalization of cytosolic mRNAs to the rough ER membrane increases their protein expression.

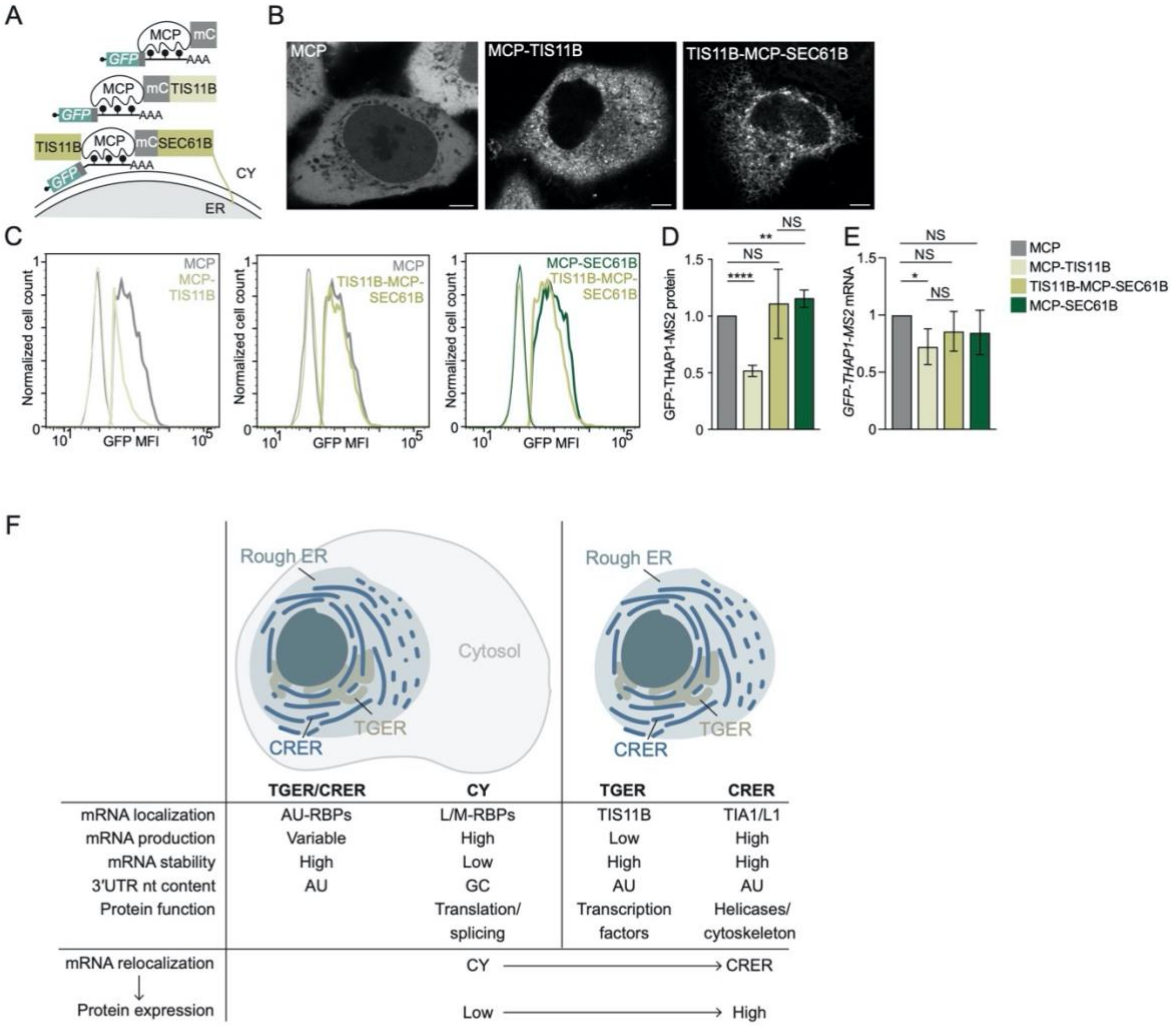

(A) Schematic of a GFP-tagged reporter mRNA bound by TIS11B that allows investigation of localization-dependent GFP protein expression. Fusion of MCP and TIS11B localizes the mRNA reporter to the cytosol, whereas the TIS11B-MCP-SEC61B fusion localizes the mRNA to the rough ER membrane.
(B) Confocal live cell imaging of HeLa cells expressing the indicated constructs (described in A). Scale bar, 5 µm.
(C) GFP protein expression of the mRNA reporter measured by FACS in HeLa cells coexpressing the mRNA reporter together with the indicated MCP-fusion constructs. Representative histograms are shown. GFP-negative populations are plotted on the left side.
(D) Quantification of the experiment from (C). Shown is the mean ± std of four independent experiments. T-test for independent samples, ****, $P < 0.0001$, **, $P = 0.03$, NS, not significant.
(E) *GFP* reporter mRNA abundance measured by qRT-PCR in HeLa cells co-expressing the mRNA reporter together with the indicated MCP-fusion constructs. Shown in the mean ± std of three independent experiments after normalization to *GAPDH*. *, $P = 0.037$, NS, not significant.
(F) Model. Characteristics of subcytoplasmic compartments. Shown are mRNA features of compartment-enriched mRNAs. mRNA relocalization from the cytosol to the ER increased protein expression by two-fold independently of the bound RBPs. nt, nucleotide.

Figure 2.14 Redirecting mRNA localization from the cytosol to the rough ER overcomes the repressive effect of a bound RBP.

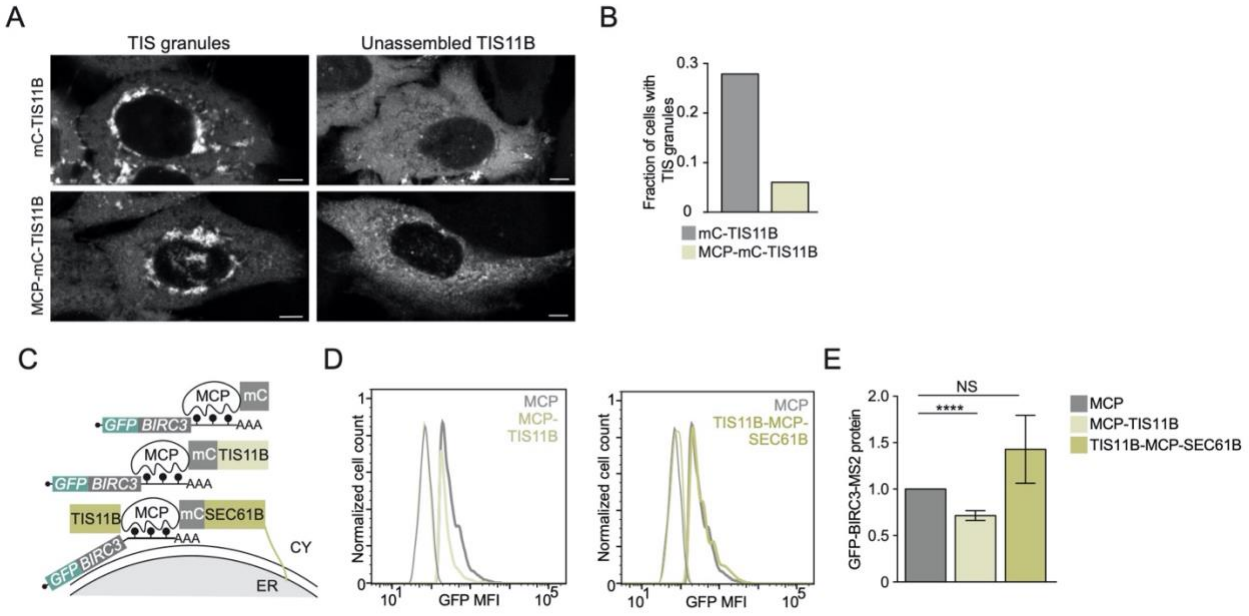

(A) Confocal live cell imaging of HeLa cells expressing the indicated constructs. Shown are representative images with TIS granules or unassembled TIS11B. mC, mCherry. Scale bar, 5 µm.
(B) Quantification from (A). The fraction of HeLa cells with TIS granules is shown after transfection of the indicated TIS11B fusion constructs. *N* = 165 cells were analyzed for mCherry-TIS11B and *N* = 198 cells were analyzed for MCP-mCherry-TIS11B. MCP-mCherry-TIS11B largely prevents TIS granule formation.
(C) Schematic of a second TIS11B-bound mRNA reporter that allows investigation of mRNA localization-dependent GFP expression. The coding region of the reporter is provided by BIRC3, followed by MS2 binding sites. Tethering of MCP or TIS11B localizes the mRNA reporter to the cytosol, whereas the MCP-TIS11B-SEC61B fusion localizes the mRNA reporter to the rough ER.
(D) GFP protein expression of the reporter mRNA from (C) in HeLa cells, coexpressing the indicated MCP-fusion constructs, measured by FACS. Representative histograms are shown. The histograms on the left indicate GFP-negative cell populations.
(E) Quantification of the experiment from (D). Shown is the mean ± std of four independent experiments. T-test for independent samples, ****, $P < 0.0001$, MCP vs TIS11B-SEC61B: $P = 0.058$; NS).

Table 2.1 Characteristics of mRNAs validated by RNA-FISH.

	Partition coefficient		
Genes	**TGER**	**CRER**	**CY**
LHPP	0.14	0.25	0.61
PTP4A3	0.24	0.23	0.53
MAP2K2	0.21	0.21	0.58
MLST8	0.21	0.17	0.62
SF3A2	0.23	0.26	0.51
FOS	0.82	0.15	0.04
THAP1	0.66	0.17	0.17
FBXL3	0.54	0.23	0.23
HSPA1B	0.75	0.19	0.06
DNAJB1	0.77	0.10	0.13
BAG3	0.62	0.22	0.16
DUSP1	0.71	0.16	0.12
ALDH18A1	0.35	0.51	0.14
TES	0.39	0.53	0.08
IQGAP3	0.34	0.54	0.12

Table 2.2. Mann-Whitney statistical test values.

Related to Figure	**Comparison**	***Z* Score**	***P* Value**
2.3A	UB vs TGER	-20.6	5.5E-94
2.3A	UB vs CRER	-0.87	0.39
2.3A	UB vs CY	-5.0	8.9E-40
2.3B	UB vs TGER	-11.6	3.5E-31
2.3B	UB vs CRER	-7.4	1.5E-13
2.3B	UB vs CY	-5.0	5.4E-7
2.3C	UB vs TGER	-10.6	2.5E-26
2.3C	UB vs CRER	-4.3	1.8E-5
2.3C	UB vs CY	-18.0	1.0E-72
2.3D	UB vs TGER	-3.7	2.4E-4
2.3D	UB vs CRER	-5.3	8.5E-8
2.3D	UB vs CY	-8.6	6.1E-18
2.5F	No RBP vs AU-RBP	-15.0	1.1E-50
2.5F	No RBP vs L/M-RBP	-8.7	2.5E-18
2.5F	AU-RBP vs L/M-RBP	-20.1	4.9E-90
2.5G	No RBP vs AU-RBP	-12.8	1.8E-37
2.5G	No RBP vs L/M-RBP	-6.8	1.1E-11
2.5G	AU-RBP vs L/M-RBP	-17.0	1.1E-64
2.5H	No RBP vs AU-RBP	-20.2	5.3E-91
2.5H	No RBP vs L/M-RBP	-11.9	6.7E-33
2.5H	AU-RBP vs L/M-RBP	-26.3	6.9E-153
2.5L	No RBP vs AU-RBP	-28.7	1.0E-181
2.5L	No RBP vs L/M-RBP	-4.3	1.5E-5
2.5L	AU-RBP vs L/M-RBP	-28.2	4.9E-175
2.5M	No RBP vs AU-RBP	-45	0
2.5M	No RBP vs L/M-RBP	-4.4	1.3E-5
2.5M	AU-RBP vs L/M-RBP	-31.2	2.2E-213
2.5N	No RBP vs AU-RBP	-24.6	1.0E-133
2.5N	No RBP vs L/M-RBP	-5.3	1.0E-7
2.5N	AU-RBP vs L/M-RBP	-17.9	6.0E-72
2.7B	No RBP vs TIS11B+	-13.3	2.0E-40
2.7B	No RBP vs TIS11B+++/TIA1-L1+	-15.2	3.7E-52
2.7B	No RBP vs TIS11B++/TIA1-L1+++	-6.2	4.7E-10
2.7B	No RBP vs TIA1-L1++	-3.6	3.2E-4
2.7C	No RBP vs TIS11B+	-7.5	5.5E-14

2.7C	No RBP vs TIS11B+++/TIA1-L1+	-3.8	1.5E-4
2.7C	No RBP vs TIS11B++/TIA1-L1+++	-13.7	1.7E-42
2.7C	No RBP vs TIA1-L1++	-7.8	5.5E-15
2.7D	No RBP vs TIS11B+	-31.1	4.6E-212
2.7D	No RBP vs TIS11B+++/TIA1-L1+	-32.0	5.3E-225
2.7D	No RBP vs TIS11B++/TIA1-L1+++	-30.7	1.3E-207
2.7D	No RBP vs TIA1-L1++	-14.3	1.3E-46
2.7D	TIS11B+/TIA1-L1++	-11.9	8.5E-33
2.7E	No RBP vs TIS11B+	-31.1	4.6E-212
2.7E	No RBP vs TIS11B+++/TIA1-L1+	-15.5	7.3E-54
2.7E	No RBP vs TIS11B++/TIA1-L1+++	-13.4	7.2E-41
2.7E	No RBP vs TIA1-L1++	-2.9	4.3E-3
2.7E	TIS11B+/TIA1-L1++	-9.7	4.0E-22
2.7F	No RBP vs TIS11B+	-17.1	2.0E-65
2.7F	No RBP vs TIS11B+++/TIA1-L1+	-15.2	2.1E-52
2.7F	No RBP vs TIS11B++/TIA1-L1+++	-17.7	7.7E-70
2.7F	No RBP vs TIA1-L1++	-8.3	2.1E-16
2.7F	TIS11B+/TIA1-L1++	-4.5	8.5E-6
2.7G	No RBP vs TIS11B+	-3.1	0.002
2.7G	No RBP vs TIS11B+++/TIA1-L1+	-1.2	0.222
2.7G	No RBP vs TIS11B++/TIA1-L1+++	-9.7	4.2E-22
2.7G	No RBP vs TIA1-L1++	-9.0	2.8E-19
2.7G	TIS11B+/TIA1-L1++	-7.3	2.2E-13
2.7H	No RBP vs TIS11B+	-0.343	0.7
2.7H	No RBP vs TIS11B+++/TIA1-L1+	-2.0	0.043
2.7H	No RBP vs TIS11B++/TIA1-L1+++	-5.8	4.7E-9
2.7H	No RBP vs TIA1-L1++	-6.7	1.9E-11
2.7H	TIS11B+/TIA1-L1++	-5.8	7.4E-9
2.4A	UB vs TGER	-20.6	5.9E-94
2.4A	UB vs CRER	-2.6	0.008
2.4A	UB vs CY	-13.2	1.1E-39
2.4B	UB vs TGER	-2.7	0.007
2.4B	UB vs CRER	-0.193	0.85
2.4B	UB vs CY	-15.2	2.6E-52
2.4C	UB vs TGER	-12.9	4.7E-38
2.4C	UB vs CRER	-6.1	1.4E-9
2.4C	UB vs CY	-20.0	5.3E-89
2.4D	UB vs TGER	-7.3	2.9E-13
2.4D	UB vs CRER	-3.6	3.5E-4

2.4D	UB vs CY	-20.5	2.7E-93
2.4E	UB vs TGER	-2.4	0.016
2.4E	UB vs CRER	-20.3	1.1E-91
2.4E	UB vs CY	-22.2	1.3E-109
2.4D	No RBP vs Any RBP, TGER	-9.4	8.6E-21
2.4D	No RBP vs Any RBP, CRER	-9.0	3.1E-19
2.4D	No RBP vs Any RBP, CY	-12.2	4.4E-34
2.6F	No RBP vs LARP4B	-10.3	5.6E-25
2.6F	No RBP vs METAP2	-6.6	3.0E-11
2.6F	No RBP vs LARP4B/METAP2	-8.3	1.0E-16
2.6H	No RBP vs AU-RBP	-42.0	0
2.6H	No RBP vs L/M-RBP	-10.0	1.8E-23
2.6H	AU-RBP vs L/M-RBP	-27.2	2.9E-162
2.6I	No RBP vs AU-RBP	-21.8	6.2E-105
2.6I	No RBP vs L/M-RBP	-11.7	1.3E-31
2.6I	AU-RBP vs L/M-RBP	-27.3	2.3E-164
2.10A	No RBP vs TIS11B	-13.3	2.0E-40
2.10A	No RBP vs HuR	-6.4	1.8E-10
2.10A	No RBP vs PUM2	-4.8	1.0E-6
2.10A	No RBP vs TIS11B/HuR/PUM2	-15.6	1.4E-54
2.10C	No RBP vs TIS11B+	-28.2	6.7E-175
2.10C	No RBP vs TIS11B+++/TIA1-L1+	-29.2	6.0E-187
2.10C	No RBP vs TIS11B++/TIA1-L1+++	-28.0	8.8E-173
2.10C	No RBP vs TIA1-L1++	-11.1	1.2E-28
2.10C	TIS11B+/TIA1-L1++	-11.2	2.6E-29
2.10D	No RBP vs TIS11B+	-17.9	1.2E-71
2.10D	No RBP vs TIS11B+++/TIA1-L1+	-19.9	4.1E-88
2.10D	No RBP vs TIS11B++/TIA1-L1+++	-19.1	4.2E-81
2.10D	No RBP vs TIA1-L1++	-8.9	8.0E-19
2.10D	TIS11B+/TIA1-L1++	-3.7	1.9E-4

CHAPTER 3: DISCUSSION

Using fluorescent particle sorting and digitonin extraction, we determined differential mRNA localization under steady-state cultivation conditions for TGER, CRER and cytosol. We confirmed that the rough ER membrane is the predominant site of protein synthesis for membrane and secretory proteins as 79% of these mRNAs (*N* = 1688) are strongly enriched there (Fazal *et al.*, 2019; Jan *et al.*, 2014). However, we detected even more mRNAs that encode non-membrane proteins with a biased localization to ER (*N* = 2165), representing 31% of mRNAs encoding non-membrane proteins in our dataset (Fig. 2.1F). Our findings indicate that the ER membrane is a general site of translation for both membrane and non-membrane proteins. We confirm previous reports (Chen *et*

al., 2011; Cui *et al.*, 2012; Diehn *et al.*, 2006; Lerner *et al.*, 2003; Reid and Nicchitta, 2012; Voigt *et al.*, 2017), but we expand substantially the number of mRNAs that encode non-membrane proteins on the rough ER. As this group of mRNAs has not been characterized, we focused our analysis on these mRNAs.

Compartment-specific translation of functionally related genes

We observed that 52% of mRNAs that encode non-membrane proteins have a biased mRNA transcript localization pattern towards a single cytoplasmic compartment. We used RNA-FISH on endogenous and transfected mRNAs to validate the results of our subcytoplasmic mRNA localization dataset and confirmed the predicted mRNA enrichment in their respective compartments (Fig. 2.1, 2.5, and 2.7). One of our most striking findings was that within each cytoplasmic compartment a different group of functionally related mRNAs is translated (Fig. 2.3). Moreover, the compartment-enriched mRNAs are characterized by substantially different production and degradation rates as well as expression levels of their encoded proteins (Fig. 2.3). These features are consistent with the compartment-enriched gene groups, indicating that the cytoplasm is strongly partitioned into different functional and regulatory compartments that are not enclosed by membranes.

For example, we observed that low-abundance proteins are translated in the TGER region. mRNAs encoding zinc finger proteins and transcription factors were substantially enriched (Fig. 2.3E), likely because these gene classes are usually expressed at lower levels than other gene classes (Vaquerizas *et al.*,

2009). Transcription factors may also take advantage of other, so far unknown, features of the TGER environment that may allow for regulation of protein complex assembly. This idea is based on the previous observation that membrane proteins that are translated in the TGER domain are able to establish protein complexes that cannot be formed when the proteins are translated on the ER membrane outside of TIS granules (Ma and Mayr, 2018).

In contrast, mRNAs that are the most stable and encode the most highly expressed proteins are enriched on the CRER and include helicases, cytoskeleton-bound proteins, and chromatin regulators (Fig. 2.3). It was previously shown that global translation is inhibited during stress, including hypoxia, but local translation on the ER is sustained. Active translation of hypoxia-induced genes was accomplished through their increased ER localization during stress (Staudacher et al., 2015). Our findings show that the rough ER membrane is not only a privileged site of protein synthesis during stress, but also promotes high protein expression for a selected group of genes in steady-state cultivation conditions.

It was previously assumed that the majority of non-membrane protein-encoding mRNAs are translated in the cytosol (Fazal *et al.*, 2019; Jan *et al.*, 2014). Although for nearly all mRNAs some transcripts localize to the cytosol, we show that for only ~21% of these mRNAs the majority of transcripts localizes there. The group of mRNAs overrepresented in the cytosol had the highest production and degradation rates (Fig. 2.3). They are enriched in proteins involved in mRNA processing and translation factors, whose abundance levels require tight control.

Taken together, despite not being separated by membranes, we observed strong evidence for the functional compartmentalization of the subcytoplasmic space.

A combinatorial code of 3'UTR-bound RBPs controls subcytoplasmic mRNA localization

According to the RNA regulon hypothesis, functionally related mRNAs are coregulated by specific RBPs that orchestrate the different regulatory steps during their lifetime (Keene, 2007). As compartment-enriched mRNAs differed substantially in their mRNA features, we determined the RBPs responsible for subcytoplasmic localization. In polarized cells, differential mRNA localization has been described between soma and neurites or between apical and basal compartments (Hüttelmaier *et al.*, 2005; Miller et al., 2002; Moor *et al.*, 2017). Although HEK293T cells lack such polarity, we identified a hierarchy in subcytoplasmic mRNA localization. Differential mRNA localization between the perinuclear region, containing the TGER/CRER, and the cytosol was largely determined by the antagonistic effects of 3′UTR-bound AU-RBPs and LARP4B. mRNAs bound by AU-RBPs tend to localize to the perinuclear region, TGER/CRER, whereas lack of AU-RBPs or the presence of LARP4B promotes cytosolic localization (Fig. 2.5E-H).

However, not all mRNAs bound by AU-RBPs behave similarly. TIS11B-bound mRNAs are biased towards TGER, whereas TIA1/L1-bound mRNAs are biased towards the CRER. For mRNAs that are co-bound by both RBPs, the ratio of TIS11B to TIA1/L1 is the best discriminator for biased mRNA localization

between TGER and CRER (Fig. 2.7). Early mRNA localization studies performed in fibroblasts and neurons detected unique localization signals (Chao et al., 2010; Lawrence and Singer, 1986; Miller *et al.*, 2002). Our study did not identify such signals, but instead, we found that 3′UTR-bound RBPs had cumulative effects on mRNA localization. For example, we observed that increasing levels of a 3′UTR-bound RBP enhanced its respective effect on mRNA localization, but when two RBPs with opposing effects were bound to the same mRNA, they neutralized each other's contribution (Fig. 2.7).

TIA1/L1 localizes mRNAs to the CRER and promotes protein expression

We discovered a previously undescribed role for 3′UTR-bound TIA1/L1 in mRNA localization to CRER and identified TIAL1 as a strong positive regulator of mRNA and protein expression (Fig. 2.7G-H). So far, TIA1 and TIAL1 have mostly been described as regulators of pre-mRNA splicing and as translational repressors in the context of cellular stress where they assemble into stress granules (Gilks et al., 2004; Kedersha et al., 1999). However, in the absence of stress, TIA1/L1 has been reported to promote polysome association which supports our findings (Mazan-Mamczarz et al., 2006; Meyer *et al.*, 2018).

We generated a reporter system to investigate mRNA localization-dependent regulation of protein expression. By using this new experimental system, we observed a 3.5 to 4-fold increase in protein expression caused by TIAL1 (Fig. 2.9G, 2.11H). This increase is partially achieved by the intrinsic activity of TIAL1 but the full increase in protein expression was only accomplished through

cooperative action between TIAL1 and the rough ER membrane environment (Fig. 2.11H). Taken together, our data suggest that highly expressed non-membrane proteins take advantage of the translation-promoting environment of the rough ER through recruitment of TIA1/L1. The mechanistic nature of the translation-promoting environment is not yet understood and may be a combination of direct effects on translation and indirect effects, such as protection of TIS11B-bound mRNAs from degradation.

mRNA localization to the rough ER membrane promotes protein expression

Surprisingly, we observed that mRNA localization to the rough ER membrane also promoted protein expression for TIS11B-bound mRNAs. Unassembled TIS11B localizes to the cytosol and was previously found to repress expression of specific mRNAs (Galloway *et al.*, 2016; Lykke-Andersen and Wagner, 2005; Stoecklin *et al.*, 2002). We confirmed this result by showing that cytosolic unassembled TIS11B represses reporter mRNA and protein expression. However, translation of a TIS11B-bound mRNA on the rough ER membrane overrode the intrinsically repressive effects of cytosolic, unassembled TIS11B (Fig. 2.13D).

Taken together with the results obtained from endogenous mRNAs, our findings strongly suggest that the rough ER membrane represents a privileged site for protein expression. Translation of highly abundant mRNAs results in highly expressed proteins. Notably, the TGER seems to ensure that low-abundance mRNAs are effectively translated into low-abundance proteins, effectuating

control over the protein synthesis of a class of proteins strongly enriched in transcription factors.

The mechanism by which the rough ER membrane generates a stimulating environment for protein expression is currently unknown. It was shown previously that mRNAs are bound by more ribosomes when translated on the ER instead of the cytosol (Voigt *et al.*, 2017). Furthermore, ER-resident enzymes may modulate the translation machinery or the 3′UTR-bound RBPs to boost translation (Bertolotti, 2018). We speculate that the environment on the rough ER, which is generated in part by the enriched mRNAs and their bound RBPs, may exclude repressive factors that seem to be active in the cytosol. This idea is supported by our observation that cytosolic mRNAs have the highest degradation rates and that the repressive effects of TIS11B on mRNA expression are mitigated when TIS11B is localized to the ER (Fig. 2.3D, 2.5N and Fig. 2.13E).

In our dataset, cytosolically-enriched mRNAs have a higher GC-content and the lowest mRNA stability values, which is consistent with previous reports showing that GC-rich 3′UTRs are destabilizing, whereas mRNAs with AU-rich 3′UTRs are more stable (Courel *et al.*, 2019; Litterman *et al.*, 2019). There are currently two models that are consistent with the observed data. According to the prevailing model, mRNA stability is regulated by the mRNA-bound RBPs (Gebauer et al., 2021), meaning the RBPs that bind to AU-rich mRNAs would stabilize them. However, our data also support an alternative model that takes into account subcellular localization. In this model, mRNAs with AU-rich 3′UTRs use RBPs to preferentially localize to the rough ER, a region that might be inherently protected

from degradation. This latter model is supported by our reporter experiments. We observed that redirecting mRNAs to the rough ER membrane increased their protein levels independently of 3′UTR sequence, which was kept constant in the relocalization experiments (Fig. 2.11I, 2.13D). For TIS11B-bound reporter mRNAs, increased mRNA stability contributes to the increase in protein expression observed at the ER (Fig. 2.13E). However, mRNA stability was unchanged for reporter mRNAs bound by TIAL1 or SEC61B, suggesting additional ER-specific factors stimulate translation in that environment (Fig. 2.9H, 2.11E).

Our study revealed a surprisingly high degree of cytoplasmic compartmentalization. This is the basis for the translation of functionally related proteins in defined environments that strongly affect mRNA stability and protein expression (Fig. 2.13F). Our results highlight the contribution of spatial regulation whose consequences go beyond the effects mediated by the mRNA-bound proteins. In the future, our findings may provide the basis for biotechnology applications that make use of engineered 3′UTR sequences to boost protein expression in experimental settings or to increase protein production of mRNA vaccines.

Limitations of our study

To obtain sufficient material for TGER and CRER particle sorting, we used transfected, fluorescently labeled proteins instead of endogenous proteins. As TGER and the CRER are tightly associated (Fig. 2.1C), for some mRNAs that

encode membrane proteins, differential mRNA localization to TGER or the CRER could not be resolved. However, despite their tight association, TGER- and CRER-enriched mRNAs that encode non-membrane proteins differed substantially in their functional gene classes and in their mRNA and protein features, suggesting that our purification method was successful.

The RNA-seq experiments in this study did not include ERCC spike-in controls. As such, we can only make conclusions on the relative enrichment of mRNAs in a given subcytoplasmic compartment. Absolute abundance values would be required to make any claims about absolute enrichment. Additionally, the sequencing method used in this study does not provide transcript-level information, therefore we are unable assess the contribution of alternative 3′UTR isoform expression on subcytoplasmic localization of mRNA. For example, it was shown experimentally that alternative 3′UTR isoform usage determines *CD47* mRNA localization but more sophisticated sequencing methods such as 3′-seq (Lianoglou et al., 2013) would be required to address this question on a global scale.

The reporter relocalization experiments showed that RNA-binding proteins influence the subcytoplasmic location of translation. However, this study does not directly assess the role of individual RNA-binding proteins on mRNA localization. In principle this could be achieved by genetic knockdown/knockout of individual RNA-binding proteins and performing mRNA localization analysis. However, our regression analysis suggests that the majority of mRNAs are bound by a combination of RNA-binding proteins and currently it is unclear how the

perturbation of one RNA-binding protein will affect the balance of the rest. While we are very interested in performing these experiments, it is a complex research focus onto its own and therefore outside the scope of the current study.

CHAPTER 4: OUTLOOK AND FUTURE DIRECTIONS

I began my thesis work with the intention to uncover the biological significance of a newly described membraneless organelle, TIS granules. However, the complex biology of TIS11B necessitated a systems-level approach to understanding the function of TIS granules in the broader context of subcytoplasmic compartmentalization and cellular organization. Sequencing the transcriptomes from three cytoplasmic compartments generated an incredibly rich dataset that allowed us to develop of map of distinct regulatory environments generalizable across the entire mRNA transcriptome. I hope that other groups will use this map to guide their own investigations as well as build upon it. There are three highlights in our study that I believe are most compelling for further investigation: functional regulation of TIS granules, the translational environment of the CRER, and the combinatorial RBP code for mRNA localization.

Functional Regulation of TIS granules

All experimental evidence so far supports the hypothesis that TIS granules provide a specific environment to promote protein-protein interactions of lowly expressed proteins. Mechanistic characterization of this environment and how its regulated remain an active research focus in the lab. A simple hypothesis to explain the protein-protein interactions promoted in TIS granules is that two molecules have a higher likelihood of interacting within the confined space of the

granule network than the same two molecules in the cytosol. However, ongoing work in the lab identified an additional and fascinating level of regulation to the protein-protein interactions facilitated within TGER. Postdoctoral researcher Vicky Luo observed that TIS granules are required for the binding of SNIP1 and MYC, and this interaction is both proximity-dependent and mRNA-dependent. NMR experiments demonstrated that upon exposure to TGER-enriched mRNA, MYC protein undergoes a conformational shift exposing SNIP1 binding sites (Luo *et al.*, 2023).This identifies a novel function of mRNA as a molecular chaperone and highlights the unique biomolecular interactions promoted in the TGER environment. mRNA can be considered a TGER client when undergoing translation in the granule and can contribute to the functional environment when acting as a molecular chaperone. With greater understanding of how mRNAs and proteins are targeted to TIS granules as well as how the dual functionality of cytosolic and assembled TIS11B is regulated, we can potentially exploit the unique translational environment for therapeutic purpose.

Translational Environment of the ER

Our results confirm previous observations suggesting the ER membrane is a hub for efficient translation in the cytoplasm (Reid and Nicchitta, 2012; Voigt *et al.*, 2017), but the factors responsible remain unknown. Our reporter experiments show that TIAL1 has some intrinsic ability to promote translation of mRNAs bound by TIAL1 in their 3′UTRs, but its stimulatory effects are mitigated by 50% when TIAL1 is not localized to the ER (Fig. 6I). One hypothesis to explain this

observation is that an ER-resident kinase or phosphatase alters the post-translational modification landscape of TIAL1 to promote its interaction with translation initiation or elongation factors. This is purely speculative but would be interesting to explore experimentally. Further, some of my unpublished experiments suggest that the intrinsically disordered region (IDR) of TIAL1 is critical to its ability to promote translation at the ER. Perhaps IDRs of TIA1/L1 interact with the ER membrane to co-localize membrane-resident translation factors in a confined space. There are many potential applications in biotech for a system that can increase the protein payload of a single mRNA and thus the novel function of TIA family proteins in promoting translation and how this is potentiated at the ER is worth exploring.

The Combinatorial RBP Code

The work described in this thesis takes the first step in describing a hierarchical RBP code for mRNA localization, opening the door to many future studies. One future direction that I find particularly exciting is investigating the dynamic nature of the system. We show that the ratio of TIS11B/TIAL1 bound in the 3′UTR determines whether an mRNA is localized to TGER or CRER in steady-state equilibrium, but it would be interesting to study how the interplay between RBPs changes under different perturbation conditions. For example, we show that mRNAs encoding transcription factor proteins are enriched in TGER. Among

these mRNAs are many so called immediate-early genes. These mRNAs are lowly expressed at steady state but become rapidly transcribed in response to specific stimuli (Karin, 1996). *FOS* and *JUN* are well-characterized immediate-early genes and both exhibit localization bias to TGER at steady state. Do these mRNAs change their localization in response to stimuli? Do they shift into the CRER region to take advantage of the translational environment there? How does the landscape of RBPs bound to these mRNAs change in response to stimuli?

Perhaps the most surprising aspect of the combinatorial code presented in this thesis is that none of the RBPs we identify as significantly deterministic to subcytoplasmic localization were previously characterized as such. Is it possible that mRNA localization is a salient feature of RNA-binding proteins but the previously unknown hierarchy among co-bound molecules has thus far precluded our observation of this? Greater understanding of how RNA-binding proteins function as a system to support subcellular localization will help facilitate therapeutic targeting of RNA-binding proteins in the future.

CHAPTER 5: MATERIALS AND METHODS

Constructs

Fluorescently-tagged TIS11B and SEC61B constructs. The eGFP/mCherry/BFP fusion constructs for TIS11B and SEC61B expression were described previously (Ma and Mayr, 2018). They were generated in the pcDNA3.1-puro expression

vector. The TIS11B and SEC61B coding regions were PCR amplified from HeLa cDNA and inserted downstream of eGFP/mCherry/BFP using BsrGI/EcoRI or BsrGI/HindIII restriction sites, respectively.

Constructs for RNA-FISH. All coding regions were amplified from HeLa cDNA with their respective F and R primers and inserted in-frame, downstream of GFP (GFP lacking a stop codon) between BsrGI and XbaI sites into pcDNA3.1-puro-GFP vector. The corresponding 3′UTRs were amplified from HeLa genomic DNA and inserted downstream of the stop codon into the multiple cloning site using XbaI and ApaI. All primers are listed in Table 5.1.

Constructs to generate the mRNA localization reporter. To investigate the influence of RBPs on mRNA localization of a GFP mRNA reporter, RBPs were fused to MCP and tethered to a GFP mRNA reporter containing MS2 binding sites as 3′UTR (Berkovits and Mayr, 2015; Bertrand *et al.*, 1998). To investigate mRNA localization-dependent protein expression of the GFP mRNA reporter, subcellular localization signals were fused to MCP or to MCP-RBP fusions.

GFP mRNA reporter. To generate the GFP mRNA reporter, the GFP-BIRC3-MS2-SU (Lee and Mayr, 2019) vector was used the BIRC3 coding region was replaced with the THAP1 coding region. It was PCR amplified from the GFP-THAP1 vector using THAP1-MS2 F and THAP1-MS2 R primers and inserted between the BsrGI and AgeI sites. The SU fragment was removed with HindIII and XhoI and blunt end ligated, resulting in GFP-THAP1-MS2.

MCP-mCherry RBP fusion constructs. To generate MCP-mCherry, the MCP coding sequence was PCR amplified from UBC NLS-HA-2XMCP-tagRFPt vector

(Addgene 64541) using MCP F and MCP R primers and inserted in-frame, upstream of mCherry (mCherry lacking a start codon) between BmtI and BamHI sites in pcDNA3.1-puro-mCherry vector (Ma and Mayr, 2018). To generate MCP-mCherry-TIS11B and MCP-mCherry-TIAL1, their coding sequences were inserted in-frame, downstream of mCherry between the BsrGI and XbaI sites. The TIS11B coding sequence was amplified from pcDNA3.1-puro-GFP-TIS11B using TIS11B MCP F and TIS11B MCP R primers and the TIAL1 coding sequence was PCR amplified from pFRT_TO_FlagHA_TIAL1 (Addgene 106090) using TIAL1 MCP F and TIAL1 MCP R primers.

MCP-mCherry fusion constructs with subcellular localization signals. To generate pcDNA3.1-puro-MCP-mCherry-SEC61B, the MCP-mCherry coding sequence was cut from MCP-mCherry vector using BmtI and BsrGI and pasted in-frame, upstream of SEC61B in pcDNA3.1-mCherry-SEC61B (replacing mCherry). To generate the TIS11B-MCP-mCherry-SEC61B vector, TIS11B coding sequence was PCR amplified from pcDNA3.1-puro-GFP-TIS11B using TIS-SEC F and TIS-SEC R primers and pasted in-frame, upstream of MCP into the BmtI site in the MCP-mCherry-SEC61B vector. To generate TRAPα-MCP-mCherry, the TRAPα coding sequence (encoded by the *SSR1* gene) was PCR amplified from HeLa cDNA using TRAPα MCP F and TRAPa MCP R and inserted in-frame, upstream of MCP in the pcDNA3.1-puro-MCP-mCherry vector.

For plasma membrane localization, the CAAX prenylation signal was added to the C-terminus of MCP-mCherry or MCP-mCherry-TIAL1. The CAAX coding sequence was purchased as a gene fragment from Azenta as described (Yan *et*

al., 2016) and PCR amplified using TIAL1 CAAX F and CAAX R primers. It was inserted in-frame using the BsrGI and ApaI sites, located downstream of mCherry to generate pcDNA3.1-puro-MCP-mCherry-CAAX. It was inserted in-frame using EcoNI and ApaI sites to generate MCP-mCherry-TIAL1-CAAX.

SunTag constructs. To generate the SunTag-FOS vector, the FOS coding region was PCR amplified from HeLa cDNA using FOS 2F and FOS 2R primers and inserted between AgeI and BmtI sites in pcDNA4-TO-24xGCN4_v4-KIF18B-24xPP7 vector (Addgene 74928), replacing KIF18B. The FOS 3′UTR was PCR amplified from HeLa genomic DNA using FOS UTR 2F and FOS UTR 2R primers and inserted in EcoRI site downstream of the PP7 region in SunTag-FOS.

Isolation of subcytoplasmic compartments

Transfection. HEK293T cells were seeded in six 10 cm dishes at 80% confluency in antibiotic free media. After 24 hours, cells were transfected by calcium phosphate with either 3 µg mCherry-TIS11B or 3 µg GFP-SEC61B per dish.

Particle purification. 20 hours after transfection, cells were rinsed once with ice-cold PBS, scraped in 10 ml ice-cold PBS, and pelleted at 300 x g. Pellets from two plates were resuspended in 1 ml ice-cold hypotonic isolation buffer (225 mM mannitol, 75 mM sucrose, 20 mM Tris-HCl pH 7.4, 0.1 mM EDTA). Cells were lysed with 50 strokes in a 1 ml dounce-homogenizer with pestle on ice in order to shear the nuclei from the ER. Nuclei were pelleted with a two-minute spin at 600 x g. The supernatant contains the cytoplasmic membrane fraction, which was

pelleted with a 15-minute spin at 7000 x g and resuspended in ice-cold PBS for fluorescent particle sorting.

Fluorescent particle sorting. Particles were sorted on a BD FACSAria III cell sorter equipped with a 70 µm nozzle. The forward-scatter threshold was decreased from 5,000 to 800 in order to visualize subcellular particles. Particles were first detected by fluorescence using the 594 nm and 488 nm excitation lasers, for mCherry-TIS11B and GFP-SEC61B respectively, and 405 nm excitation laser for DAPI. A sorting gate was drawn on particles that were either mCherry-positive or GFP-positive, but DAPI-negative, to exclude any remaining nuclei. Sorting was performed in purity mode with an average speed of 150 particles/second. Particles were sorted directly into 1 ml of TRIzol solution in Eppendorf tubes, holding 180,000 particles per tube. RNA extraction was performed for each tube separately and total RNA for each sample was combined for library preparation. Three biological replicates for each particle prep were sequenced. For each replicate, about 1.5 million TIS11B granule particles and 2.0 million ER particles were collected.

Cytosol extraction. The cytosol was extracted as previously described (Liu and Fagotto, 2011). HEK293T cells were plated in a six-well plate at 80% confluency. After 24 hours, cells were rinsed once in the dish with ice-cold PBS. After aspirating PBS, 300 µl ice-cold digitonin solution (40 µg/ml digitonin, 150 mM NaCl, 20 mM HEPES pH 7.4, 0.2 mM EDTA, 2 mM DTT, 2 mM MgCl2) was added and incubated on a shaker at 4°C for ten minutes. After incubation, the digitonin-derived cytosolic extract was pipetted from the plate and spun at 20,000

x g for one minute to pellet any floating cells. 200 µl of cytosolic extract was added to 1 ml TRIzol solution for RNA extraction.

RNA-seq library preparation

RiboGreen RNA Reagent (ThermoFisher) was used for RNA quantification and quality control was performed by Agilent BioAnalyzer. 50-500 ng of total RNA underwent polyA selection and TruSeq library preparation according to instructions provided by Illumina (TruSeq Stranded mRNA LT Kit, catalog # RS-122-2102), with eight cycles of PCR. Samples were barcoded and run on a HiSeq 4000 in a PE50 run, using the HiSeq 3000/4000 SBS Kit (Illumina). An average of 27 million paired reads was generated per sample.

Western Blotting

For whole cell lysate preparation, cells were trypsinized and washed twice with PBS and lysed in 2x Laemmli Sample buffer (Alfa Aesar, J61337). For cytosolic lysate, cytosol was extracted with digitonin as described above and one volume of 2x Laemmli Sample buffer was added. Laemmli lysates were boiled for 10 min at 95°C. Samples were subjected to SDS-PAGE on NuPAGE 4%–12% Bis-Tris gradient protein gel (Invitrogen). Imaging was captured on the Odyssey DLx imaging system (Li-Cor). The antibodies used are listed in the Key Resources Table.

TIS11B iCLIP

Transfection. HEK293T cells were seeded in 10 cm dishes at 80% confluency in antibiotic free media. After 24 hours, cells were transfected by calcium phosphate with either 3 µg GFP-TIS11B or 1.5 µg GFP-only per dish.

Sample preparation. 20 hours after transfection, cells were rinsed once with ice-cold PBS and 6 ml of fresh PBS was added to each plate before crosslinking. Cells were irradiated once with 150 mJ/cm^2 in a Spectroline UV Crosslinker at 254 nm. Irradiated cells were scraped into Eppendorf tubes, spun at 500 x g for one minute, and snap-frozen. Crosslinked cell pellets were lysed in iCLIP lysis buffer (50 mM Tris-HCl pH 7.4, 100 mM NaCl, 1% Igepal CA-630 (Sigma I8896), 0.1% SDS, 0.5% sodium deoxycholate), sonicated with the Bioruptor Pico for 10 cycles 30 seconds ON/30 seconds OFF, and supplemented with 0.5 U of RNase I per 1 mg/ml lysate for RNA fragmentation. Lysates were pre-cleared by centrifugation at 20,000 x g at 4°C. A mix of Protein A/G Dynabeads (50 µl of each per sample, Life Technologies) were coupled to 10 µg of rabbit anti-GFP antibody (Abcam ab290). TIS11B protein-RNA complexes were immunoprecipitated from 1 ml of crosslinked lysate and washed with high salt and PNK buffer (NEB). RNA was repaired by 3′ dephosphorylation and ligated to L3-IR adaptor on beads (Zarnegar et al., 2016). Excess adaptor was removed by incubation with 5′ deadenylase and the exonuclease RecJf (NEB). TIS11B protein-RNA complexes were eluted from the beads by heating at 70°C for one minute. The complexes were then visualized via the infrared-labeled adaptor, purified with SDS-PAGE, and transferred to nitrocellulose membrane. cDNA was synthesized with Superscript IV Reverse Transcriptase (Life Technologies) and

circularized by CircLigase II. Circularized cDNA was purified with AmPURE bead-based purification (A63880, Beckman Coulter), amplified by PCR and sequenced by Novaseq.

RNA-FISH

Single molecule RNA-FISH for endogenous mRNAs. Probe design. Primary probes were designed using the ProbeDealer package in MATLAB (Hu et al., 2020). Each primary probe contains 30 transcript-targeting nucleotides preceded by 20 common nucleotides that are complementary to the secondary probe. At least 30 probes were designed for each transcript, purchased in a pool from IDT. The secondary probes are 5′ conjugated to AlexaFluor 633 and were purchased from IDT.

Transfection. Prior to cell seeding, 35 mm glass cover slips were sterilized with ethanol then incubated in 1 µg/ml fibronectin in PBS at room temperature for one hour. Cover slips were rinsed in PBS and HeLa cells were seeded at 100,000 per coverslip. 24 hours after seeding, cells were transfected with 500 ng GFP-TIS11B using Lipofectamine 3000 (Invitrogen).

Sample preparation. 20 hours after transfection, cells were rinsed once with PBS then fixed in 4% paraformaldehyde for 10 minutes at room temperature. All steps were performed at room temperature if not otherwise noted. Cells were rinsed twice with PBS and permeabilized with 0.5% Triton-X solution for 10 minutes. Cells were rinsed twice with PBS and incubated for five minutes in pre-hybridization buffer (2xSSC, 50% formamide). Cells were incubated in primary

probe hybridization solution (40 µM primary probe, 2xSSC, 50% formamide, 10% dextran sulfate (Sigma), 200 µg/ml yeast tRNA (Sigma), 1:100 Murine RNase Inhibitor (NEB)), for at least 15 hours at 37°C. To remove excess or unbound primary probes, cells were then rinsed twice in 2xSSC + 0.1% Tween for 15 minutes at 60°C then once more for 15 minutes at room temperature. Cells were incubated in secondary probe solution (4 nM secondary probe, 2xSSC, 50% ethylene carbonate, 1:100 Murine RNase Inhibitor) for 30 minutes in the dark. Secondary probes were rinsed twice in 50% ethylene carbonate, 2xSSC solution for five minutes then mounted with Prolong Diamond mounting solution (Invitrogen). For both endogenous and GFP-fusion constructs, RNA-FISH images were captured using confocal ZEISS LSM 880 with Airyscan super-resolution mode.

Cytosol extraction. To visualize and validate cytosolic versus ER-associated endogenous mRNAs, HeLa cells were seeded as described above, then incubated in 2 ml digitonin solution described above (40 µg/ml digitonin, 150 mM NaCl, 20 mM HEPES pH 7.4, 0.2 mM EDTA, 2 mM DTT, 2 mM MgCl2) for 10 min at 4°C. Digitonin solution was removed, coverslips were rinsed with 2 ml PBS, and RNA-FISH was performed as described above.

Line profile analysis. To quantify colocalization of two fluorescence signals (mRNA vs TGER or mRNA vs ER), line profiles were generated with FIJI (ImageJ). For each cell, 2-4 straight lines were drawn to cross TGER (or the ER) in different directions, indicated by the white arrows shown in the figures. Fluorescence signal along the straight line of TGER (or ER) and the examined

mRNA was calculated for each channel using the plot profile tool in FIJI. The values of the Pearson's correlation coefficient r were calculated using Excel. Perfect correlation of protein-mRNA is indicated by r = 1, perfect exclusion is indicated by r = -1, and random distribution is indicated by r = 0.

Enrichment analysis of endogenous mRNAs. Enrichment of endogenous mRNAs in TGER was determined using FIJI. The total area of the cell and the total area occupied by TIS granules was calculated for each cell. A mask was created from the GFP-TIS11B signal and the mask area was divided by the total cell area to generate the granule area fraction. The total number of transcripts per cell (number of foci) was quantified. This value was multiplied by the granule area fraction to yield the number of transcripts expected to be present in TIS granules by chance. The observed number of transcripts in the TIS granule area was then divided by the expected value to obtain the enrichment fold-change. The fold-change values were log2-transformed. An enrichment score of 0 indicates 'no enrichment' and is observed when the observed and expected numbers of transcripts in TIS granules are the same. A positive enrichment score indicates that there are more transcripts localized to TIS granules than one would expect by chance and a negative enrichment score indicates fewer transcripts in TIS granules than one would expect by chance.

RNA-FISH after transfection of constructs. RNA-FISH experiments probing for GFP-fusion constructs were performed as described previously (Ma and Mayr, 2018). Stellaris FISH probes for eGFP with Quasar 670 Dye were used.

Confocal microscopy

Confocal imaging was performed using ZEISS LSM 880 with Airyscan super-resolution mode. A Plan-Apochromat 63x/1.4 Oil objective (Zeiss) was used. For live cell imaging, cells were incubated with a LiveCell imaging chamber (Zeiss) at 37°C and 5% CO2 and imaged in cell culture media. Excitations were performed sequentially using 405, 488, 594 or 633 nm laser wavelength and imaging conditions were experimentally optimized to minimize bleed-through. Images were prepared with FIJI (ImageJ) software.

TMT mass spectrometry

To obtain protein expression levels, TMT mass spectrometry analysis was performed on HEK293T cells cultivated in steady-state conditions. Cells were trypsinized and washed three times with ice-cold PBS. Pelleted cells were snap-frozen in liquid nitrogen. Cell pellets were lysed with 200 µl buffer containing 8 M urea and 200 mM EPPS (pH at 8.5) with protease inhibitor (Roche) and phosphatase inhibitor cocktails 2 and 3 (Sigma). Benzonase (Millipore) was added to a concentration of 50 µg/ml and incubated at room temperature for 15 min followed by water bath sonication. Samples were centrifuged at 14,000 g at 4°C for 10 min, and supernatant extracted. The Pierce bicinchoninic acid (BCA) protein concentration assay was used to determine protein concentration. Protein disulfide bonds were reduced with 5 mM tris (2-carboxyethyl) phosphine at room temperature for 15 min, and alkylated with 10 mM iodoacetamide at room temperature for 30 min in the dark. The reaction was quenched with 10 mM

dithiothreitol at room temperature for 15 min. Aliquots of 100 µg were taken for each sample and diluted to 100 µl with lysis buffer. Samples were subject to chloroform/methanol precipitation as previously described (Navarrete-Perea et al., 2018). Pellets were reconstituted in 200 mM EPPS buffer and digested with Lys-C (1:50 enzyme-to-protein ratio) and trypsin (1:50 enzyme-to-protein ratio), and digested at 37°C overnight.

Peptides were TMT-labeled as described (Navarrete-Perea *et al.*, 2018). Briefly, peptides were TMT-tagged by the addition of anhydrous ACN and TMTPro reagents (16plex) for each respective sample and incubated for 1 hour at room temperature. A ratio check was performed by taking a 1 µl aliquot from each sample and desalted by StageTip method (Rappsilber et al., 2007). TMT tags were then quenched with hydroxylamine to a final concentration of 0.3% for 15 min at room temperature. Samples were pooled 1:1 based on the ratio check and vacuum-centrifuged to dryness. Dried peptides were reconstituted in 1 ml of 3% ACN/1% TFA, desalted using a 100 mg tC18 SepPak (Waters), and vacuum-centrifuged overnight.

Peptides were centrifuged to dryness and reconstituted in 1 ml of 1% ACN/25mM ABC. Peptides were fractionated into 48 fractions. Briefly, an Ultimate 3000 HPLC (Dionex) coupled to an Ultimate 3000 Fraction Collector using a Waters XBridge BEH130 C18 column (3.5 um 4.6 x 250 mm) was operated at 1 ml/min. Buffer A, B, and C consisted of 100% water, 100% ACN, and 25mM ABC, respectively. The fractionation gradient operated as follows: 1% B to 5% B in 1 min, 5% B to 35% B in 61 min, 35% B to 60% B in 5 min, 60% B to 70% B in 3

min, 70% B to 1% B in 10 min, with 10% C the entire gradient to maintain pH. The 48 fractions were then concatenated to 12 fractions, (i.e. fractions 1, 13, 25, 37 were pooled, followed by fractions 2, 14, 26, 38, etc.) so that every 12th fraction was used to pool. Pooled fractions were vacuum-centrifuged and then reconstituted in 1% ACN/0.1% FA for LC-MS/MS.

Fractions were analyzed by LC-MS/MS using a NanoAcquity (Waters) with a 50 cm (inner diameter 75 µm) EASY-Spray Column (PepMap RSLC, C18, 2 µm, 100 Å) heated to 60°C coupled to an Orbitrap Eclipse Tribrid Mass Spectrometer (Thermo Fisher Scientific). Peptides were separated by direct injection at a flow rate of 300 nl/min using a gradient of 5 to 30% acetonitrile (0.1% FA) in water (0.1% FA) over 3 hours and then to 50% ACN in 30 min and analyzed by SPS-MS3. MS1 scans were acquired over a range of m/z 375-1500, 120K resolution, AGC target (standard), and maximum IT of 50 ms. MS2 scans were acquired on MS1 scans of charge 2-7 using isolation of 0.5 m/z, collision-induced dissociation with activation of 32%, turbo scan, and max IT of 120 ms. MS3 scans were acquired using specific precursor selection (SPS) of 10 isolation notches, m/z range 110-1000, 50K resolution, AGC target (custom, 200%), HCD activation of 65%, max IT of 150 ms, and dynamic exclusion of 60 s.

Visualization of translation in TGER

The SunTag system was used to visualize mRNA translation in the cytosol and the TGER domain. Stable expression of td-PP7-3xmCherry (Addgene 74926) and scFv-GCN4-sfGFP (Addgene 60907) was achieved by generating virus in

HEK293T cells and transducing HeLa cells. Cells were seeded on 3.5 cm glass bottom dishes (Cellvis, D35-20-1-N). 20 hours later, cells were transfected with either the SunTag vector expressing KIF18B (Addgene 74928) or SunTag-FOS-UTR. At 15 hours post transfection, cells were treated with 100 ng/ml doxycycline for one hour to induce SunTag expression. Confocal imaging was performed as described above. Colocalization of puncta was quantified using FIJI.

mRNA localization-dependent GFP protein expression

Transfection. HeLa cells were seeded in 12-well plates at 80% confluency and transfected with 250 ng GFP-THAP1-MS2 and 250 ng of the MCP-mCherry fusion constructs indicated in the figure (Lipofectamine 3000, Invitrogen). When indicated, GFP-THAP1 or GFP-BIRC3-MS2-SU was used instead of GFP-THAP1-MS2. At 13-15 hours post transfection, cells were analyzed by FACS. For RNA-FISH experiments, cells were seeded at 80% confluency in 4-well slide chambers (Millipore Sigma) and cotransfected with 75 ng GFP-THAP1-MS2, 100 ng BFP-SEC61B, and 75 ng of the indicated MCP-mCherry fusion constructs.

FACS analysis to measure GFP protein expression. Cells were trypsinized, washed once in complete media, then resuspended in FACS buffer (PBS plus 1% FCS). At least 5,000 cells were measured on a BD LSR-Fortessa Cell Analyzer and FACS data were analyzed using FlowJo software. GFP protein expression corresponds to GFP mean fluorescence intensity (MFI). To determine the effect of MCP-tethered RBPs on protein output of the GFP reporter mRNA, only cells that were successfully cotransfected with both the MCP-mCherry

fusion and the GFP reporter constructs were analyzed. To do so, the double-positive cells (mCherry+/GFP+) were gated, and all single positive and unstained cells were excluded from the analysis. The reported GFP MFI was calculated from the double-positive cells. Untransfected cells were used to draw the gates for mCherry+ or GFP+ cells.

qPCR analysis to measure *GFP* mRNA abundance. Cells were trypsinized, washed once in complete media, then resuspended in FACS buffer (PBS plus 1% FCS). To determine the effect of MCP-tethered RBPs on GFP reporter mRNA stability, cells were sorted based on expression of both the MCP-mCherry fusion and the GFP reporter constructs. The BD FACSAria III cell sorter was used to collect 50,000 cells from each co-transfected population. Cells were sorted directly into 1 mL of TRIzol solution in Eppendorf tubes for total RNA was extraction. cDNA synthesis was performed on 200ng of RNA per sample using the SuperScript IV VILO ezDNase Master Mix (Invitrogen). ezDNase enzyme was included to eliminate plasmid DNA contamination. To measure the relative expression levels of reporter mRNA by qRT-PCR, FastStart Universal SYBR Green Master Mix (ROX) from Roche was used together with GFP-qPCR F/R primers. GAPDH was used as a housekeeping gene.

RNA-seq of subcytoplasmic fractions

RNA-seq. Raw reads were processed by trimmomatic (version: 0.39) to trim low-quality ends (average quality per base < 15, 4 bp window) and adapters (Bolger et al., 2014). Trimmed reads were mapped to the human genome (hg19) using

hisat2 (version: 2.1.0) (Kim et al., 2019). Reads mapped to each gene were counted using featureCounts (version: 1.6.4) (Liao et al., 2014). RPKM values for each gene were calculated using a custom Perl script. The mean RPKM values of all biological replicates were calculated and used for downstream analyses. Only protein-coding genes were analyzed. A gene is considered expressed if the RPKM value is 3 or greater. The RPKM values of the biological replicates correlated strongly (Fig. 2.2E).

Classification of membrane/secretory proteins versus non-membrane proteins. Information on the presence of transmembrane domains or a signal sequence was obtained from uniprot. All expressed genes were separated into mRNAs that encode membrane/secretory proteins or non-membrane proteins. If a protein contains a signal sequence but not a transmembrane domain, it is considered as secretory protein. All proteins with transmembrane domains are considered membrane proteins and all remaining proteins are classified as non-membrane proteins. Among the 9155 mRNAs expressed in HEK293T cells, 2140 were classified as membrane/secretory proteins, whereas 7015 were classified as non-membrane proteins (Table 1).

Compartment-specific partition coefficients. The sum of RPKM values obtained from TGER particles, CRER particles, and the cytosol was considered as total cytoplasmic mRNA expression. For each gene, the fraction of transcripts that localize to each of the three compartments was calculated by dividing its compartment-specific RPKM value by the total cytoplasmic mRNA expression

(Fig. S1F). The compartment-specific partition coefficient of a gene is the fraction of mRNA transcripts that localize to the compartment.

Compartment-specific enrichment of mRNAs that encode membrane/secretory proteins. We considered an mRNA to be CRER-enriched if the ratio of partition coefficients (CRER/TGER) was greater than 1.25 and classified it as TGER-enriched if it was smaller than 0.8. The median partition coefficient of membrane/secretory mRNAs in the cytosol was 0.09. If the cytosolic partition coefficient of an mRNA was greater than 0.36, it was considered enriched in the cytosol. If the CRER and TGER-specific partition coefficients were similar and the cytosolic partition coefficient was smaller than 0.18, the mRNA was assigned to the CRER, whereas it was considered not localized if the cytosolic partition coefficient was smaller than 0.18 (Fig. 2.2G).

Compartment-specific enrichment of mRNAs that encode non-membrane proteins. For all mRNAs that encode non-membrane proteins, the medians of the partition coefficients for each compartment were calculated. For TGER particles the median was 0.32, for CRER particles, it was 0.30 and for the cytosol, the median was 0.34. An mRNA was considered to have a biased localization to a specific compartment if its compartment-specific partition coefficient exceeded 1.25-fold of the median partition coefficient of the compartment. For example, the minimum partition coefficient for TGER-enriched mRNAs was 0.42, it was 0.38 for CRER-enriched mRNAs, and 0.43 for CY-biased mRNAs. If the enrichment was observed in two compartments, the mRNA was assigned to the compartment with the higher value. This strategy resulted in 1246 mRNAs

considered to be TGER-enriched, 919 mRNAs to be ER-enriched, and 1481 mRNAs to be enriched in the cytosol. The remaining 3369 mRNAs (48%) do not have a compartment-biased mRNA localization pattern and were called (unbiased, UB).

mRNA and protein features of the localized mRNAs

RPKM values of mRNAs were obtained from RNA-seq data of unfractionated HEK293T cells and were determined for the compartment-biased mRNAs. Pro-seq and RNA-seq from HEK293 cells were obtained from GEO (GSE140365: PRO-seq; GSE142895: RNA-seq) (Patel *et al.*, 2020). Raw reads were processed by trimmomatic (version: 0.39) to trim low-quality ends (average quality per base < 15, 4 bp window) and adapters (Bolger *et al.*, 2014). Trimmed reads were mapped to the human genome (hg19) using hisat2 (version: 2.1.0) (Kim *et al.*, 2019). Reads mapped to each gene were counted by featureCounts (version: 1.6.4) (Liao *et al.*, 2014). To estimate mRNA stability rates, log2-normalized counts of Pro-seq data were divided by the log2-normalized RNA-seq data, as described previously (Blumberg *et al.*, 2021). 3′UTR length of each mRNA was obtained from Ref-seq. The longest 3′UTR isoform of each gene is reported. AU-content in 3′UTRs is the sum of all adenosines and uridines in annotated 3′UTRs divided by the total number of nucleotides in 3′UTRs. The number of AUUUAs (AU-rich elements) in 3′UTRs were counted. Protein length was obtained from Uniprot.

Protein expression

Protein expression was obtained from TMT-based quantitative mass spectrometry analysis of unfractionated HEK293T cells. Precursor protein abundance was calculated for each protein and scaled to the TMT abundance for each channel. Relative abundance was then calculated by averaging biological replicates.

CLIP data analysis

iCLIP analysis of TIS11B in HEK293T cells. Raw fastq files were demultiplexed using the iCount python package (https://icount.readthedocs.io). 5′ and 3′ adapters were trimmed by Cutadapt (Martin, 2011). Trimmed reads were mapped to human genome using STAR and reads mapping to tRNA/rRNA were discarded (Dobin et al., 2013). Crosslink sites were called from bam files using the “xlsites” function of iCount. CLIP-seq analysis was carried out on the iMaps platform (https://imaps.genialis.com/iclip), where peak calling was performed by analysing cDNA counts at crosslink sites using Paraclu (Frith et al., 2008). Motif analysis was carried out using HOMER software. Enrichment was calculated within the genomic coordinates of a total of 57,714 TIS11B CLIP peaks found in 3′UTRs. Total peaks: 190,920; peaks in 3′UTRs: 57,714.

POSTAR3 CLIP data. CLIP data on 168 RBPs were downloaded from Postar3 (Zhao *et al.*, 2021) and peak counts that overlapped with annotated 3′UTRs from Ref-seq in all mRNAs that encode non-membrane proteins were recorded. For each RBP, the median number of 3′UTRs CLIP peaks was calculated and all

3′UTRs with peaks counts greater than the median were considered as targets. Based on the fraction of mRNAs that are considered compartment-specific (TG: 17.8%; ER 13.1%; CY: 21.1%; unbiased: 48.0%), we determined the expected number of target genes for each compartment. If the observed number of targets divided by the expected number of targets in a compartment was greater than 1.5, the RBP was added to our short-list (Table S4). As TIS11B and TIA1/L1 are known to bind to AU-rich sequences, we added the processed PAR-CLIP data of the LARP4B RBP as it was reported to bind to AU-rich elements (Küspert *et al.*, 2015).

Logistic regression. The R package `nnet` (v7.3-17) was used to fit a logistic regression model using the CLIP peak counts from the RBPs on the short list (N = 25) to predict the subcytoplasmic mRNA localization of non-membrane proteins. Covariates with missing values were imputed as zeros. All covariates were first `sqrt` transformed and then standardized. The 'not localized' category was used as the base level. The R package `broom` (v0.8.0) was used to compute t-test statistics for the model coefficients. The code is available on github (github.com/Mayrlab/tiger-seq).

Confirmation of the logistic regression. To validate the contribution of each individual RBP, we used more stringent criteria to determine their targets. Among all mRNAs that encode non-membrane proteins with at least one CLIP peak in the 3′UTR, we considered the top third of mRNAs as targets of each RBP (TIS11B: 1781 targets; TIA1/L1: 1313 targets; LARP4B: 1621 targets; METAP2: 256 targets; HuR: 1124 targets; PUM2: 427 targets; HNRNPC: 232 targets).

Intersection of membrane/secretory mRNAs with previous datasets

The mRNAs that are coexpressed in our RNA-seq dataset (*N* = 9155 mRNAs) and the ER membrane-localized mRNAs from the APEX-seq dataset (*N* = 1045) were determined (Fazal *et al.*, 2019). The overlapping 845 mRNAs were intersected with the mRNAs that encode membrane/secretory proteins found to be enriched on the ER in our analysis (*N* = 1476). We detected 673 mRNAs which correspond to 80% of all APEX-seq mRNAs that are considered to be ER membrane-enriched. The universe used to test for enrichment were all mRNAs that encode non-membrane proteins (*N* = 2140). A similar analysis was performed for the fractionation dataset from Reid (2012) (Reid and Nicchitta, 2012). Among the 385 coexpressed mRNAs that are enriched on the ER according to Reid, we detected 308 in our ER-enriched fraction when focusing on membrane/secretory protein encoding mRNAs. This group represents 80% of all ER-enriched mRNAs detected by Reid.

Gene ontology analysis

Gene ontology (GO) analysis was performed using DAVID (Huang da *et al.*, 2009).

Further statistical analysis

Statistical parameters are reported in the figures and figure legends, including the definitions and exact values of *N* and experimental measures (mean ± std or boxplots depicting median, 25th and 75th percentile (boxes) and 5% and 95% confidence intervals (error bars). Pair-wise transcriptomic feature comparisons were performed using a two-sided Mann-Whitney test. For transcriptomic analyses, statistical significance is indicated by asterisks *, $1 \times 10^{-3} > P > 1 \times 10^{-9}$; **, $1 \times 10^{-10} > P > 1 \times 10^{-20}$; ***, $1 \times 10^{-21} > P > 1 \times 10^{-80}$; ****, $1 \times 10^{-81} > P > 0$. Enrichment was determined using a X^2 test. The *P* value was calculated using a two-sided Fisher's exact test. When indicated, a two-sided t-test with assumption of equal variance was applied. Statistical significance for experimental data is indicated by asterisks *, $P < 0.05$, **, $P < 0.01$, ***, $P < 0.001$, ****, $P < 0.0001$.

Data and code availability

The mass spectrometry data are reported in Table S1. The RNA-seq samples obtained from the subcytoplasmic fractionation and the TIS11B iCLIP data obtained from HEK293T cells are available at GEO (Accession number: GSE215770). The code for logistic regression is available on github.

Table 5.1 Sequences of oligonucleotides used in this study.

Sequences of primers for PCR	
FOS F	5´-CAGTTGTACAAGATGTTCTCGGGCTTCAAC-3´
FOS R	5´-TATATCTAGATCACAGGGCCAGCAGCGT-3´
FOS UTR F	5´-TATATCTAGAGGGCAGGGAAGGGGAGGCA-3´
FOS UTR R	5´-CGCGTCTAGATCGCATTCAACTTAAATGCT-3´
THAP1 F	5´-TAATTGTACAGTGCAGTCCTGCTCCGCC-3´
THAP1 R	5´-ACTGTCTAGATTATGCTGGTACTTCAACTA-3´

THAP1 UTR F	5´-CAGTTCTAGAAAAAATGAAATGTGTATTGA-3´
THAP1 UTR R	5´-TAATGGGCCCTGCCATTGTTTCACACCT-3´
DNAJB1 F	5´-CAGTTGTACAGGTAAAGACTACTACCAG-3´
DNAJB1 R	5´-ACTGTCTAGACTATATTGGAAGAACCTG-3´
DNAJB1 UTR F	5´-CAGTTCTAGACTATCTGAGCTCCCCAAG-3´
DNAJB1 UTR R	5´-ACTGTCTAGATGAGGTTTAGCATCAGTC-3´
HSPA1B F	5´-TAATTGTACAGCCAAAGCCGCGGCGATC-3´
HSPA1B R	5´-ACTGTCTAGACTAATCCACCTCCTCAATGG-3´
HSPA1B UTR F	5´-CATCTCTAGAGGGCCTTTGTTCTTTAGTAT-3´
HSPA1B UTR R	5´-CGTGGGGCCCAAAGTTTAACATTTTATT-3´
FBXL3 F	5´-CAGTTGTACAAAACGAGGAGGAAGAGATAG-3´
FBXL3 R	5´-TAATTCTAGATTACCAAGTGGGCATCATGT-3´
FBXL3 UTR F	5´-CAGTTCTAGAAAACTGCATGATGAATAGCA-3´
FBXL3 UTR R	5´-AATTGGGCCCAGCATTAGTAACTTTTTATT-3´
LHPP F	5´-TATATGTACAGCACCGTGGGGCAAGC-3´
LHPP R	5´-TATATCTAGATCACTTGTCGGCGTGCTG-3´
LHPP UTR F	5´-TATATCTAGATGGCCTCCTGGGAGAGCC-3´
LHPP UTR R	5´-TATGTCTAGATGCTGGTCAAGGCAGAGT-3´
PTP4A3 F	5´-TATATGTACAGCTCGGATGAACCGCCCG-3´
PTP4A3 R	5´-TATATCTAGACTACATAACGCAGCACCGGG-3´
PTP4A3 UTR F	5´-TAATTCTAGAGCTCAGGACCTTGGCTGGG-3´
PTP4A3 UTR R	5´-GACGTCTAGATTCACCCAACATGCATTGG-3´
THAP1 MS2 F	5´-ATATTGTACAAGGTGCAGTCCTGCTCCG-3´
THAP1 MS2 R	5´-CAGTACCGGTTTATGCTGGTACTTCAACTA-3´
MCP F	5´-CAGTGCTAGCATGGCTTCTAACTTTACTCA-3´
MCP R	5´-TATAGGATCCGTAGATGCCGGAGTTTGCTG-3´
TIS11B MCP F	5´-ATATGTACAAGACCACCACCCTCGTGT-3´
TIS11B MCP R	5´-CAGGTCTAGATTAGTCATCTGAGATGGAAA-3´
TIA1 MCP F	5´-TATATGTACAAGGAGGACGAGATGCCCAAG-3´

TIA1 MCP R	5´-CAGTTCTAGATCACTGGGTTTCATACCCTG-3´
TIAL1 MCP F	5´-TATATGTACAAGATGGAAGACGACGGGCAG-3´
TIAL1 MCP R	5´-GCGATCTAGATCACTGTGTTTGGTAACTTG-3´
TIS-SEC F	5´-TAATGCTAGCATGACCACCACCCTCGTGTC-3´
TIS-SEC R	5´-CAGTGCTAGCGTCATCTGAGATGGAAAGTC-3´
TRAPA MCP F	5´-TAATGCTAGCATGAGACTCCTCCCCCGCTT-3´
TRAPA MCP R	5´-CAGTGCTAGCCTCATCAGATCCCACTGATC-3´
TIAL1 CAAX F	5´-AGGTCCTCCCCAAGGACAAGCTCCTCC-3´
TIAL1 CAAX R	5´-CCTAGGGCCCTTACATGATAACACACTTGG-3´
CAAX F	5´-CAGTCTGTACAAGATGGGTGGAGGTTCTGG-3´
FOS 2F	5´-TATTACCGGTCAATGTTCTCGGGCTTCAAC-3´
FOS 2R	5´-TATAGCTAGCTCACAGGGCCAGCAGCGT-3´
FOS UTR 2F	5´-TTAAGAATTCGGGGCAGGGAAGGGGAGG-3´
FOS UTR 2R	5´-CCGCGAATTCTCGCATTCAACTTAAATGCT-3´
Sequences of RNA-FISH oligos	**5´- -3´**
2_BAG3 -_Seq_2	GGGATGTATTGAAGGAGGATGTCGCGGTCACCGTTGCCGGACGCCACCTG
4_BAG3 -_Seq_4	GGGATGTATTGAAGGAGGATTGTGGTCCACGAAGAAGGGCCAGCCGGTCT
5_BAG3 -_Seq_5	GGGATGTATTGAAGGAGGATGCGGGTCGTTCCACGTAGTGGTGCGGCTGT
7_BAG3 -_Seq_7	GGGATGTATTGAAGGAGGATCCTCCCGGGAAGGGCCATTGGCAGAGGAT
8_BAG3 -_Seq_8	GGGATGTATTGAAGGAGGATGGCCTTCCCTAGCAGGCGGCAGCCTAGAGC
10_BAG3 -_Seq_10	GGGATGTATTGAAGGAGGATCGCCTTCATGGAGCACAGGAATGGGAATGT
11_BAG3 -_Seq_11	GGGATGTATTGAAGGAGGATCATGGAAAGGGTGCACCTGCCGGTTCTCAG
13_BAG3 -_Seq_13	GGGATGTATTGAAGGAGGATTCTGAGGAGCCGCTGCTGCCGCCTCAGTTC
14_BAG3 -_Seq_14	GGGATGTATTGAAGGAGGATTCTGGCATGCCCCGCAGAGGTGACTGGGAC
16_BAG3 -_Seq_16	GGGATGTATTGAAGGAGGATGGCTGGGGGCTGGGCTGCCGCCGCCGCTGC

17_BAG3 - _Seq_17	GGGATGTATTGAAGGAGGATTGGAGACTGGGACCGCTCAG GTCCGTGGGA
19_BAG3 - _Seq_19	GGGATGTATTGAAGGAGGATGCTCCTGCCGGAGGAAGGC AGGCTGGCCGA
20_BAG3 - _Seq_20	GGGATGTATTGAAGGAGGATCCCCCGCGGGAGCTGGTGA CTGCCCAGGCT
22_BAG3 - _Seq_22	GGGATGTATTGAAGGAGGATTGGTGGAAGGAGGGCTGGG CTGCTGGCCGG
23_BAG3 - _Seq_23	GGGATGTATTGAAGGAGGATTGCTGCGCTGGGTAGTGCGT CTTCTGGGCT
25_BAG3 - _Seq_25	GGGATGTATTGAAGGAGGATGGCTCCCAGTCATCCCCCTG GATCTTGTGG
26_BAG3 - _Seq_26	GGGATGTATTGAAGGAGGATGACCTGAACGGGGATGCCG CCCGCAGGGGC
28_BAG3 - _Seq_28	GGGATGTATTGAAGGAGGATTGGAGTGGCGTGCTGCTCCT GGCTGGTGAG
29_BAG3 - _Seq_29	GGGATGTATTGAAGGAGGATACGGTGTGCACACGGATGGG CGAGGGGGAG
31_BAG3 - _Seq_31	GGGATGTATTGAAGGAGGATTCAGGCTGGGAAACAGGTGC AGTTTCTCGA
32_BAG3 - _Seq_32	GGGATGTATTGAAGGAGGATACTGGGCCTGGCTTACTTTC TGGTTTGTTT
34_BAG3 - _Seq_34	GGGATGTATTGAAGGAGGATGAATCCACCTCTTTGCGGAT CACTTGAATT
35_BAG3 - _Seq_35	GGGATGTATTGAAGGAGGATGGAGGTGGGGGCTTCTGGG AAACAGGTTTA
37_BAG3 - _Seq_37	GGGATGTATTGAAGGAGGATGGGCTGGGAGGAGGACAAG GAACTGGAGCA
39_BAG3 - _Seq_39	GGGATGTATTGAAGGAGGATGGGGCTGCCCTCTCTTCTGT AGCCACACTC
40_BAG3 - _Seq_40	GGGATGTATTGAAGGAGGATGGAGGTGTAGCTTCTGCAGG GGCAGTGCTG
42_BAG3 - _Seq_42	GGGATGTATTGAAGGAGGATATGGCTTCCACTTTCAGCACT CCTGGATGT
43_BAG3 - _Seq_43	GGGATGTATTGAAGGAGGATGCCTGCTCCAGCCCCTGTAC CTTCTCCAGG
45_BAG3 - _Seq_45	GGGATGTATTGAAGGAGGATAAATACTCTTCGATCATCAGG TACTTTTTG
46_BAG3 - _Seq_46	GGGATGTATTGAAGGAGGATACTGAATCCAGGGCCAGCAG CTCTTTGGTC
48_BAG3 - _Seq_48	GGGATGTATTGAAGGAGGATTGAACCTTCCTGACACCGTC TCTCCTGGCC
49_BAG3 - _Seq_49	GGGATGTATTGAAGGAGGATGCTTTCTGTTCAAGTTTTTCC AAGATGGTC
51_BAG3 - _Seq_51	GGGATGTATTGAAGGAGGATTCTGCTTCAAGGTTGCTGGG CTGGAGTTCA

52_BAG3 - _Seq_52	GGGATGTATTGAAGGAGGATCCCATCTCCATGATTGCCTG CAGTGGCTGA
54_BAG3 - _Seq_54	GGGATGTATTGAAGGAGGATTCTGTGTGGGGATCTTCTGC ATTTCCAGCA
55_BAG3 - _Seq_55	GGGATGTATTGAAGGAGGATGCTGCTGCTGTGGCTTCTGG CTGCTGGGTT
57_BAG3 - _Seq_57	GGGATGTATTGAAGGAGGATAGAGGCTACGGTGCTGCTGG GTTACCAGGG
58_BAG3 - _Seq_58	GGGATGTATTGAAGGAGGATCATCGGTTCCGAGTCTGATTT TTACAGGGC
60_BAG3 - _Seq_60	GGGATGTATTGAAGGAGGATTAAAAACCAACTGACTTAAAG TCTCTGAAA
61_BAG3 - _Seq_61	GGGATGTATTGAAGGAGGATCACCCAAGTTACTGCATACC AAGCAGCTAA
63_BAG3 - _Seq_63	GGGATGTATTGAAGGAGGATCAGAGTAAGAATATAGAAGA AAAGCATCAT
64_BAG3 - _Seq_64	GGGATGTATTGAAGGAGGATCTCAAACAACAAGCAACTTCT TTATTTGTA
66_BAG3 - _Seq_66	GGGATGTATTGAAGGAGGATAGGTGGTGGGGGTGCCCAA GTAGACAGGGC
67_BAG3 - _Seq_67	GGGATGTATTGAAGGAGGATTACAAAAGACAGTGCACAAC CACAGCTAAC
69_BAG3 - _Seq_69	GGGATGTATTGAAGGAGGATCTGATAAATGTTTCATATTTAT GTGATGGG
70_BAG3 - _Seq_70	GGGATGTATTGAAGGAGGATGAAGAAAATCATCTCATTAAA ATGGCAACA
72_BAG3 - _Seq_72	GGGATGTATTGAAGGAGGATATATTCCTATGGCTCCTGGCA CATTTTACT
73_BAG3 - _Seq_73	GGGATGTATTGAAGGAGGATAATGTAGCATTAAAGTCATCC AACATACAG
2_DUSP1 - _Seq_2	GGGATGTATTGAAGGAGGATTCGCTCCCCCAGCAGCGCCC GCAGGCCTCC
3_DUSP1 - _Seq_3	GGGATGTATTGAAGGAGGATGCGGCAGTCCAGCAGCAGG CATTGCGCCGC
4_DUSP1 - _Seq_4	GGGATGTATTGAAGGAGGATGATGTGGCCGGCGTTGAAAG CGAAGAAGGA
5_DUSP1 - _Seq_5	GGGATGTATTGAAGGAGGATGGTGCTGAAGCGCACGTTGA CAGAGCCGGC
6_DUSP1 - _Seq_6	GGGATGTATTGAAGGAGGATCTCCAGGCCCATGGCGCCCT TGGCCCGGCG
7_DUSP1 - _Seq_7	GGGATGTATTGAAGGAGGATCAGCAACACCACGGCGTGGT AGGCGCCGGC
8_DUSP1 - _Seq_8	GGGATGTATTGAAGGAGGATCCAGGGTGCCGTCGCGCTTG GCGCCGTCCA
9_DUSP1 - _Seq_9	GGGATGTATTGAAGGAGGATTTGAGGAAGAAGACTTGCGC GGCGCGCGCC

10_DUSP1 - _Seq_10	GGGATGTATTGAAGGAGGATCAGGAAGCCGAAAACGCTTC GTATCCTCCT
11_DUSP1 - _Seq_11	GGGATGTATTGAAGGAGGATGGGGGTCGACTGTTTGCTGC ACAGCTCCGG
12_DUSP1 - _Seq_12	GGGATGTATTGAAGGAGGATGCTAGTACTCAGGGGAAGGC TGAGCCCCAT
13_DUSP1 - _Seq_13	GGGATGTATTGAAGGAGGATACTGCACCCAGATTCCGCGC TGTCAGGGAC
15_DUSP1 - _Seq_15	GGGATGTATTGAAGGAGGATGTACAGAAAGGGCAGGATTT CCACCGGGCC
16_DUSP1 - _Seq_16	GGGATGTATTGAAGGAGGATCTTGCGGGAAGCGTGATACG CACTGCCCAG
17_DUSP1 - _Seq_17	GGGATGTATTGAAGGAGGATGGCAGTGATGCCCAAGGCAT CCAGCATGTC
18_DUSP1 - _Seq_18	GGGATGTATTGAAGGAGGATGTTGGGACAATTGGCTGAGA CGTTGATCAA
19_DUSP1 - _Seq_19	GGGATGTATTGAAGGAGGATGCTCTTGTACTGGTAGTGAC CCTCAAAATG
20_DUSP1 - _Seq_20	GGGATGTATTGAAGGAGGATGTCTGCCTTGTGGTTGTCCT CCACAGGGAT
21_DUSP1 - _Seq_21	GGGATGTATTGAAGGAGGATGTCAATGGCCTCGTTGAACC AGGAGCTGAT
22_DUSP1 - _Seq_22	GGGATGTATTGAAGGAGGATTCCTCCAGCATTCTTGATGGA GTCTATGAA
23_DUSP1 - _Seq_23	GGGATGTATTGAAGGAGGATAATGCCTGCCTGGCAGTGGA CAAACACCCT
24_DUSP1 - _Seq_24	GGGATGTATTGAAGGAGGATGTAAGCAAGGCAGATGGTGG CTGACCGGGA
25_DUSP1 - _Seq_25	GGGATGTATTGAAGGAGGATGTCCAGCTTGACTCGATTAG TCCTCATAAG
26_DUSP1 - _Seq_26	GGGATGTATTGAAGGAGGATTCGCCTCTGCTTCACAAACTC AAAGGCCTC
28_DUSP1 - _Seq_28	GGGATGTATTGAAGGAGGATCACCTGGGACTCAAACTGCA GCAGCTGGCC
29_DUSP1 - _Seq_29	GGGATGTATTGAAGGAGGATCCCAGCCTCTGCCGAACAGT GCGGAGCCAG
30_DUSP1 - _Seq_30	GGGATGTATTGAAGGAGGATGAGGTGCCTCGGTCGAGCAC AGCCATGGCG
31_DUSP1 - _Seq_31	GGGATGTATTGAAGGAGGATGAGACGGGGAAGTTGAACAC GGTGGTGGTG
32_DUSP1 - _Seq_32	GGGATGTATTGAAGGAGGATAGCGCACTGTTCGTGGAGTG GACAGGGATG
33_DUSP1 - _Seq_33	GGGATGTATTGAAGGAGGATGAGGTCGTAATGGGGCTCTG AAGGTAGCTC
34_DUSP1 - _Seq_34	GGGATGTATTGAAGGAGGATTCACCTCCCGTGGCCTTTCA GCAGCTGGGA

35_DUSP1 - _Seq_35	GGGATGTATTGAAGGAGGATGCATGGAGTCCCAATGGGAT GTGAAGAGCC
36_DUSP1 - _Seq_36	GGGATGTATTGAAGGAGGATCCAGAGTTATTGCATTTCTCC TCTCAAGGA
37_DUSP1 - _Seq_37	GGGATGTATTGAAGGAGGATTAAATAAGGACCAGCCCTCT CGAGCCCCTC
38_DUSP1 - _Seq_38	GGGATGTATTGAAGGAGGATGAAACCCAGAGGAACTCGGG TGAAGTTAAA
39_DUSP1 - _Seq_39	GGGATGTATTGAAGGAGGATTTGACGCTAAGTCATCACCAT AACTGCTTA
41_DUSP1 - _Seq_41	GGGATGTATTGAAGGAGGATAGATGGACTTGATGTACCCA CTATATATTG
42_DUSP1 - _Seq_42	GGGATGTATTGAAGGAGGATTGAGTCCTTTCTCTTCTGCCC CATTTTGTC
43_DUSP1 - _Seq_43	GGGATGTATTGAAGGAGGATGGGCGAGCAAAAAGAAACCG GATCACACAC
44_DUSP1 - _Seq_44	GGGATGTATTGAAGGAGGATTATGTCAAGCATGAAGAGATT CTACAAAAA
45_DUSP1 - _Seq_45	GGGATGTATTGAAGGAGGATATATGTGTCGTCGGGAATAAT ACTGGTAGG
46_DUSP1 - _Seq_46	GGGATGTATTGAAGGAGGATCAGACACCTACACAAAAATAA ATAAGGTAT
47_DUSP1 - _Seq_47	GGGATGTATTGAAGGAGGATTCTAGGAGTAGACAATGACA TTTGTGAAGG
48_DUSP1 - _Seq_48	GGGATGTATTGAAGGAGGATCTCAAAAACAAAAATTGAGGT ATTTGGTTC
49_DUSP1 - _Seq_49	GGGATGTATTGAAGGAGGATGCTTAAGATATATTTACAGGA TAGTACAGT
50_DUSP1 - _Seq_50	GGGATGTATTGAAGGAGGATGTATTTTCCATCAGTGCTGAA AACAAACCT
51_DUSP1 - _Seq_51	GGGATGTATTGAAGGAGGATAGCAAACATACAACTGTTGG CAACTAAAAA
52_DUSP1 - _Seq_52	GGGATGTATTGAAGGAGGATCCTTATGTAACAAAATGTCTT CTTAGAAGA
1_SF3A2 - _Seq_1	GGGATGTATTGAAGGAGGATCTTGCCCCCGGGGCGATGCT GGAAGTCCAT
2_SF3A2 - _Seq_2	GGGATGTATTGAAGGAGGATGGAGGAGGAGGCCACGCCC CCGCTCCCGGT
3_SF3A2 - _Seq_3	GGGATGTATTGAAGGAGGATGAGGCGCTCCCTGCGGTCAC GGTTGCTCTC
4_SF3A2 - _Seq_5	GGGATGTATTGAAGGAGGATGTGGTTCTTCATGAAGTACG GGTCCTTGTT
5_SF3A2 - _Seq_6	GGGATGTATTGAAGGAGGATCAGGCAGAGTTTGCATTCAT AGGAGCCCAG
6_SF3A2 - _Seq_7	GGGATGTATTGAAGGAGGATCAGGTAGCTCCCCTCATTGT TGTGAAGTGT

7_SF3A2 - _Seq_8	GGGATGTATTGAAGGAGGATGGTCTGGTGCTTCTTCCCCT GCGTATGTGC
8_SF3A2 - _Seq_9	GGGATGTATTGAAGGAGGATGGCCTCCTTGGCTGCTCGCC GGGCCAGGTT
9_SF3A2 - _Seq_10	GGGATGTATTGAAGGAGGATTGACCTTCTCAGGCGCGGGC TGGGCAGGGG
10_SF3A2 - _Seq_11	GGGATGTATTGAAGGAGGATCGATCTTCACAAACTTCTTCA CCTCCACCT
11_SF3A2 - _Seq_12	GGGATGTATTGAAGGAGGATTCTGCTTGGTCACTTTGTAGC CCGGGCGGC
12_SF3A2 - _Seq_13	GGGATGTATTGAAGGAGGATGGAGGCTCTGCTGGCCCATC TCCGAGTCTC
13_SF3A2 - _Seq_14	GGGATGTATTGAAGGAGGATCGGCGATCTCAGGGTAGTCA ATCTGGAAGA
14_SF3A2 - _Seq_15	GGGATGTATTGAAGGAGGATACATGAAGCGGTGACGTGGC ATGATGCCCT
15_SF3A2 - _Seq_16	GGGATGTATTGAAGGAGGATCCGGAGGCTCGATCCTCTGC TCGTACGCAG
16_SF3A2 - _Seq_17	GGGATGTATTGAAGGAGGATTCGGCGGCCATGAGCAGGTA CTGCCAGCGC
17_SF3A2 - _Seq_18	GGGATGTATTGAAGGAGGATGGCACCTTGAAGGCAATGGT CTCGTAGGGC
18_SF3A2 - _Seq_19	GGGATGTATTGAAGGAGGATTTGCCCTCCGCCTTGTCGAT CTCTCTGCTC
19_SF3A2 - _Seq_20	GGGATGTATTGAAGGAGGATTTGGTCTCCCGGTTCCAGTG TGTCCAGAAC
20_SF3A2 - _Seq_22	GGGATGTATTGAAGGAGGATGGGAGGCTGGGTGGAGCCG GGGGCTTCTCC
21_SF3A2 - _Seq_23	GGGATGTATTGAAGGAGGATCGGGGGTGGAGGCCGCTTC ACCCCAGGGGG
22_SF3A2 - _Seq_24	GGGATGTATTGAAGGAGGATCGGTGGCCGAGGGGGCAGA CCGTTCATCAG
23_SF3A2 - _Seq_25	GGGATGTATTGAAGGAGGATTGGCGGGGGCGGTGGCAAA GACTCAGGCAG
24_SF3A2 - _Seq_26	GGGATGTATTGAAGGAGGATTAGCTGGGGTGGTCCCGGG GGCCCTGAGGG
25_SF3A2 - _Seq_27	GGGATGTATTGAAGGAGGATTGCAGGGGGATGCACCACTG GGGCCGGGGG
26_SF3A2 - _Seq_28	GGGATGTATTGAAGGAGGATGACGCCAGGAGCTGGGGGA TGGACCCCAGA
27_SF3A2 - _Seq_29	GGGATGTATTGAAGGAGGATGGCTGGGGGATGGACGCCA GGAGCTGGGGG
28_SF3A2 - _Seq_30	GGGATGTATTGAAGGAGGATGACCCCAGAGGTTGGTGGGT GGACCCCAGG
29_SF3A2 - _Seq_31	GGGATGTATTGAAGGAGGATGGCTGGAGGGTGGACTCCA GGAGCTGGGGG

30_SF3A2 - _Seq_32	GGGATGTATTGAAGGAGGATGACTCCGGGGGCTGGTGGG TGAACCCCGGG
31_SF3A2 - _Seq_33	GGGATGTATTGAAGGAGGATTGGTGGGTGAACCCCAGGG GCTGGTGGGTG
32_SF3A2 - _Seq_34	GGGATGTATTGAAGGAGGATCGCTGATGGGGGAGGATGG ACCCCTGGGGC
33_SF3A2 - _Seq_35	GGGATGTATTGAAGGAGGATTGGGTGCACCCCCGGGGCC TGGGGGTGAAC
34_SF3A2 - _Seq_36	GGGATGTATTGAAGGAGGATTGGGGCCTGAGGGTGAACG GCGGGGGCTGC
35_SF3A2 - _Seq_37	GGGATGTATTGAAGGAGGATAGGGTGCATCCCTGGGGCTG GTGGGTGCAC
36_SF3A2 - _Seq_38	GGGATGTATTGAAGGAGGATGGGAGGTTGGGGGTGGACC CCCGGGGCCTG
37_SF3A2 - _Seq_39	GGGATGTATTGAAGGAGGATGGTGGACCCCAGGAGCCGA CGGATGGACCC
38_SF3A2 - _Seq_40	GGGATGTATTGAAGGAGGATGATTTGAGGGGTGAACTCCC GGAGGCTGAG
39_SF3A2 - _Seq_41	GGGATGTATTGAAGGAGGATCCTCAGCATTGGGGGCATGG GAGTTGGGGG
40_SF3A2 - _Seq_42	GGGATGTATTGAAGGAGGATGTTCCCTGGGCCTTCGGAGG GAAGTGGGGG
41_SF3A2 - _Seq_43	GGGATGTATTGAAGGAGGATTTCTCAGTTGGTTGGGGGAG GGGGAGGTAT
42_SF3A2 - _Seq_44	GGGATGTATTGAAGGAGGATTGGCGCTGGGCTTGCTGGG GGAGGGAGCAG
43_SF3A2 - _Seq_45	GGGATGTATTGAAGGAGGATCTTCTCTCAGTGGGAAAAGG CAAGAGCACC
1_MLST8 ._Seq_1	GGGATGTATTGAAGGAGGATACTGCCCACCGTGCCTGGGG AGGTGTTCAT
2_MLST8 ._Seq_2	GGGATGTATTGAAGGAGGATGTAGCCTGCAGTGGCCAGGA TGACCGGGTC
3_MLST8 ._Seq_3	GGGATGTATTGAAGGAGGATGTGGGCCTGCCAGAAGCGC ACGGTGTGGTC
4_MLST8 ._Seq_4	GGGATGTATTGAAGGAGGATGTGCTGCACCGTCCGGGTGC AGATGCCGCT
5_MLST8 ._Seq_5	GGGATGTATTGAAGGAGGATGACCTCCAAGGCATTCACCT GGGAGTCCTG
6_MLST8 ._Seq_6	GGGATGTATTGAAGGAGGATTGCAGCAGCAATCATGCTGC GGTCCGGTGT
7_MLST8 ._Seq_7	GGGATGTATTGAAGGAGGATGAGATCATACATGCGGATGT GCTGGTAACC
8_MLST8 ._Seq_8	GGGATGTATTGAAGGAGGATGCTGATGATGGGGTTAGGGT TATTGGAGTT
9_MLST8 ._Seq_9	GGGATGTATTGAAGGAGGATAGACGCGATGTTCTTGTTGA CGCCGTCGTA

10_MLST8._Seq_10	GGGATGTATTGAAGGAGGATCATCCAGCGGCCGTCTTCGTGGAAGCCCAC
11_MLST8._Seq_11	GGGATGTATTGAAGGAGGATCCTGGCTGTGCAGTCCTCGCCGCCCGTGTA
12_MLST8._Seq_12	GGGATGTATTGAAGGAGGATCTGCAGGTTCCGGGACCTGAGGTCCCAGAT
13_MLST8._Seq_13	GGGATGTATTGAAGGAGGATGGGTGCGTTCACCTGGAAGATCCGCTGGCA
14_MLST8._Seq_14	GGGATGTATTGAAGGAGGATCTGGTTGGGGTGCAGGCACACGCAGTTAAT
15_MLST8._Seq_15	GGGATGTATTGAAGGAGGATCCCGCTCTGGTCACCCACGATGAGCTCTGC
16_MLST8._Seq_16	GGGATGTATTGAAGGAGGATGTCTGTTTTCAAGTCCCAGATGTGGATAGC
17_MLST8._Seq_17	GGGATGTATTGAAGGAGGATCTCGGGCTCAGGGATCAGCTGCTCGTTGTG
18_MLST8._Seq_18	GGGATGTATTGAAGGAGGATGGGATCGATGTGGGCGGACGTGATGGAGAC
19_MLST8._Seq_19	GGGATGTATTGAAGGAGGATGCTATTGACAGCTGCCATGTAGCTGGCGTC
20_MLST8._Seq_20	GGGATGTATTGAAGGAGGATCGTCAGATTCCAGACATAGCAGTTTCCGGT
21_MLST8._Seq_21	GGGATGTATTGAAGGAGGATGAGCTGGGTCACCTCGTCACCAATGCCCCC
22_MLST8._Seq_22	GGGATGTATTGAAGGAGGATCGTGTGGGCAGGGATCTTAGTCTTGGGGAT
23_MLST8._Seq_23	GGGATGTATTGAAGGAGGATGGGGCTGAAGCGACACTGCAGGGCGTAGCG
24_MLST8._Seq_24	GGGATGTATTGAAGGAGGATAGCCGAGCAGGTGGCGAGGAGCGTGGAGTC
25_MLST8._Seq_25	GGGATGTATTGAAGGAGGATGGACGTCCTCCAGATCTTGCACGTCTGATC
26_MLST8._Seq_26	GGGATGTATTGAAGGAGGATGATGCTCAGCTCCGTCATCAGGGAGAAGTT
27_MLST8._Seq_27	GGGATGTATTGAAGGAGGATGCGGGAGGACTCCCCGGGGTTGCCGCTCTT
28_MLST8._Seq_28	GGGATGTATTGAAGGAGGATCCCCGAGAAGGCGCAGCCCCACATCCAGCC
29_MLST8._Seq_29	GGGATGTATTGAAGGAGGATCGAGGAAGCAGTGACGATGTACTGGGAGTC
30_MLST8._Seq_30	GGGATGTATTGAAGGAGGATCTCCACACACCAGAGCCGGGCCAGGTTGTC
31_MLST8._Seq_31	GGGATGTATTGAAGGAGGATGCCGCCATACTCTCTCTTGATCTCTCCAGT
32_MLST8._Seq_32	GGGATGTATTGAAGGAGGATGAAGGCCAGGCAGACAACAGCCTTCTGGTG

33_MLST8._Seq_33	GGGATGTATTGAAGGAGGATGGTCACAGGCTAGCCCAGCACACTGTCATT
34_MLST8._Seq_34	GGGATGTATTGAAGGAGGATTGCCACCACCTGCACCAGGCAGTCCCGAGG
35_MLST8._Seq_35	GGGATGTATTGAAGGAGGATTGACCTGGGTGCTGCATGGGTCCCTCCAGC
36_MLST8._Seq_36	GGGATGTATTGAAGGAGGATTGGCGCAGGCCGGCAGGGGAGGGTCTGCTC
37_MLST8._Seq_37	GGGATGTATTGAAGGAGGATAAGGCGCCACAGGGGGCCATCAGGTCCAGC
38_MLST8._Seq_38	GGGATGTATTGAAGGAGGATGGCTGAGAGTCCCAGGGCAGCCTGGCCCAG
39_MLST8._Seq_39	GGGATGTATTGAAGGAGGATAGCTCTGTCACATCTGGATAAGCAACTGGG
40_MLST8._Seq_40	GGGATGTATTGAAGGAGGATGTCCAGGAGTGTGCAGCCTGGCTTGGGTCG
41_MLST8._Seq_41	GGGATGTATTGAAGGAGGATCGACTTTCCCAGGCAGTGCAGGCTAGCCCA
42_MLST8._Seq_42	GGGATGTATTGAAGGAGGATCAGACCCCTCAGCAGCTTTGGGCCCTCGGC
43_MLST8._Seq_43	GGGATGTATTGAAGGAGGATACACACTAGCTTGGGGGTGGGCACCAGCCT
44_MLST8._Seq_44	GGGATGTATTGAAGGAGGATCCCTGAAACGCGGGCAGGGAGGGGCAGAGA
45_MLST8._Seq_45	GGGATGTATTGAAGGAGGATCATGGTGGTGGTGTTCTCTATGGACCGAGG
1_MAP2K2-_Seq_1	GGGATGTATTGAAGGAGGATCGGCAGCACCGGCTTCCTCCGGGCCAGCAT
2_MAP2K2-_Seq_3	GGGATGTATTGAAGGAGGATGGAGGCGCCCTCGCTGGTAGGGGATGGGCC
3_MAP2K2-_Seq_8	GGGATGTATTGAAGGAGGATCGCGCCCAGCTCTGAGATCCTTTCGAAGTC
4_MAP2K2-_Seq_12	GGGATGTATTGAAGGAGGATCTGCAGCTCGCGGATGATCTGGTTCCGGAT
5_MAP2K2-_Seq_13	GGGATGTATTGAAGGAGGATGATGTACGGCGAGTTGCATTCGTGCAGGAC
6_MAP2K2-_Seq_14	GGGATGTATTGAAGGAGGATGTCACTGTAGAAGGCCCCGTAGAAGCCCAC
7_MAP2K2-_Seq_15	GGGATGTATTGAAGGAGGATCATGTGTTCCATGCAAATGCTGATCTCCCC
8_MAP2K2-_Seq_16	GGGATGTATTGAAGGAGGATTTTCAGCACCTGGTCCAGGGAGCCGCCGTC
9_MAP2K2-_Seq_17	GGGATGTATTGAAGGAGGATCAGGATCTCCTCGGGAATCCTCTTGGCCTC
10_MAP2K2-_Seq_18	GGGATGTATTGAAGGAGGATGCCCCGGAGAACCGCGATGCTGACTTTCCC

11_MAP2K2-_Seq_20	GGGATGTATTGAAGGAGGATGATGTTGGAGGGCTTCACATCTCGGTGCAT
12_MAP2K2-_Seq_25	GGGATGTATTGAAGGAGGATGATGTCCGACTGCACCGAGTAATGTGTGCC
13_MAP2K2-_Seq_26	GGGATGTATTGAAGGAGGATCAGCTCCACCAGGGACAGGCCCATGCTCCA
14_MAP2K2-_Seq_27	GGGATGTATTGAAGGAGGATGGCCTCCAGCTCTTTGGCGTCGGGCGGGGG
15_MAP2K2-_Seq_28	GGGATGTATTGAAGGAGGATTTCCCCGTCGACCACGGGCCGGCCAAAGAT
16_MAP2K2-_Seq_29	GGGATGTATTGAAGGAGGATCCGAGGCGAGATGCTGTGAGGCTCTCCTTC
17_MAP2K2-_Seq_30	GGGATGTATTGAAGGAGGATCCATCCCGTGACCGCTGACGGGGCGCCCGG
18_MAP2K2-_Seq_31	GGGATGTATTGAAGGAGGATGTTCAAAGATGGCCATGGCAGGCCGGCTAT
19_MAP2K2-_Seq_32	GGGATGTATTGAAGGAGGATGAGGTGGCTCGTTCACAATATAGTCCAGGA
20_MAP2K2-_Seq_35	GGGATGTATTGAAGGAGGATATCTTCAGGTCCGCCCGCTCCGCTGGGTTC
21_MAP2K2-_Seq_36	GGGATGTATTGAAGGAGGATGACCGCTTGATGAAGGTGTGGTTTGTGAGC
22_MAP2K2-_Seq_37	GGGATGTATTGAAGGAGGATCAGCCGGCAAAATCCACTTCTTCCACCTCG
23_MAP2K2-_Seq_38	GGGATGTATTGAAGGAGGATGGCTGGTTCAGCCGCAGGGTTTTACACAAC
24_MAP2K2-_Seq_39	GGGATGTATTGAAGGAGGATCACTGTCACACGGCGGTGCGCGTGGGTGTG
25_MAP2K2-_Seq_40	GGGATGTATTGAAGGAGGATGACGGTGGGCAGGTCACCAGCGGGACGCAG
26_MAP2K2-_Seq_41	GGGATGTATTGAAGGAGGATCCTCAGCTGGAAGGGCGGGGCATGGACAGG
27_MAP2K2-_Seq_42	GGGATGTATTGAAGGAGGATGGTGAGGCAGGAGGGTGGGTGGAGGCGCCA
28_MAP2K2-_Seq_43	GGGATGTATTGAAGGAGGATCATGCGCTGTCGCCCCGCCACCGGTGCTCTC
29_MAP2K2-_Seq_44	GGGATGTATTGAAGGAGGATGACGGGCAGGAGAGGAGACCCCCGTTCCTG
30_MAP2K2-_Seq_45	GGGATGTATTGAAGGAGGATGTCGCCCGTCCCCAGAGGCACCCCGGCCAG
31_MAP2K2-_Seq_46	GGGATGTATTGAAGGAGGATAGCAGAGCCTCTGAGACCACACACAGCAGC
32_MAP2K2-_Seq_47	GGGATGTATTGAAGGAGGATCTCTCCCTGTTTTGTTTTGTAACCTAAGGA
5_IQGAP3-_Seq_5	GGGATGTATTGAAGGAGGATCTCCTTCAGGCAGGCCTCCATCCAGCGCTT

9_IQGAP3 -_Seq_9	GGGATGTATTGAAGGAGGATCTGCTCCACATCGTAGATCTTCTTCAAGGG
13_IQGAP3-_Seq_13	GGGATGTATTGAAGGAGGATATAGATGTCCGTGGTCTCTGGGAAGAAGGT
17_IQGAP3-_Seq_17	GGGATGTATTGAAGGAGGATCTCAGCTGTGAATTTCACTTTCCCGTATAG
21_IQGAP3-_Seq_21	GGGATGTATTGAAGGAGGATAGCTGCATGGACTGCAGCCTCATCCACCGA
25_IQGAP3-_Seq_25	GGGATGTATTGAAGGAGGATCTCTTGGTAGACGGCTGCCAGAGGCTCTCG
29_IQGAP3-_Seq_29	GGGATGTATTGAAGGAGGATATGGTTGATATTGCCCTGGATTTCAGCCTG
33_IQGAP3-_Seq_33	GGGATGTATTGAAGGAGGATAAAGTCTCTCCTCACCCCTCGCAGGGCCAG
37_IQGAP3-_Seq_37	GGGATGTATTGAAGGAGGATCTTTGTGTTGGCTGCAGCCACACCAGCCTG
42_IQGAP3-_Seq_42	GGGATGTATTGAAGGAGGATCAGCTGGTACATAGACGATGCAACAGGGTA
46_IQGAP3-_Seq_46	GGGATGTATTGAAGGAGGATACTGGCATCCCGGGCCTCCAGGGCCCGGTT
50_IQGAP3-_Seq_50	GGGATGTATTGAAGGAGGATAGTCCTCACCCATCCCACGCTCCTGTCGCA
54_IQGAP3-_Seq_54	GGGATGTATTGAAGGAGGATCAGGGCTGCCTTTGTCCAGAGCCTCATTGA
58_IQGAP3-_Seq_58	GGGATGTATTGAAGGAGGATCTGTCACCTGGGCCTTCTGCCTTTTGGCTG
62_IQGAP3-_Seq_62	GGGATGTATTGAAGGAGGATTGATGGCTTGATTGATGGCAGCCACACCAA
66_IQGAP3-_Seq_66	GGGATGTATTGAAGGAGGATTCTTTGCCATGGCACTTTCCAGGGCTCGCT
70_IQGAP3-_Seq_70	GGGATGTATTGAAGGAGGATTGAGGGGGCAGCCAGGAGGTTGCTCCCAGA
74_IQGAP3-_Seq_74	GGGATGTATTGAAGGAGGATGGCGGGCCTGGAGCTGGATAACAAAGCCGA
78_IQGAP3-_Seq_78	GGGATGTATTGAAGGAGGATGGTAAATCTTCCGCTGCCTATAACCCCGCC
83_IQGAP3-_Seq_83	GGGATGTATTGAAGGAGGATAAAATGCCTGGATCTTCACAATGGAGTTAA
87_IQGAP3-_Seq_87	GGGATGTATTGAAGGAGGATCAGCCAAGAAGTCTTGCTGGCTTTGATTCA
91_IQGAP3-_Seq_91	GGGATGTATTGAAGGAGGATTGATCCGGTTCTTCACCAGCAGGCCAATCT
95_IQGAP3-_Seq_95	GGGATGTATTGAAGGAGGATGCCGTTTCTCTTTGCTCAGCGACTTTAAAC
99_IQGAP3-_Seq_99	GGGATGTATTGAAGGAGGATAAATCACTGCCTCCATGAACTTGGTGGTTT

103_IQGAP3 - _Seq_103	GGGATGTATTGAAGGAGGATCTGTCACCACGTCCTGGGGCTGCTCCACCT
107_IQGAP3 - _Seq_107	GGGATGTATTGAAGGAGGATCGCTGAGCACTTTGTCTTCTAGCACATCCT
111_IQGAP3 - _Seq_111	GGGATGTATTGAAGGAGGATCCTCGGGGTGGCTCAAGGCCTGCTCCGGGG
115_IQGAP3 - _Seq_115	GGGATGTATTGAAGGAGGATGGACTTTGGCCACATATCGCATCCCATACG
120_IQGAP3 - _Seq_120	GGGATGTATTGAAGGAGGATGGGCTCCACCAGCTGCCATGGCCACAATGT
124_IQGAP3 - _Seq_124	GGGATGTATTGAAGGAGGATGGTGTGTTTCCTCCAGATAGTCATTCAGGA
128_IQGAP3 - _Seq_128	GGGATGTATTGAAGGAGGATCCACGGTGATGTACACCATGGGTTTGGCCA
132_IQGAP3 - _Seq_132	GGGATGTATTGAAGGAGGATGGTCAGGGATGGTGGGCAGCTCCCCAAGAT
136_IQGAP3 - _Seq_136	GGGATGTATTGAAGGAGGATTACGGGTGTTGGAGTCATCAGCATCTGCCT
140_IQGAP3 - _Seq_140	GGGATGTATTGAAGGAGGATGCTGCTTGTGGGCTGCTTCTTGCTCTCTGG
144_IQGAP3 - _Seq_144	GGGATGTATTGAAGGAGGATTAGGTTCCGCAGGACGCGCCGCTGCTTCTC
148_IQGAP3 - _Seq_148	GGGATGTATTGAAGGAGGATCAGCTCTGCCTTCCGCCTGTGCCTGTGTCT
152_IQGAP3 - _Seq_152	GGGATGTATTGAAGGAGGATCTTGGAGTCGGGGGCCAGGTGGTCCAGGCA
156_IQGAP3 - _Seq_156	GGGATGTATTGAAGGAGGATAAAGATGACGTTTCTGAAGTGAGAGGCGGG
161_IQGAP3 - _Seq_161	GGGATGTATTGAAGGAGGATTTTGGCCTTGTTGAAGAGTTTCATGACAGC

165_IQGAP3 -_Seq_165	GGGATGTATTGAAGGAGGATGTGAGTTAGTGTTAAAGAAAGCATCCAGAG
169_IQGAP3 -_Seq_169	GGGATGTATTGAAGGAGGATCCAATTAGAAGATACACTGTCTGTGGCCAG
173_IQGAP3 -_Seq_173	GGGATGTATTGAAGGAGGATACACAAGAGTAATGGCTTTCCCAGGTCAAG
177_IQGAP3 -_Seq_177	GGGATGTATTGAAGGAGGATGGAGGTAGGGATGGGGAGCCTGGCCCTGGC
181_IQGAP3 -_Seq_181	GGGATGTATTGAAGGAGGATACATGGGCACTAACACACACTGCATCCCCC
185_IQGAP3 -_Seq_185	GGGATGTATTGAAGGAGGATAGAGTGTAAGGATGGGAGAAAGAATAAATA
189_IQGAP3 -_Seq_189	GGGATGTATTGAAGGAGGATAACCTAAGGTGACTTTAAATCCAAGGTAAA
193_IQGAP3 -_Seq_193	GGGATGTATTGAAGGAGGATGAAGAGTCAGCTGTAAGGGATGAGAATCCT
197_IQGAP3 -_Seq_197	GGGATGTATTGAAGGAGGATTGGGAGTAACAGCTGCTTTTATTAACATCA
3_ALDH18A1 -_Seq_3	GGGATGTATTGAAGGAGGATATGAGATCTGAAGACGGTTGTACACTTGAC
5_ALDH18A1 -_Seq_5	GGGATGTATTGAAGGAGGATAGTGATAAACGGGATGTTGCTCCAAGAACG
7_ALDH18A1 -_Seq_7	GGGATGTATTGAAGGAGGATGGCATGCTTCAGCTCACTGCGGTGGGCGAA
9_ALDH18A1 -_Seq_9	GGGATGTATTGAAGGAGGATCAGGCCACATTCATCCCCTCGGGTCACCAC
11_ALDH18A1 -_Seq_11	GGGATGTATTGAAGGAGGATTCTGCCCTGATTCTGCAGCACTGATACCTG
13_ALDH18A1 -_Seq_13	GGGATGTATTGAAGGAGGATCTCATGGCGCAAGCGTTGTTTGCCAAAGGC
15_ALDH18A1 -_Seq_15	GGGATGTATTGAAGGAGGATTTCTTTCAGCTGGTTCTGCCCCGAGTGGAG

17_ALDH18A1 - _Seq_17	GGGATGTATTGAAGGAGGATCATCAGCCCACTCTGTCCGGCAGCTGCACA
20_ALDH18A1 - _Seq_20	GGGATGTATTGAAGGAGGATGCGCTTCTGCTCATCATGGAAATCCAAATT
22_ALDH18A1 - _Seq_22	GGGATGTATTGAAGGAGGATGTTGACAATGGGGACAATGTTCATTCTAAG
24_ALDH18A1 - _Seq_24	GGGATGTATTGAAGGAGGATGCTATCATTATCTTTAACACTAATAACCCC
26_ALDH18A1 - _Seq_26	GGGATGTATTGAAGGAGGATTACATCTGAAAGAACAATCAAGAGATCAGT
28_ALDH18A1 - _Seq_28	GGGATGTATTGAAGGAGGATAGACTGCTGATCTCCGGGATAAAATATATC
30_ALDH18A1 - _Seq_30	GGGATGTATTGAAGGAGGATTGCTTTCACCTTGGCTTCCATGCCACCCAT
32_ALDH18A1 - _Seq_32	GGGATGTATTGAAGGAGGATCTTTGGGTGGGTTCCATTGGCAATAACAAC
34_ALDH18A1 - _Seq_34	GGGATGTATTGAAGGAGGATTGAAAAGAAGGTACCAACTTTCTTCCCCTC
37_ALDH18A1 - _Seq_37	GGGATGTATTGAAGGAGGATCTGCTCAGGTTCCAAGGTGGCCAACATCCT
39_ALDH18A1 - _Seq_39	GGGATGTATTGAAGGAGGATCAGGATCTCATCACGCTGGTCCGTCAACAG
41_ALDH18A1 - _Seq_41	GGGATGTATTGAAGGAGGATGGCTTAAACGTTTCAGCAGAGGAGCTGCAA
43_ALDH18A1 - _Seq_43	GGGATGTATTGAAGGAGGATGGGAGGAGGCTGCGATCTGTCGCAGACCGA
45_ALDH18A1 - _Seq_45	GGGATGTATTGAAGGAGGATGTTCCAGTTCCAAGTTTTTGGCGATTCGGG
47_ALDH18A1 - _Seq_47	GGGATGTATTGAAGGAGGATGTAGACAGTCAGGACGAGATTCAAAGATCA

49_ALDH18A1 - _Seq_49	GGGATGTATTGAAGGAGGATCCTTCCCTCCTTTGAGTAACAAGCCATTGC
51_ALDH18A1 - _Seq_51	GGGATGTATTGAAGGAGGATCATGGATTGAGAGAGCCTCCTGGGTCAGGA
54_ALDH18A1 - _Seq_54	GGGATGTATTGAAGGAGGATGTGGAATGATCAGATCTATCATTTTGTCTA
56_ALDH18A1 - _Seq_56	GGGATGTATTGAAGGAGGATCCATCACTGGAATCCCCTTAGCAGCTTTCT
58_ALDH18A1 - _Seq_58	GGGATGTATTGAAGGAGGATTGACCTTATCAACACTGGCCTCGGAATCCA
60_ALDH18A1 - _Seq_60	GGGATGTATTGAAGGAGGATAAGTCTCCAAAGCATTACAGGCAGCTGGAT
62_ALDH18A1 - _Seq_62	GGGATGTATTGAAGGAGGATTCAGCATATCAATGATCTGGTCAAATAATG
64_ALDH18A1 - _Seq_64	GGGATGTATTGAAGGAGGATGGCTGAAGGTCAGATAGGAGGCAAATTTGG
66_ALDH18A1 - _Seq_66	GGGATGTATTGAAGGAGGATCTACTTCAATGCATAATTCCAGGTCCCCAT
68_ALDH18A1 - _Seq_68	GGGATGTATTGAAGGAGGATCATCCGTGTGGGAGCTGCCATACTTGTGGA
71_ALDH18A1 - _Seq_71	GGGATGTATTGAAGGAGGATAAAAGCGAGTGCTGGCATTCCAGAACACAC
73_ALDH18A1 - _Seq_73	GGGATGTATTGAAGGAGGATCGTGGATTCTCGATGTACTGATTCCCACTT
75_ALDH18A1 - _Seq_75	GGGATGTATTGAAGGAGGATCCTTCCCTCGCAGCAGCCACTTAGTAGTAA
77_ALDH18A1 - _Seq_77	GGGATGTATTGAAGGAGGATGGAGGTTCTCATGAAGATATTTTAAACTTC
79_ALDH18A1 - _Seq_79	GGGATGTATTGAAGGAGGATCTTTTGGAAAATTCCCGGGTTTTCCTGGCT

81_ALDH18A1 - _Seq_81	GGGATGTATTGAAGGAGGATCAGGAACTGGGAGACAAGAGCGGGCTCTCT
83_ALDH18A1 - _Seq_83	GGGATGTATTGAAGGAGGATTGCTATTGCCAAACGGAGCCCAGAAGCATC
85_ALDH18A1 - _Seq_85	GGGATGTATTGAAGGAGGATCTATCGGTAGCAACTATTTTCTTACTTTAA
88_ALDH18A1 - _Seq_88	GGGATGTATTGAAGGAGGATAAGGGGGACTGTAAGTCACTGAGGTGACAC
90_ALDH18A1 - _Seq_90	GGGATGTATTGAAGGAGGATGATGACTACATGTGAAAGAAATAAAATGTG
92_ALDH18A1 - _Seq_92	GGGATGTATTGAAGGAGGATTCTGATGAGAATGCTAAAAAGAAGAGTTGC
94_ALDH18A1 - _Seq_94	GGGATGTATTGAAGGAGGATCAAATAAATACAAAAGGTCAATCTTCCCAG
96_ALDH18A1 - _Seq_96	GGGATGTATTGAAGGAGGATCACAGCATCTCCTGGATGCAGGAAGCTGCA
98_ALDH18A1 - _Seq_98	GGGATGTATTGAAGGAGGATGGAACATCCTGAAACTTGCATCTCCTGCTG
100_ALDH18A1 - _Seq_100	GGGATGTATTGAAGGAGGATGGTAGGACGACAAAATAATTCATACAAAAA
102_ALDH18A1 - _Seq_102	GGGATGTATTGAAGGAGGATAAAAGGGGGAAGAATCCAAAGTATTAAAAT
2_TES - _Seq_2	GGGATGTATTGAAGGAGGATGGCTCCAAATCCTTGCTCGTGACCTAAGCC
4_TES - _Seq_4	GGGATGTATTGAAGGAGGATTACGACATATTTTTCTCCAGAAGTGCAGTT
5_TES - _Seq_5	GGGATGTATTGAAGGAGGATCATCATGCTCTTCTTGGCCACACTTGCAGT
7_TES - _Seq_7	GGGATGTATTGAAGGAGGATTATACTTGGTGTCTTCAAAAAGTTTTCCCA
8_TES - _Seq_8	GGGATGTATTGAAGGAGGATCATCTGACTTTAGTTTTGCAATCAGAGTGG
10_TES - _Seq_10	GGGATGTATTGAAGGAGGATTCTTCTTGGCAGCAACTGGATTCGTCAATA

11_TES - _Seq_11	GGGATGTATTGAAGGAGGATACTCATAGGTAACTGTATTGA TGGAGACAT
13_TES - _Seq_13	GGGATGTATTGAAGGAGGATCCTTGGGTAGCATCTGCATG TACTGCCTGG
14_TES - _Seq_14	GGGATGTATTGAAGGAGGATCCCCCTCTGAGCCTGCTACT GGCTGCTTTT
16_TES - _Seq_16	GGGATGTATTGAAGGAGGATTTGAAGGGTCCTGGTCATGT GCAGGGAGCT
17_TES - _Seq_17	GGGATGTATTGAAGGAGGATTCACCTCTCTGGGAGACAAC TCATGGCACT
19_TES - _Seq_19	GGGATGTATTGAAGGAGGATTGACATCTCCTACTCCCAGA GCTTCGCTCT
20_TES - _Seq_20	GGGATGTATTGAAGGAGGATGGCCTTGGGCATCCATCTCA CAGGGAAGTT
22_TES - _Seq_22	GGGATGTATTGAAGGAGGATCCATGGCCCCCACTGCTGCT GGGGTGCTTC
23_TES - _Seq_23	GGGATGTATTGAAGGAGGATGAGTTCTTTTGTGCTCAGCA GATTTGTCCT
25_TES - _Seq_25	GGGATGTATTGAAGGAGGATCGGCATAGATGGCTGGGTCA CCTTCTTTCA
26_TES - _Seq_26	GGGATGTATTGAAGGAGGATGGTGCCACAGTTTATCATAG CCAGCCCTTT
28_TES - _Seq_28	GGGATGTATTGAAGGAGGATTCCAAAAATAAATCATGTCAA CCAGGAGTT
29_TES - _Seq_29	GGGATGTATTGAAGGAGGATAATGTCTGCCACAGTATAGCT TCTCATTCT
31_TES - _Seq_31	GGGATGTATTGAAGGAGGATACTCATTGCTGAATATCAGCT CGTCACAGC
32_TES - _Seq_32	GGGATGTATTGAAGGAGGATGGTGCCAATTCTGGTTTTCTG CCTGGGTAT
34_TES - _Seq_34	GGGATGTATTGAAGGAGGATCCATCACGTATATCTCCCCA GCTAGAATGC
35_TES - _Seq_35	GGGATGTATTGAAGGAGGATAGCAGGGCTTGCACACGGG CTTGTCATTGA
37_TES - _Seq_37	GGGATGTATTGAAGGAGGATGCACTTCTGGGTCGATGGCA TTGTGGCATC
39_TES - _Seq_39	GGGATGTATTGAAGGAGGATAAGAGCACAGAAAGCACTCT GTGGATGCAT
40_TES - _Seq_40	GGGATGTATTGAAGGAGGATACTTCTGCCCAATGAGGCAT TTGCTGCAGC
42_TES - _Seq_42	GGGATGTATTGAAGGAGGATCCTAAGACATCCTCTTCTTAC ATTCCACTG
43_TES - _Seq_43	GGGATGTATTGAAGGAGGATCTATGGCTCGATACTTCTGG GTGCCCTCCT
45_TES - _Seq_45	GGGATGTATTGAAGGAGGATATCTCTTGGTTTCCTTTACAG TTTCTTTTT

46_TES - _Seq_46	GGGATGTATTGAAGGAGGATAAACCAAGTTTAAAAGTTGAG ACCGAAAAA
48_TES - _Seq_48	GGGATGTATTGAAGGAGGATTAATGAGATCCAAGCTTCCAA AAATGATTT
49_TES - _Seq_49	GGGATGTATTGAAGGAGGATGTGGCACAAATGGAATAGAG ACATGAAGTT
51_TES - _Seq_51	GGGATGTATTGAAGGAGGATAAAAGAAGTGTAGAACTAGG AATGCTCATC
52_TES - _Seq_52	GGGATGTATTGAAGGAGGATTTTTCTTTTCATTTTACACATG AGGGGGAA
54_TES - _Seq_54	GGGATGTATTGAAGGAGGATAAAGGTCAGTGAATAAGACG AGGCAATAAA
55_TES - _Seq_55	GGGATGTATTGAAGGAGGATTGTCAAAAAGAATTCACTGTG TATCATTAC
57_TES - _Seq_57	GGGATGTATTGAAGGAGGATGAAAGAGTAAATGCATAGGC ATTAAAACAG
58_TES - _Seq_58	GGGATGTATTGAAGGAGGATTAAAGAAAATGCCACCTCTG CCTAAATCAG
60_TES - _Seq_60	GGGATGTATTGAAGGAGGATGGCCACAGATGCAAGTCACC AACTTACAAA
61_TES - _Seq_61	GGGATGTATTGAAGGAGGATGATACTGTTATGCCACATGTG ATAATAAAA
63_TES - _Seq_65	GGGATGTATTGAAGGAGGATGGCTAACATGGTGAAAACCT GTCTCTACTA
64_TES - _Seq_68	GGGATGTATTGAAGGAGGATCAGGCATGGTGGCTCCCACA CCTGTAATCC
66_TES - _Seq_70	GGGATGTATTGAAGGAGGATGGTGGCTTGGCTTTTATGTC CAAGCCAAAA
67_TES - _Seq_71	GGGATGTATTGAAGGAGGATGGTACAAAAACTATACATGTT CTTTGGATT
69_TES - _Seq_73	GGGATGTATTGAAGGAGGATCCATTAGGAAAGAATAAAAAC CATGCAAAA
70_TES - _Seq_74	GGGATGTATTGAAGGAGGATGACAGGCTTGGAAGTATTAT AAAACAGGAT
72_TES - _Seq_76	GGGATGTATTGAAGGAGGATGAATAAACATTAGAAATACCT AGCCATGAA
73_TES - _Seq_77	GGGATGTATTGAAGGAGGATGCATAGCTATGTGTAGAAGT ACACAGGGAA

REFERENCES

Badonyi, M., and Marsh, J.A. (2022). Large protein complex interfaces have evolved to promote cotranslational assembly. Elife *11*. 10.7554/eLife.79602.

Berkovits, B.D., and Mayr, C. (2015). Alternative 3' UTRs act as scaffolds to regulate membrane protein localization. Nature *522*, 363-367. 10.1038/nature14321.

Bertolotti, A. (2018). The split protein phosphatase system. Biochem J *475*, 3707-3723. 10.1042/bcj20170726.

Bertrand, E., Chartrand, P., Schaefer, M., Shenoy, S.M., Singer, R.H., and Long, R.M. (1998). Localization of ASH1 mRNA particles in living yeast. Mol Cell *2*, 437-445. 10.1016/s1097-2765(00)80143-4.

Biederer, T., Sara, Y., Mozhayeva, M., Atasoy, D., Liu, X., Kavalali, E.T., and Südhof, T.C. (2002). SynCAM, a synaptic adhesion molecule that drives synapse assembly. Science *297*, 1525-1531. 10.1126/science.1072356.

Biever, A., Donlin-Asp, P.G., and Schuman, E.M. (2019). Local translation in neuronal processes. Curr Opin Neurobiol *57*, 141-148. 10.1016/j.conb.2019.02.008.

Blumberg, A., Zhao, Y., Huang, Y.-F., Dukler, N., Rice, E.J., Chivu, A.G., Krumholz, K., Danko, C.G., and Siepel, A. (2021). Characterizing RNA stability genome-wide through combined analysis of PRO-seq and RNA-seq data. BMC biology *19*, 30. 10.1186/s12915-021-00949-x.

Bolger, A.M., Lohse, M., and Usadel, B. (2014). Trimmomatic: a flexible trimmer for Illumina sequence data. Bioinformatics *30*, 2114-2120. 10.1093/bioinformatics/btu170.

Bonifacino, J.S., Cosson, P., and Klausner, R.D. (1990). Colocalized transmembrane determinants for ER degradation and subunit assembly explain the intracellular fate of TCR chains. Cell *63*, 503-513. 10.1016/0092-8674(90)90447-m.

Boraas, L., Hu, M., Thornton, L., Vejnar, C.E., Zhen, G., Giraldez, A.J., Mayr, C., Wang, S., and Nicoli, S. (2021). Non-coding function for mRNAs in Focal Adhesion Architecture and Mechanotransduction. bioRxiv, 2021.2010.2004.463097. 10.1101/2021.10.04.463097.

Buxbaum, A.R., Haimovich, G., and Singer, R.H. (2015). In the right place at the right time: visualizing and understanding mRNA localization. Nat Rev Mol Cell Biol *16*, 95-109. 10.1038/nrm3918.

Chao, J.A., Patskovsky, Y., Patel, V., Levy, M., Almo, S.C., and Singer, R.H. (2010). ZBP1 recognition of beta-actin zipcode induces RNA looping. Genes Dev *24*, 148-158. 10.1101/gad.1862910.

Chen, Q., Jagannathan, S., Reid, D.W., Zheng, T., and Nicchitta, C.V. (2011). Hierarchical regulation of mRNA partitioning between the cytoplasm and the endoplasmic reticulum of mammalian cells. Mol Biol Cell *22*, 2646-2658. 10.1091/mbc.E11-03-0239.

Courel, M., Clément, Y., Bossevain, C., Foretek, D., Vidal Cruchez, O., Yi, Z., Bénard, M., Benassy, M.N., Kress, M., Vindry, C., et al. (2019). GC content shapes mRNA storage and decay in human cells. Elife *8*. 10.7554/eLife.49708.

Cui, X.A., Zhang, H., and Palazzo, A.F. (2012). p180 promotes the ribosome-independent localization of a subset of mRNA to the endoplasmic reticulum. PLoS Biol *10*, e1001336. 10.1371/journal.pbio.1001336.

Diehn, M., Bhattacharya, R., Botstein, D., and Brown, P.O. (2006). Genome-scale identification of membrane-associated human mRNAs. PLoS Genet *2*, e11. 10.1371/journal.pgen.0020011.

Dobin, A., Davis, C.A., Schlesinger, F., Drenkow, J., Zaleski, C., Jha, S., Batut, P., Chaisson, M., and Gingeras, T.R. (2013). STAR: ultrafast universal RNA-seq aligner. Bioinformatics *29*, 15-21. 10.1093/bioinformatics/bts635.

Fazal, F.M., Han, S., Parker, K.R., Kaewsapsak, P., Xu, J., Boettiger, A.N., Chang, H.Y., and Ting, A.Y. (2019). Atlas of Subcellular RNA Localization Revealed by APEX-Seq. Cell *178*, 473-490.e426. 10.1016/j.cell.2019.05.027.

Frith, M.C., Valen, E., Krogh, A., Hayashizaki, Y., Carninci, P., and Sandelin, A. (2008). A code for transcription initiation in mammalian genomes. Genome Res *18*, 1-12. 10.1101/gr.6831208.

Galloway, A., Saveliev, A., Łukasiak, S., Hodson, D.J., Bolland, D., Balmanno, K., Ahlfors, H., Monzón-Casanova, E., Mannurita, S.C., Bell, L.S., et al. (2016). RNA-binding proteins ZFP36L1 and ZFP36L2 promote cell quiescence. Science *352*, 453-459. 10.1126/science.aad5978.

Gebauer, F., Schwarzl, T., Valcárcel, J., and Hentze, M.W. (2021). RNA-binding proteins in human genetic disease. Nat Rev Genet *22*, 185-198. 10.1038/s41576-020-00302-y.

Gilks, N., Kedersha, N., Ayodele, M., Shen, L., Stoecklin, G., Dember, L.M., and Anderson, P. (2004). Stress granule assembly is mediated by prion-like

aggregation of TIA-1. Molecular biology of the cell *15*, 5383-5398. 10.1091/mbc.e04-08-0715.

Glock, C., Biever, A., Tushev, G., Nassim-Assir, B., Kao, A., Bartnik, I., Tom Dieck, S., and Schuman, E.M. (2021). The translatome of neuronal cell bodies, dendrites, and axons. Proc Natl Acad Sci U S A *118*. 10.1073/pnas.2113929118.

Hafner, A.S., Donlin-Asp, P.G., Leitch, B., Herzog, E., and Schuman, E.M. (2019). Local protein synthesis is a ubiquitous feature of neuronal pre- and postsynaptic compartments. Science *364*. 10.1126/science.aau3644.

Hafner, M., Landthaler, M., Burger, L., Khorshid, M., Hausser, J., Berninger, P., Rothballer, A., Ascano, M., Jungkamp, A.C., Munschauer, M., et al. (2010). PAR-CliP--a method to identify transcriptome-wide the binding sites of RNA binding proteins. Journal of visualized experiments : JoVE. 10.3791/2034.

Hu, M., Yang, B., Cheng, Y., Radda, J.S.D., Chen, Y., Liu, M., and Wang, S. (2020). ProbeDealer is a convenient tool for designing probes for highly multiplexed fluorescence in situ hybridization. Sci Rep *10*, 22031. 10.1038/s41598-020-76439-x.

Huang da, W., Sherman, B.T., and Lempicki, R.A. (2009). Systematic and integrative analysis of large gene lists using DAVID bioinformatics resources. Nat Protoc *4*, 44-57. 10.1038/nprot.2008.211.

Hubstenberger, A., Courel, M., Benard, M., Souquere, S., Ernoult-Lange, M., Chouaib, R., Yi, Z., Morlot, J.B., Munier, A., Fradet, M., et al. (2017). P-Body Purification Reveals the Condensation of Repressed mRNA Regulons. Mol Cell *68*, 144-157 e145. 10.1016/j.molcel.2017.09.003.

Hüttelmaier, S., Zenklusen, D., Lederer, M., Dictenberg, J., Lorenz, M., Meng, X., Bassell, G.J., Condeelis, J., and Singer, R.H. (2005). Spatial regulation of beta-actin translation by Src-dependent phosphorylation of ZBP1. Nature *438*, 512-515. 10.1038/nature04115.

Jan, C.H., Williams, C.C., and Weissman, J.S. (2014). Principles of ER cotranslational translocation revealed by proximity-specific ribosome profiling. Science *346*, 1257521. 10.1126/science.1257521.

Karin, M. (1996). The regulation of AP-1 activity by mitogen-activated protein kinases. Philos Trans R Soc Lond B Biol Sci *351*, 127-134. 10.1098/rstb.1996.0008.

Kedersha, N.L., Gupta, M., Li, W., Miller, I., and Anderson, P. (1999). RNA-binding proteins TIA-1 and TIAR link the phosphorylation of eIF-2 alpha to the assembly of mammalian stress granules. J Cell Biol *147*, 1431-1442. 10.1083/jcb.147.7.1431.

Keene, J.D. (2007). RNA regulons: coordination of post-transcriptional events. Nature reviews. Genetics *8*, 533-543. 10.1038/nrg2111.

Khong, A., Matheny, T., Jain, S., Mitchell, S.F., Wheeler, J.R., and Parker, R. (2017). The Stress Granule Transcriptome Reveals Principles of mRNA Accumulation in Stress Granules. Mol Cell *68*, 808-820 e805. 10.1016/j.molcel.2017.10.015.

Kim, D., Paggi, J.M., Park, C., Bennett, C., and Salzberg, S.L. (2019). Graph-based genome alignment and genotyping with HISAT2 and HISAT-genotype. Nat Biotechnol *37*, 907-915. 10.1038/s41587-019-0201-4.

Kim-Ha, J., Smith, J.L., and Macdonald, P.M. (1991). oskar mRNA is localized to the posterior pole of the Drosophila oocyte. Cell *66*, 23-35. 10.1016/0092-8674(91)90136-m.

Kuriyan, J., and Eisenberg, D. (2007). The origin of protein interactions and allostery in colocalization. Nature *450*, 983-990. 10.1038/nature06524.

Küspert, M., Murakawa, Y., Schäffler, K., Vanselow, J.T., Wolf, E., Juranek, S., Schlosser, A., Landthaler, M., and Fischer, U. (2015). LARP4B is an AU-rich sequence associated factor that promotes mRNA accumulation and translation. Rna *21*, 1294-1305. 10.1261/rna.051441.115.

Lawrence, J.B., and Singer, R.H. (1986). Intracellular localization of messenger RNAs for cytoskeletal proteins. Cell *45*, 407-415. 10.1016/0092-8674(86)90326-0.

Lebedeva, S., Jens, M., Theil, K., Schwanhausser, B., Selbach, M., Landthaler, M., and Rajewsky, N. (2011). Transcriptome-wide analysis of regulatory interactions of the RNA-binding protein HuR. Mol Cell *43*, 340-352. 10.1016/j.molcel.2011.06.008.

Lécuyer, E., Yoshida, H., Parthasarathy, N., Alm, C., Babak, T., Cerovina, T., Hughes, T.R., Tomancak, P., and Krause, H.M. (2007). Global analysis of mRNA localization reveals a prominent role in organizing cellular architecture and function. Cell *131*, 174-187. 10.1016/j.cell.2007.08.003.

Lee, S.H., and Mayr, C. (2019). Gain of Additional BIRC3 Protein Functions through 3'-UTR-Mediated Protein Complex Formation. Mol Cell *74*, 701-712 e709. 10.1016/j.molcel.2019.03.006.

Lerner, R.S., Seiser, R.M., Zheng, T., Lager, P.J., Reedy, M.C., Keene, J.D., and Nicchitta, C.V. (2003). Partitioning and translation of mRNAs encoding soluble proteins on membrane-bound ribosomes. RNA *9*, 1123-1137. 10.1261/rna.5610403.

Lianoglou, S., Garg, V., Yang, J.L., Leslie, C.S., and Mayr, C. (2013). Ubiquitously transcribed genes use alternative polyadenylation to achieve tissue-specific expression. Genes Dev *27*, 2380-2396. 10.1101/gad.229328.113.

Liao, Y., Smyth, G.K., and Shi, W. (2014). featureCounts: an efficient general purpose program for assigning sequence reads to genomic features. Bioinformatics *30*, 923-930. 10.1093/bioinformatics/btt656.

Litterman, A.J., Kageyama, R., Le Tonqueze, O., Zhao, W., Gagnon, J.D., Goodarzi, H., Erle, D.J., and Ansel, K.M. (2019). A massively parallel 3' UTR reporter assay reveals relationships between nucleotide content, sequence conservation, and mRNA destabilization. Genome Res *29*, 896-906. 10.1101/gr.242552.118.

Liu, X., and Fagotto, F. (2011). A method to separate nuclear, cytosolic, and membrane-associated signaling molecules in cultured cells. Sci Signal *4*, pl2. 10.1126/scisignal.2002373.

Luo, Y., Pratihar, S., Horste, E.H., Mitschka, S., Mey, A., Al-Hashimi, H.M., and Mayr, C. (2023). mRNA interactions with disordered regions control protein activity. bioRxiv. 10.1101/2023.02.18.529068.

Lykke-Andersen, J., and Wagner, E. (2005). Recruitment and activation of mRNA decay enzymes by two ARE-mediated decay activation domains in the proteins TTP and BRF-1. Genes Dev *19*, 351-361. 10.1101/gad.1282305.

Ma, W., and Mayr, C. (2018). A Membraneless Organelle Associated with the Endoplasmic Reticulum Enables 3'UTR-Mediated Protein-Protein Interactions. Cell *175*, 1492-1506 e1419. 10.1016/j.cell.2018.10.007.

Martin, K.C., and Ephrussi, A. (2009). mRNA localization: gene expression in the spatial dimension. Cell *136*, 719-730. 10.1016/j.cell.2009.01.044.

Martin, M. (2011). Cutadapt removes adapter sequences from high-throughput sequencing reads. 2011 *17*, 3. 10.14806/ej.17.1.200.

Mazan-Mamczarz, K., Lal, A., Martindale, J.L., Kawai, T., and Gorospe, M. (2006). Translational repression by RNA-binding protein TIAR. Mol Cell Biol *26*, 2716-2727. 10.1128/MCB.26.7.2716-2727.2006.

Meyer, C., Garzia, A., Mazzola, M., Gerstberger, S., Molina, H., and Tuschl, T. (2018). The TIA1 RNA-Binding Protein Family Regulates EIF2AK2-Mediated Stress Response and Cell Cycle Progression. Mol Cell *69*, 622-635 e626. 10.1016/j.molcel.2018.01.011.

Mili, S., Moissoglu, K., and Macara, I.G. (2008). Genome-wide screen reveals APC-associated RNAs enriched in cell protrusions. Nature *453*, 115-119. 10.1038/nature06888.

Miller, S., Yasuda, M., Coats, J.K., Jones, Y., Martone, M.E., and Mayford, M. (2002). Disruption of dendritic translation of CaMKIIalpha impairs stabilization of synaptic plasticity and memory consolidation. Neuron *36*, 507-519. 10.1016/s0896-6273(02)00978-9.

Moor, A.E., Golan, M., Massasa, E.E., Lemze, D., Weizman, T., Shenhav, R., Baydatch, S., Mizrahi, O., Winkler, R., Golani, O., et al. (2017). Global mRNA polarization regulates translation efficiency in the intestinal epithelium. Science *357*, 1299-1303. 10.1126/science.aan2399.

Moretti, F., Rolando, C., Winker, M., Ivanek, R., Rodriguez, J., Von Kriegsheim, A., Taylor, V., Bustin, M., and Pertz, O. (2015). Growth Cone Localization of the mRNA Encoding the Chromatin Regulator HMGN5 Modulates Neurite Outgrowth. Mol Cell Biol *35*, 2035-2050. 10.1128/mcb.00133-15.

Mukherjee, N., Corcoran, D.L., Nusbaum, J.D., Reid, D.W., Georgiev, S., Hafner, M., Ascano, M., Jr., Tuschl, T., Ohler, U., and Keene, J.D. (2011). Integrative regulatory mapping indicates that the RNA-binding protein HuR couples pre-mRNA processing and mRNA stability. Mol Cell *43*, 327-339. 10.1016/j.molcel.2011.06.007.

Navarrete-Perea, J., Yu, Q., Gygi, S.P., and Paulo, J.A. (2018). Streamlined Tandem Mass Tag (SL-TMT) Protocol: An Efficient Strategy for Quantitative (Phospho)proteome Profiling Using Tandem Mass Tag-Synchronous Precursor Selection-MS3. Journal of proteome research *17*, 2226-2236. 10.1021/acs.jproteome.8b00217.

Nooren, I.M., and Thornton, J.M. (2003). Diversity of protein-protein interactions. Embo J *22*, 3486-3492. 10.1093/emboj/cdg359.

Patel, R.K., West, J.D., Jiang, Y., Fogarty, E.A., and Grimson, A. (2020). Robust partitioning of microRNA targets from downstream regulatory changes. Nucleic Acids Res *48*, 9724-9746. 10.1093/nar/gkaa687.

Qin, W., Myers, S.A., Carey, D.K., Carr, S.A., and Ting, A.Y. (2021). Spatiotemporally-resolved mapping of RNA binding proteins via functional proximity labeling reveals a mitochondrial mRNA anchor promoting stress recovery. Nat Commun *12*, 4980. 10.1038/s41467-021-25259-2.

Rappsilber, J., Mann, M., and Ishihama, Y. (2007). Protocol for micro-purification, enrichment, pre-fractionation and storage of peptides for proteomics using StageTips. Nature protocols *2*, 1896-1906. 10.1038/nprot.2007.261.

Reid, D.W., and Nicchitta, C.V. (2012). Primary role for endoplasmic reticulum-bound ribosomes in cellular translation identified by ribosome profiling. J Biol Chem *287*, 5518-5527. 10.1074/jbc.M111.312280.

Shiber, A., Döring, K., Friedrich, U., Klann, K., Merker, D., Zedan, M., Tippmann, F., Kramer, G., and Bukau, B. (2018). Cotranslational assembly of protein complexes in eukaryotes revealed by ribosome profiling. Nature *561*, 268-272. 10.1038/s41586-018-0462-y.

Smalec, B.M., Ietswaart, R., Choquet, K., McShane, E., West, E.R., and Churchman, L.S. (2022). Genome-wide quantification of RNA flow across subcellular compartments reveals determinants of the mammalian transcript life cycle. bioRxiv, 2022.2008.2021.504696. 10.1101/2022.08.21.504696.

Staudacher, J.J., Naarmann-de Vries, I.S., Ujvari, S.J., Klinger, B., Kasim, M., Benko, E., Ostareck-Lederer, A., Ostareck, D.H., Bondke Persson, A., Lorenzen, S., et al. (2015). Hypoxia-induced gene expression results from selective mRNA partitioning to the endoplasmic reticulum. Nucleic Acids Res *43*, 3219-3236. 10.1093/nar/gkv167.

Stoecklin, G., Colombi, M., Raineri, I., Leuenberger, S., Mallaun, M., Schmidlin, M., Gross, B., Lu, M., Kitamura, T., and Moroni, C. (2002). Functional cloning of BRF1, a regulator of ARE-dependent mRNA turnover. EMBO J *21*, 4709-4718.

Tushev, G., Glock, C., Heumüller, M., Biever, A., Jovanovic, M., and Schuman, E.M. (2018). Alternative 3' UTRs Modify the Localization, Regulatory Potential, Stability, and Plasticity of mRNAs in Neuronal Compartments. Neuron *98*, 495-511.e496. 10.1016/j.neuron.2018.03.030.

Vaquerizas, J.M., Kummerfeld, S.K., Teichmann, S.A., and Luscombe, N.M. (2009). A census of human transcription factors: function, expression and evolution. Nat Rev Genet *10*, 252-263. 10.1038/nrg2538.

Voigt, F., Zhang, H., Cui, X.A., Triebold, D., Liu, A.X., Eglinger, J., Lee, E.S., Chao, J.A., and Palazzo, A.F. (2017). Single-Molecule Quantification of Translation-Dependent Association of mRNAs with the Endoplasmic Reticulum. Cell Rep *21*, 3740-3753. 10.1016/j.celrep.2017.12.008.

Wang, Z., Kayikci, M., Briese, M., Zarnack, K., Luscombe, N.M., Rot, G., Zupan, B., Curk, T., and Ule, J. (2010). iCLIP predicts the dual splicing effects of TIA-RNA interactions. PLoS Biol *8*, e1000530. 10.1371/journal.pbio.1000530.

Xia, C., Fan, J., Emanuel, G., Hao, J., and Zhuang, X. (2019). Spatial transcriptome profiling by MERFISH reveals subcellular RNA compartmentalization and cell cycle-dependent gene expression. Proc Natl Acad Sci U S A *116*, 19490-19499. 10.1073/pnas.1912459116.

Yan, X., Hoek, T.A., Vale, R.D., and Tanenbaum, M.E. (2016). Dynamics of Translation of Single mRNA Molecules In Vivo. Cell *165*, 976-989. 10.1016/j.cell.2016.04.034.

Yugami, M., Okano, H., Nakanishi, A., and Yano, M. (2020). Analysis of the nucleocytoplasmic shuttling RNA-binding protein HNRNPU using optimized HITS-CLIP method. PLoS One *15*, e0231450. 10.1371/journal.pone.0231450.

Zarnegar, B.J., Flynn, R.A., Shen, Y., Do, B.T., Chang, H.Y., and Khavari, P.A. (2016). irCLIP platform for efficient characterization of protein-RNA interactions. Nat Methods *13*, 489-492. 10.1038/nmeth.3840.

Zerangue, N., Schwappach, B., Jan, Y.N., and Jan, L.Y. (1999). A new ER trafficking signal regulates the subunit stoichiometry of plasma membrane K(ATP) channels. Neuron *22*, 537-548. 10.1016/s0896-6273(00)80708-4.

Zhao, W., Zhang, S., Zhu, Y., Xi, X., Bao, P., Ma, Z., Kapral, Thomas H., Chen, S., Zagrovic, B., Yang, Yucheng T., and Lu, Zhi J. (2021). POSTAR3: an updated platform for exploring post-transcriptional regulation coordinated by RNA-binding proteins. Nucleic Acids Research *50*, D287-D294. 10.1093/nar/gkab702.